Recent e⁺e⁻ Physics

G. Flügge

Institut für Kernphysik

Kernforschungszentrum Karlsruhe

KERNFORSCHUNGSZENTRUM KARLSRUHE

Institut für Kernphysik

KfK 2995

Recent e^+e^- Physics

Günter Flügge

Recent e^+e^- Physics

Abstract

Recent results from e^+e^- storage rings are discussed, with emphasis on PETRA experiments: total cross section and search for toponium; check of QED in e, μ and τ pair production; jet physics and evidence for gluon bremsstrahlung.

Neuere e^+e^- Physik

Zusammenfassung

Neuere Ergebnisse von e^+e^- Speicherringen werden diskutiert, mit Betonung der PETRA Experimente: totaler Wirkungsquerschnitt und Suche nach Toponium; Überprüfung der QED in e-, μ- und τ-Paarproduktion; Jet-Physik und Evidenz für Gluon-Bremsstrahlung.

CONTENTS

I. INTRODUCTION

These two lectures will be mainly concerned with the advances in the field of e^+e^- physics since the PETRA storage ring came into operation some 1 1/2 years ago. More complete summaries of recent e^+e^- physics can be found in ref. 1.

To get an impression of the increase in accessible energy let us look at the energy dependence of the normalized total cross section R shown in fig. 1. The respective ranges covered by DORIS/SPEAR, upgraded DORIS and PETRA/PEP are indicated.
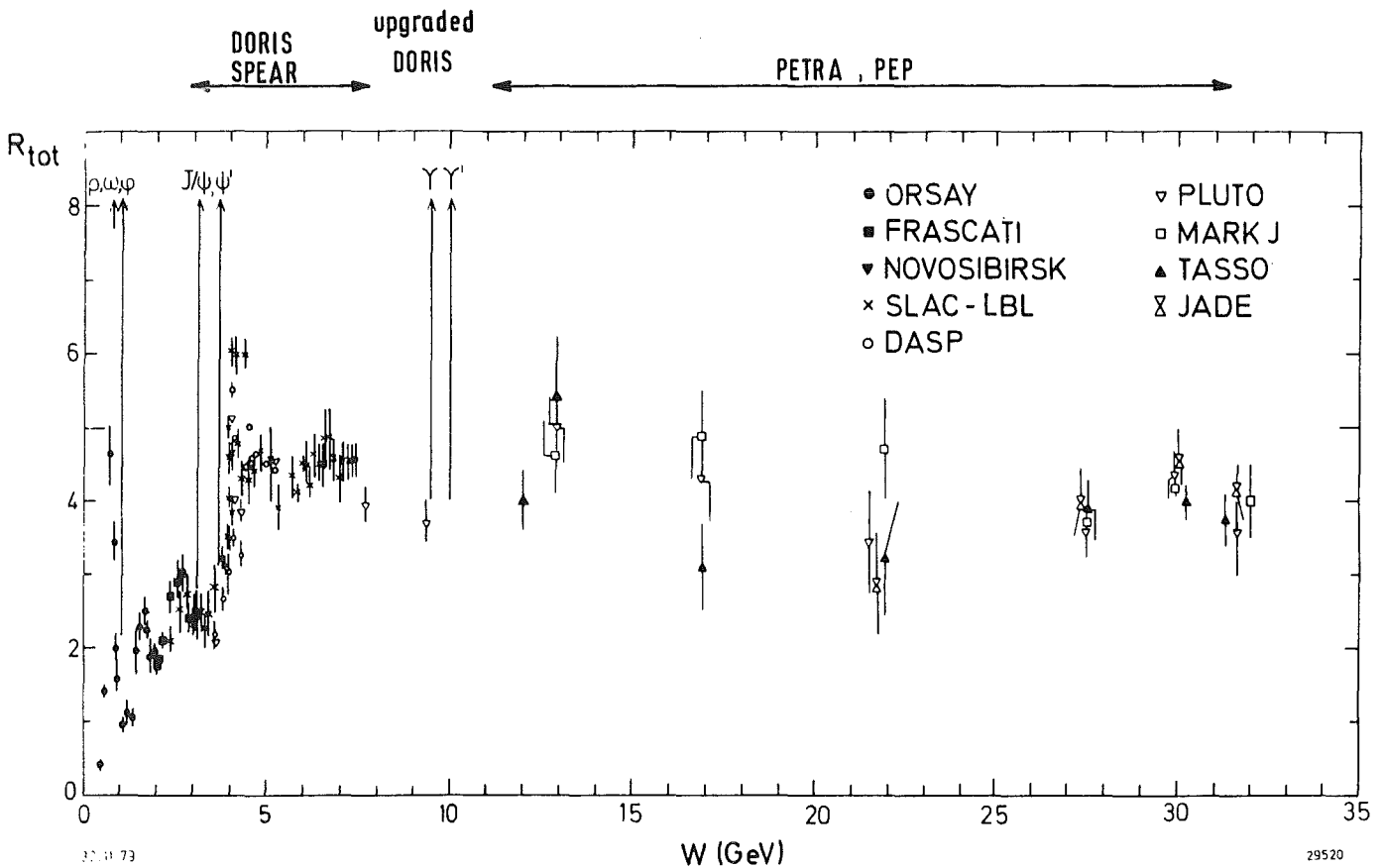

Fig. 1   The ratio $R = \sigma_{had}/\sigma_{\mu\mu}$ of hadronic to μ pair production as a function of the c.m. energy W ($\equiv E_{cm}$) (adopted from G.Wolf[1]).

The lectures are organized as follows:

A short introduction on e^+e^- storage rings and cross sections (chapter I) and a summary of our present knowledge of the heavy lepton and the bottom quark (II) will set the scene for a discussion of PETRA results: test of QED and universality of leptons (III), hadron production at PETRA and search for the top quark (IV). The second lecture will then concentrate on QCD: first a summary of QCD in quarkonia (V) and finally recent results about QCD effects in high energy jets (VI).

1. e^+e^- Storage Rings

The history of e^+e^- storage rings dates back to 1960 when B. Touschek in Frascati built the first machine of this kind[2]. The original motivation for e^+e^- storage rings was to study QED limits at large energies. Very soon, however, the prime interest turned to hadron production[3] although we see a revival of the QED tests today, in particular with a glance towards weak interference effects.

The annihilation of electrons and positrons into hadrons via the one-photon channel presents several advantages. Contrary to hadron collisions the system has the well defined quantum numbers of the photon. In (symmetric) storage rings the full energy of both beams becomes available in the head-on collisions of the stored particles.

The laboratory frame is identical with the center of mass system (for zero crossing angle and equal energies). This highly facilitates the data analysis but also requires large angular acceptance of the apparatus.

Table 0 gives a survey of e^+e^- machines which have been built[3,4].

TABLE 0 History of electron storage rings

Name	Location	First Beam	Maximum Beam Energy (GeV)
AdA	Frascati	1961	0.25
Princeton-Stanford	Stanford	1962	0.55
ACO	Orsay	1966	0.55
VEPP-2	Novosibirsk	1966	0.55
ADONE	Frascati	1969	1.55
BYPASS	Cambridge (USA)	1970	3.5
VEPP-3	Novosibirsk	1970	3.5
SPEAR	Stanford	1972	3.9
DORIS	Hamburg	1974	5.0
VEPP-2M	Novosibirsk	1975	0.67
DCI	Orsay	1976	1.8
PETRA	Hamburg	1978	19
PEP	Stanford	(1979)	18
CESR	Cornell	(1979)	8
VEPP-4	Novosibirsk	(1979)	8

PETRA:

PETRA is the first of a new generation of storage rings entering into the 30 GeV c.m. energy region[5].

The history of PETRA is summarized in table 1. It may be interesting to realize that the submission of the proposal coincides historically with the discovery of J/ψ in Nov, 1974. It took less than a year until the machine was authorized on October 20, 1975. Again one year later in autumn 1976 decisions were taken on the first round of experiments: PLUTO[7], MARK J[8], CELLO[9], JADE[10] and TASSO[11]. In the following one and a half years the construction of PETRA and of the five experiments went ahead. In July 1978 already - less than three years after authorization - an electron beam was stored and accelerated in the machine. In fall 1978 and beginning of 1979 first physics runs could be scheduled and experiments took data successfully. For these first physics shifts three detectors had been in-

Table 1   History of PETRA

Proposal submission November 1974

1975   Authorization Oct. 20, 1975

1976

Proposal up - date

Begin of tunnel construction

Call for experimental proposals

Decisions on first round of experiments

1977

Ring tunnel and halls are completed, begin of magnet installation
e^+ injection through first octant

e^- injection through second octant

1978

e^- beam storage July 15,
   acceleration to > 11 GeV July 3o
Luminosity measurements Sept. 15
installation of 3 detectors in interaction regions:
MARK J, PLUTO, TASSO
first physics runs at 2 × 8.5 GeV

1979   Shut - down, installation of additional 28 cavities + PIA
Physics runs at high energies

JADE + PIA operational

CELLO installed; additional 28 cavities

1980   Physics runs at 2 × 18 GeV

stalled in the machine: PLUTO, MARK J and TASSO. A fourth detector, JADE, came into operation in June 1979; CELLO was moved into the beam in fall 1979.

Fig. 2 shows a bird's view of the DESY site with the storage ring PETRA. PETRA - Positron-Electron-Tandem-Ring-Accelerator - is an e^+e^- storage ring designed for a maximum beam energy of 2×19 GeV. Its diameter is about 8oo m. In the original configuration all other DESY machines were used to fill the new PETRA storage ring. Two linear accelerators produce electrons and positrons. Originally positrons were preaccelerated to 2.2 GeV in the DESY synchrotron and then stacked into the DORIS storage ring. After accumulation they are reinjected into the
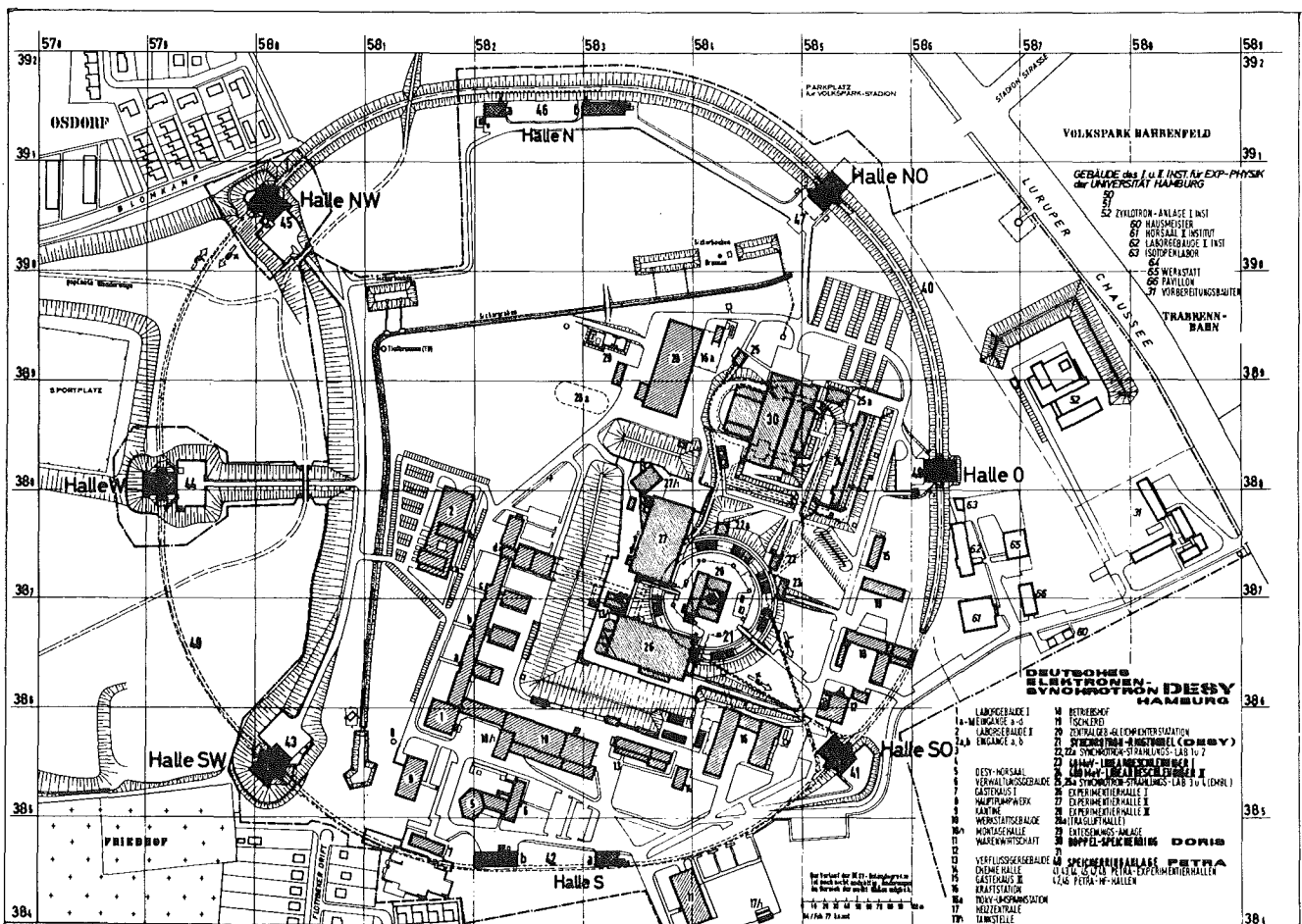

Fig. 2 The e^+e^- storage ring PETRA

DESY synchrotron and, like the electrons, accelerated to their final injection energy of 6.5 GeV. At this energy particles are injected into the PETRA tunnel where they are stacked. Typical currents of several mA are then circulating in the PETRA storage ring and can be accelerated to their final energy. Contrary to the original design of DORIS, PETRA is a single ring few bunch machine. Depending on the number of experimental areas which have to be served, the number of bunches per beam varies between one and four[12].

In March 1979 the number of active cavities in PETRA was increased from 4 to 32. Thus the accessible energy range went up to 2 × 16 GeV. Another 32 cavities were added in fall 1979 taking the machine close to its design energy.

Since the beginning of 1979 a small positron ring PIA[13] was installed and tested at the transfer between LINAC and the synchrotron. PIA was designed to accumulate positrons at 4oo MeV before injection into the synchrotron. Already in July 1979 PIA was commissioned for routine filling of PETRA and DORIS could be freed for physics runs again.

Some relevant figures on the PETRA performance are summarized in table 2.

The accomplished values for the single beam lifetime, the bunch length, and the single bunch current are close to the design figures. A maximum beam energy of $\approx$18 GeV could be obtained.

In the light of possible resonance searches it is important to note that the design value for the momentum spread of 6.5×10^{-5} GeV × p^2 (p in GeV) was observed. This guarantees an energy resolution of $\sigma = 2.3$ MeV at 10 GeV and 21 MeV at 30 GeV c.m. energy.

The best luminosity which was obtained at 2 × 15 GeV was 3×10^{3o} $cm^{-2}s^{-1}$. Compared to the designed luminosity of $\approx 10^{32}$ $cm^{-2}s^{-1}$ this is still a factor of ~30 too low. To understand this discrepancy in detail let us look at the following expression for the luminosity:

Table 2   PETRA performance (by February 1980)

Parameter	Accomplished values	Comments
- Lifetime	5 ./. 8 h	design: 9 h; improving
- Bunch length	11.4 mm (r.m.s.)	no bunch lengthening
momentum spread	0.065 MeV$\cdot p^2$(r.m.s.)	p = beam momentum in GeV
energy resolution	0.023 MeV$\cdot E_{CM}^2$(r.m.s.)	E_{CM} = c.m. energy in GeV
- Single bunch current	$\lesssim$ 18 mA	design: 20 mA
- Energy per beam	$\lesssim$ 18 GeV	design: 19 GeV
- Luminosity $\begin{cases} \text{max.} \\ \text{typical} \end{cases}$ at 2×15 GeV	3×10^{30} cm^{-2}s^{-1} 1×10^{30} cm^{-2}s^{-1}	$\begin{cases} \text{2×2 bunches; design} \\ \text{value:} \\ \approx 10^{32} \text{ cm}^{-2}\text{s}^{-1} \\ \text{(2×4 bunches)} \end{cases}$
tune shift ΔQ	0.015 ./. 0.025	design: 0.06
number of bunches B	2 × 2	design: 2 × 4
length of I.S. $\sim\sqrt{\beta_y}$	15 m	design: 10 m

$$L \sim \frac{(\Delta Q^2) \cdot B}{\beta_y} \qquad .$$

The design value of β_y is proportional to the square of the distance between the interaction quadrupoles. The product of all ratios between accomplished and design values for the tune shift ΔQ, the number of bunches B and the interaction length (table 2) explains the missing factor.

Detectors

The first experiments at PETRA were primarily motivated by the possible discovery of new degrees of freedom, in particular the proposed new quarks[14] b and t and may be even further quarks and leptons. An appropriate handle on new flavours is the total cross section.

$$\frac{\sigma_{had}}{\sigma_{\mu\mu}} = R = 3 \times \sum_{q} Q_q^2 \quad .$$

In addition topological quantities like sphericity or thrust may be even more important when looking for new thresholds. Any first round experiment should be in a position to measure these quantities. Therefore, a good detector should have a large acceptance for charged and neutral particles. For the topological studies good energy resolution both for charged and neutral particles is desirable. Two photon processes become increasingly important at larger energies. To discriminate against these processes a good measurement of the total hadronic energy is indispensable. Of course, this also ensures good suppression of beam gas, beam wall and synchrotron radiation background.

I will briefly describe the three experiments which have taken data during the first PETRA run. Fig. 3 shows the detector PLUTO[7] in its proposed final configuration at PETRA. The inner de-

PLUTO

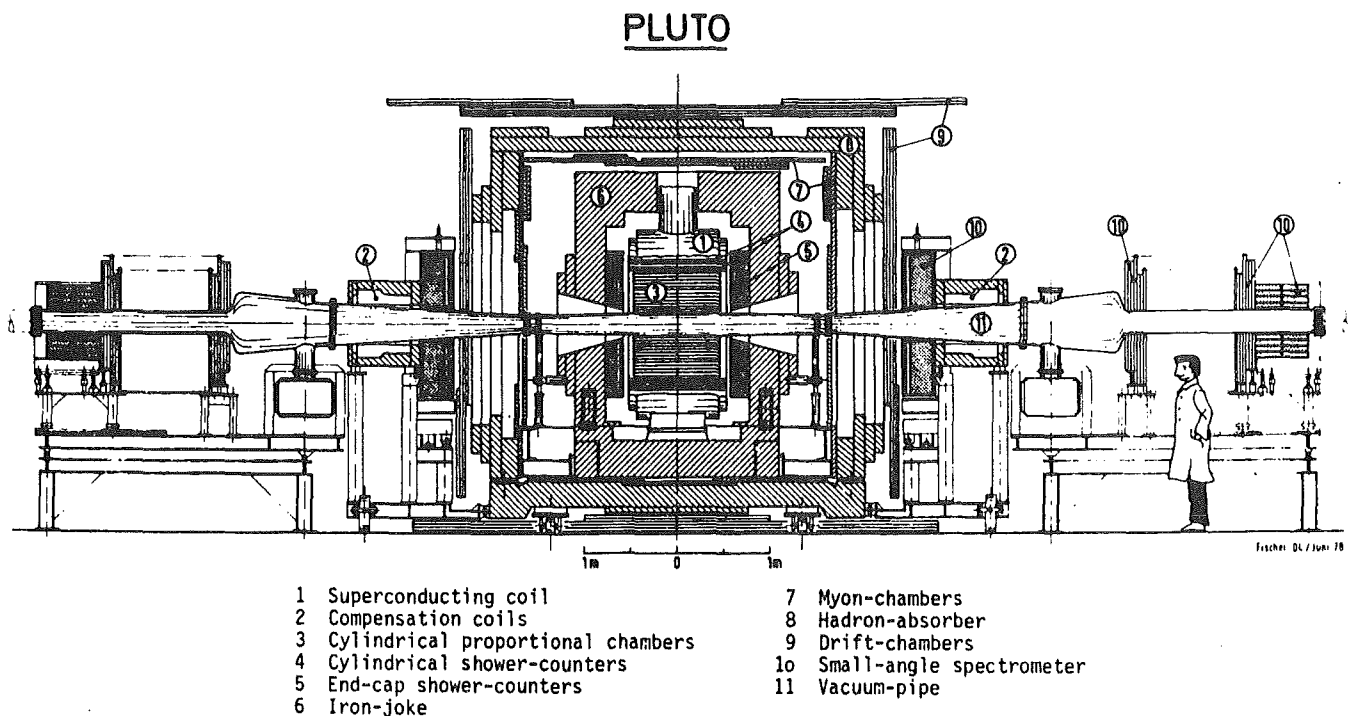| 1 | Superconducting coil | 7 | Myon-chambers |
2	Compensation coils	8	Hadron-absorber
3	Cylindrical proportional chambers	9	Drift-chambers
4	Cylindrical shower-counters	lo	Small-angle spectrometer
5	End-cap shower-counters	11	Vacuum-pipe
6	Iron-joke		

Fig. 3   The PLUTO detector in its PETRA configuration
(Aachen-Bergen-DESY-Hamburg-Maryland-Siegen-Wuppertal Collaboration)

tector had already been used at DORIS[15]. It consists of a superconducting coil which produces a magnetic field of 1.7 T. The magnetic field volume is filled with a set of cylindrical proportional chambers to detect the tracks of charged particles. Shower counters of the lead-scintillator type cover 93% of the solid angle. A set of proportional tube chambers outside the iron flux return yoke is used to separate hadrons and muons. The acceptance of such a detector for hadronic events is slightly energy dependent. In the energy range around 5 GeV for instance the event acceptance of PLUTO is of the order of 80%.

In addition to the DORIS configuration mainly two new components have been added: The magnet yoke has been surrounded by additional iron to provide a total iron thickness of 1 m for muon filtering. Large area drift chambers have been mounted outside the new iron house. The complete setup will provide a muon detection over 83% of 4π with a punchthrough and decay probability of less than three percent up to a muon momentum of 5 GeV.

Two forward spectrometers enable electron detection in the angular region between 23 and 25o mrad. Each spectrometer contains a small angle tagger (SAT) covering the angular range up to 68 mrad. It consists of a fine segmented array of lead glass blocks and two sets of proportional chambers. The remaining angular range is covered by the large angle tagger (LAT) which uses a lead scintillator sandwich preceeded by a layer of proportional tubes. The r.m.s. energy resolution in the SAT and the LAT is 8.4%/$\sqrt{E}$ and 11%/$\sqrt{E}$, respectively. The forward spectrometers are important mainly for two reasons. They extend the range for Bhabha scattering down to 23 mrad which is particularly needed for monitor purposes and they serve as tagging devices for two photon reactions.

Fig. 4 shows the MARK J detector[8]. It was built for the dedicated purpose of measuring weak-electromagnetic interference through μ pair production at high energies[16,17]. The whole apparatus is, therefore, rotatable in θ and ϕ. Essentially the setup consists of a central electromagnetic shower detector ($\sigma/E = 12\%/\sqrt{E}$) surrounded by a hadron calorimeter. Several layers of track chambers are inserted between these two calorimeters. For muon detection the hadron calorimeter is surrounded by additional iron
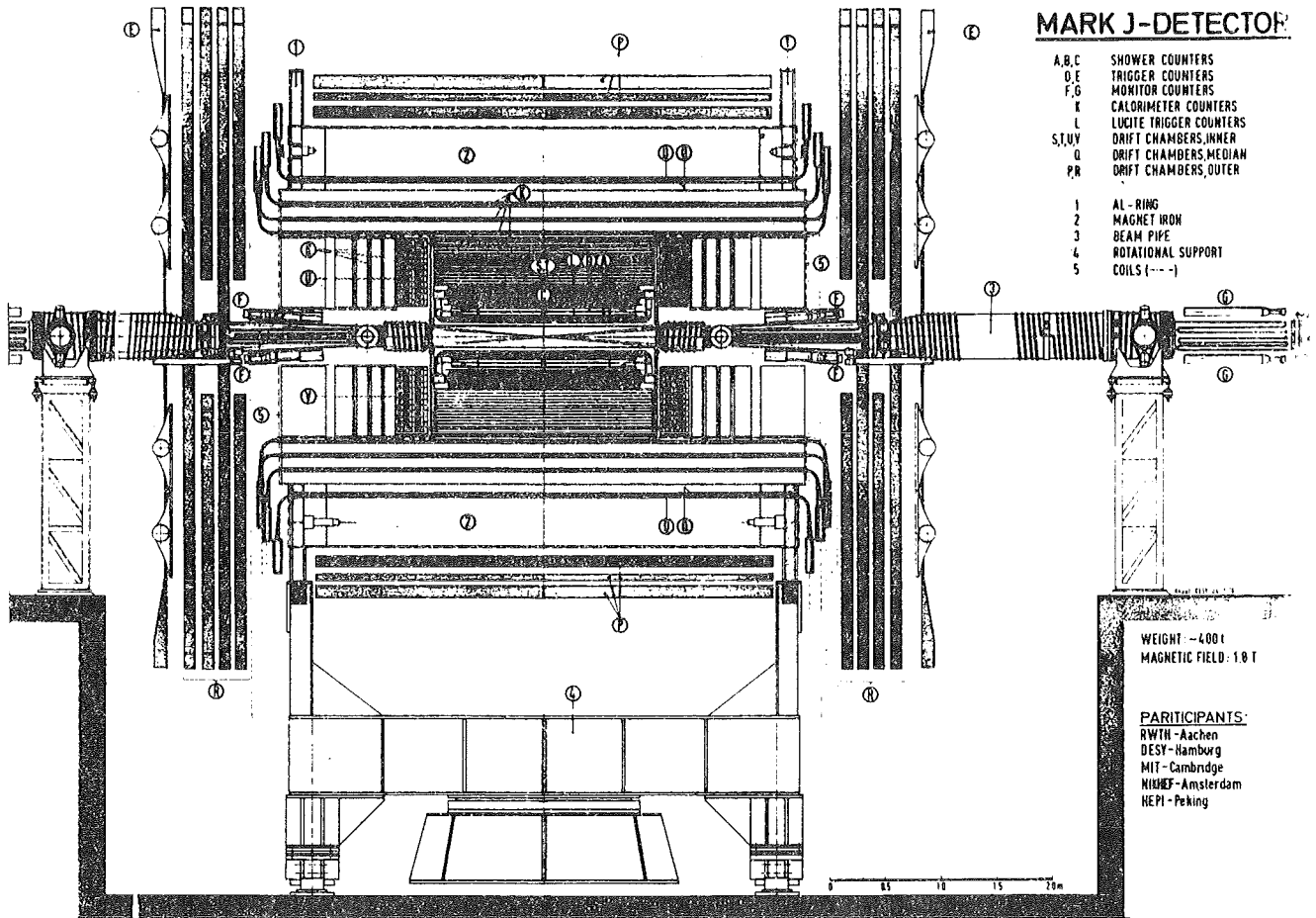
MARK J-DETECTOR

A,B,C	SHOWER COUNTERS
D,E	TRIGGER COUNTERS
F,G	MONITOR COUNTERS
K	CALORIMETER COUNTERS
L	LUCITE TRIGGER COUNTERS
S,T,U,V	DRIFT CHAMBERS,INNER
Q	DRIFT CHAMBERS,MEDIAN
P,R	DRIFT CHAMBERS,OUTER
1	AL-RING
2	MAGNET IRON
3	BEAM PIPE
4	ROTATIONAL SUPPORT
5	COILS (---)

WEIGHT ~400 t
MAGNETIC FIELD : 1.8 T

PARTICIPANTS:
RWTH-Aachen
DESY-Hamburg
MIT-Cambridge
NIKHEF-Amsterdam
HEPI-Peking

Fig. 4   The MARK J detector (Aachen-DESY-LAPP-MIT-NIKHEF-Peking colla-
boration).

which is covered by sets of multilayer drift chambers. For momentum
analysis of the muons the iron can be magnetized. The endcaps of the
detector were installed in March 1979.

Fig. 5 shows a sideview of the TASSO detector[11]. Until January '79
only the central detector consisting of a drift chamber, the time-of-
flight system, the magnet and the top and bottom μ counters were in-
stalled. Some lead-scintillator shower counters covering part of the solid
angle were added in the course of the year. The data I will report here
were essentially obtained in the magnetic detector. A warm coil pro-
vides a solenoidal field of .5 Tesla. The field volume of 4.5 m length
and 2.7 m diameter is filled with a large cylindrical drift chamber
with 15 sense wire plances, 9 radial and 6 with a stereo angle of $\pm 4^0$
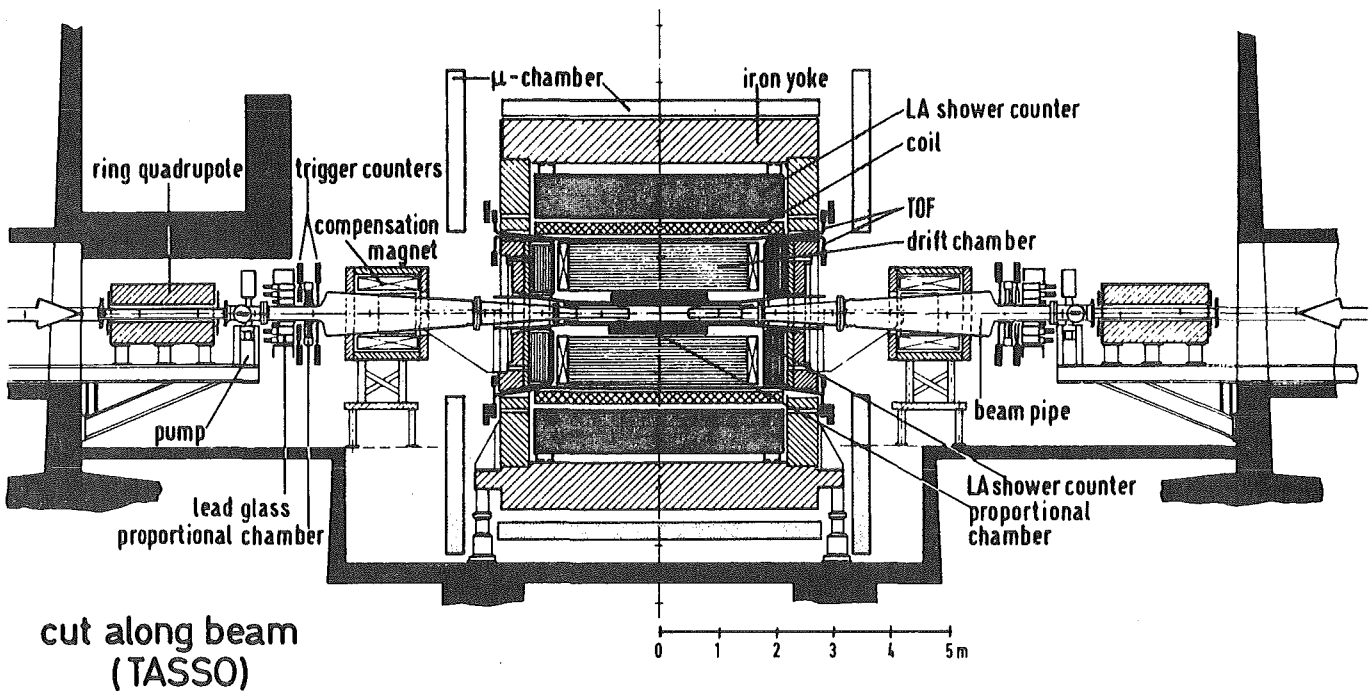
cut along beam
(TASSO)

<u>Fig. 5</u>   The TASSO detector (Aachen-Bonn-DESY-Hamburg-IC London-Oxford-
Rutherford-Weizman-Wisconsin Collaboration).

to determine the z-direction. A single wire resolution of 280 microns
(rms) has been reached which yields a momentum resolution
$\Delta p/p \simeq 2\% \times p$ (rms), p in GeV. A 4-gap proportional chamber aids the
pattern recognition and z reconstruction.

The JADE detector shown in fig.6 started data taking in June 1979.
Its warm coil, 3.5 m long, 2 m in diameter produces a field of 0.5 T.
It is filled with a novel type of high pressure drift chamber. In
addition to the momentum vector 48 dE/dx samples are measured in this
'jet chamber'. For electromagnetic shower detection the coil is
surrounded by an array of about 2700 lead glass blocks (12.5 x_o)
covering 90% of the solid angle. TOF counters inside the coil and a
μ detection array of loaded concrete interleaved with drift chambers
complete the setup.

The CELLO detector (fig.7) was moved into the beam in fall 1979.
With a thin superconducting coil (0.5 x_o) and a full coverage

1 Beam Pipe Counters
2 End Plug Lead Glass Counters
3 Pressure Tank
4 Muon Chambers
5 Jet Chambers
6 Time of Flight Counters
7 Coil
8 Central Lead Glass Counters
9 Magnet Yoke
10 Muon Filters
11 Removable End Plug
12 Beam Pipe
13 Tagging Counter
14 Compensating Coil
15 Moving Devices
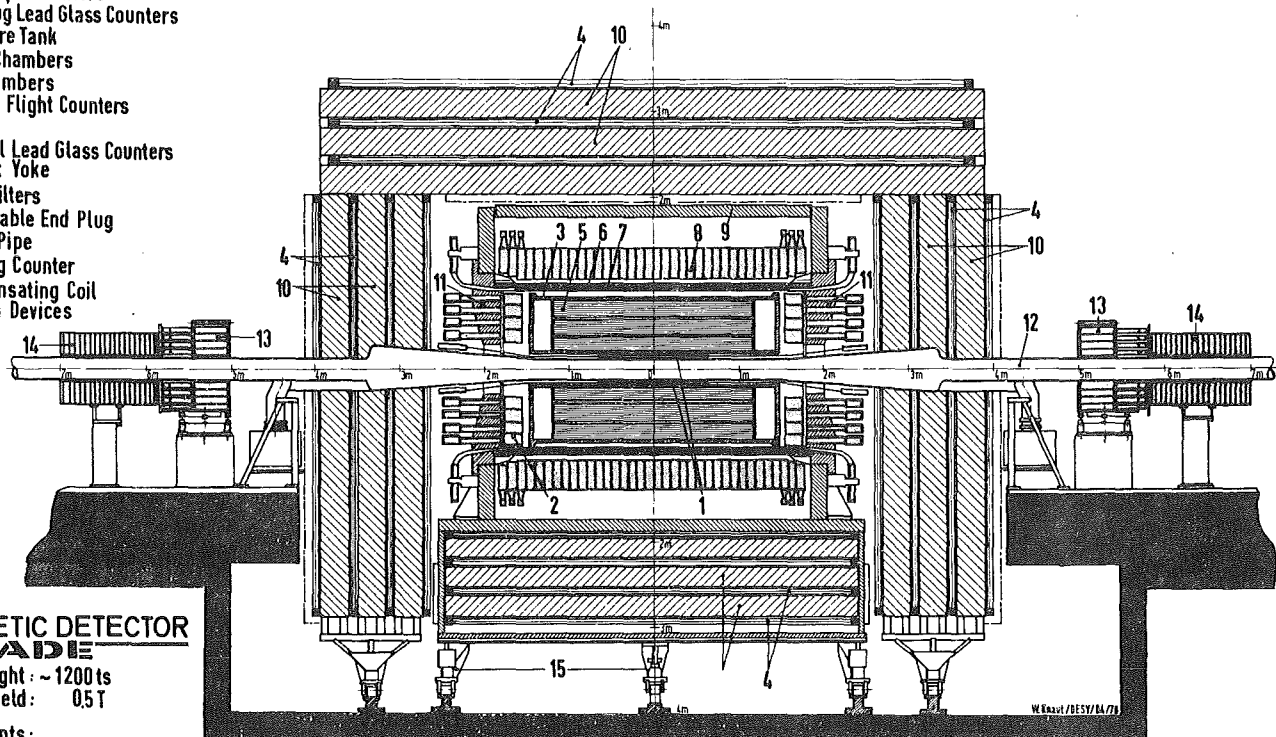
MAGNETIC DETECTOR
JADE
Total Weight : ~1200 ts
Magnet Field : 0.5 T

Participants :
DESY, Hamburg, Heidelberg,
Lancaster, Manchester, Rutherford Lab.,
Tokyo

Fig. 6   The JADE detector (DESY-Hamburg-Heidelberg-Lancaster-Manchester
Rutherford-Tokyo collaboration).

(97% solid angle) of liquid argon shower counters it has a highly
advanced technology. Since no physics results are available yet,
I will not describe this detector in detail.

A very short summary of the physics abilities of the five
detectors is given in table 3. Most detectors (except MARK J)
provide charged particle detection in large solenoidal magnetic
volumes over 80 to 90% of the solid angle. The typical momentum
resolution at 5 GeV is of the order of 5% for the drift chamber
detectors whereas it is only 15% for the proportional chamber
detector PLUTO. Myon identification over a large solid angle is
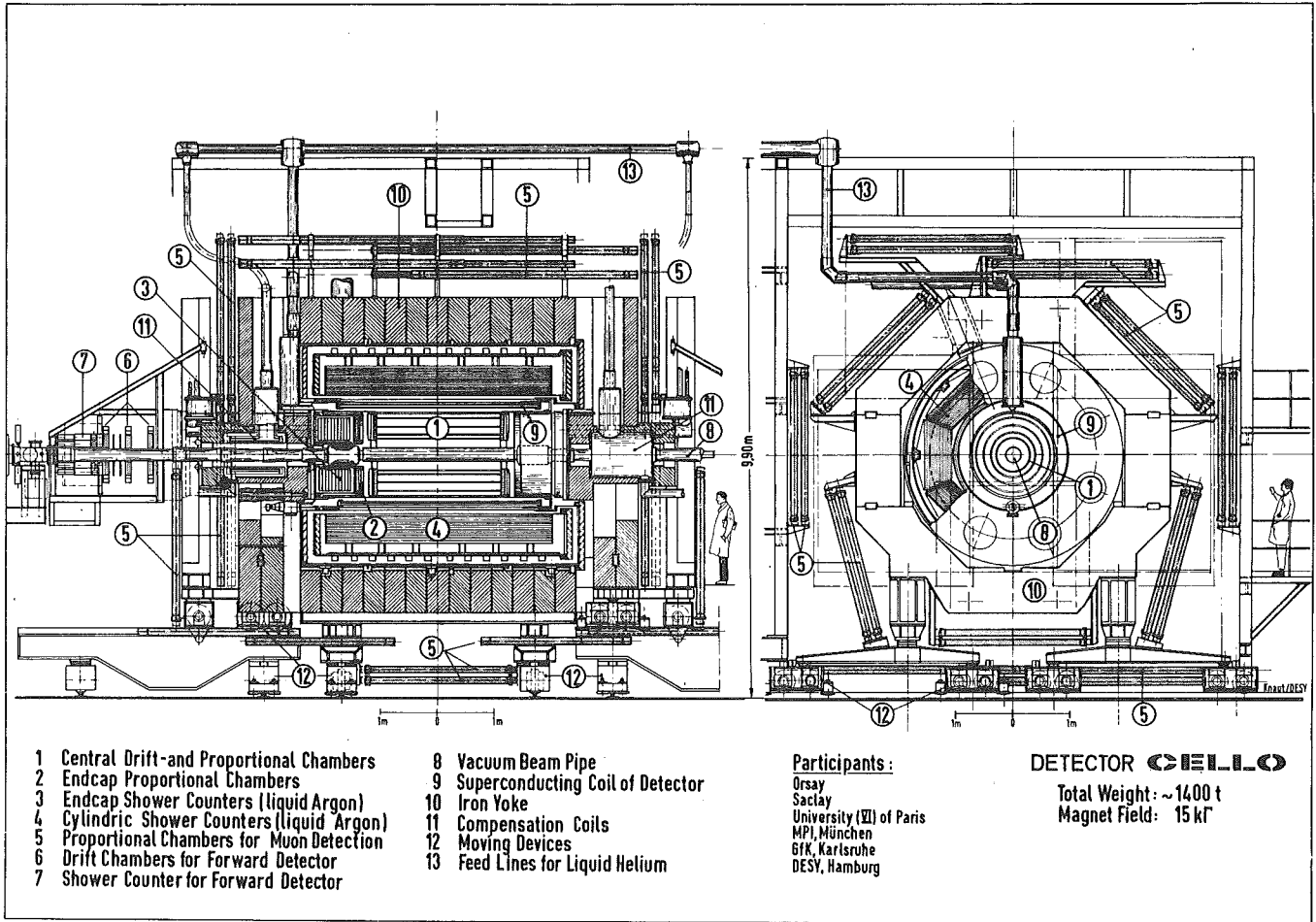available in all experiments. The same is true for electron and

1	Central Drift-and Proportional Chambers	8	Vacuum Beam Pipe
2	Endcap Proportional Chambers	9	Superconducting Coil of Detector
3	Endcap Shower Counters (liquid Argon)	10	Iron Yoke
4	Cylindric Shower Counters (liquid Argon)	11	Compensation Coils
5	Proportional Chambers for Muon Detection	12	Moving Devices
6	Drift Chambers for Forward Detector	13	Feed Lines for Liquid Helium
7	Shower Counter for Forward Detector		

Participants:
Orsay
Saclay
University (VI) of Paris
MPI, München
GfK, Karlsruhe
DESY, Hamburg

DETECTOR CELLO

Total Weight: ~1400 t
Magnet Field: 15 kΓ

Fig. 7   The CELLO detector (DESY-Karlsruhe-München-Orsay-Paris-Saclay collaboration).

photon detection. However, the method is quite different for the various detectors as indicated in table 3. In the last column I have listed a few items which are special to the different devices.

Table 3   PETRA detectors

	Main Physics Goals	Charged Hadrons σ_p/p at 5 GeV	Electrons	Special Items
PLUTO	σ_{tot}	15%	lead-scin- tillator	$\gamma\gamma$ tagging 25 ./. 250 mrad
MARK J	μ pairs	hadron calori- metry	lead-scin- tillator + tubes	rotatable
TASSO	jets + hadron identification	4-6%	liquid argon	full C-identi- fication in 2 × 1.5 sr
JADE	jets + leptons	3-5%	lead glass	"jet chamber", 48 dE/dx samples
CELLO	leptons + photons	3-5%	liquid argon	thin supercon- ducting coil 0.5 X_0

2. Cross Sections

In this section I want to give a short introduction to the main processes encountered in e^+e^- physics. The expected cross section will be estimated to provide a feeling for the rates we are dealing with.

a)   μ-Pair Production

The μ-pair production

$$e^+e^- \rightarrow \mu^+\mu^-$$

is a kind of a pilot reaction in e^+e^- physics since it is represented by the simple graph
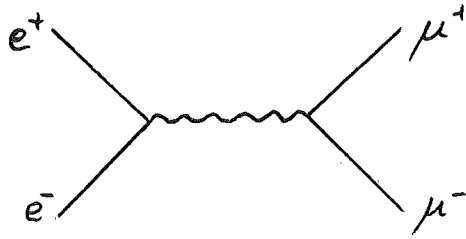
The total cross section for this reaction is given by the formula

$$\sigma_{\mu\mu} = \frac{4\pi \alpha^2}{3 \, E_{cm}^2} \approx \frac{21.7 \text{ nb}}{E_b^2 (\text{GeV}^2)} \qquad \text{(spin 1/2, pointlike, } E_{CM} \gg m_\mu,$$

$$\text{lowest order)}$$

$$E_{cm}/2 = E_b = \text{beam energy}$$

Cross sections in e^+e^- reactions will mostly be given in terms of $\sigma_{\mu\mu}$. Let us, therefore, calculate the $\mu\mu$ rates to get a feeling of the number of events one expects in e^+e^- physics. Assume an average luminosity of $3 \cdot 10^{29} \text{ s}^{-1} \text{cm}^{-2}$ at $E_{cm} = 5$ GeV varying like E_b^2. Then the energy dependence cancels out in the product $L \cdot \sigma_{\mu\mu}$ and the expected average rate will be

$$N_{\mu\mu} = L \cdot \sigma_{\mu\mu} \approx 10^{-3} \text{ s}^{-1} \approx 90 \text{ d}^{-1} \qquad .$$

b) Bhabha_Scattering

Another important QED cross section is the Bhabha scattering

$$e^+e^- \rightarrow e^+e^-$$

which is represented by the two graphs
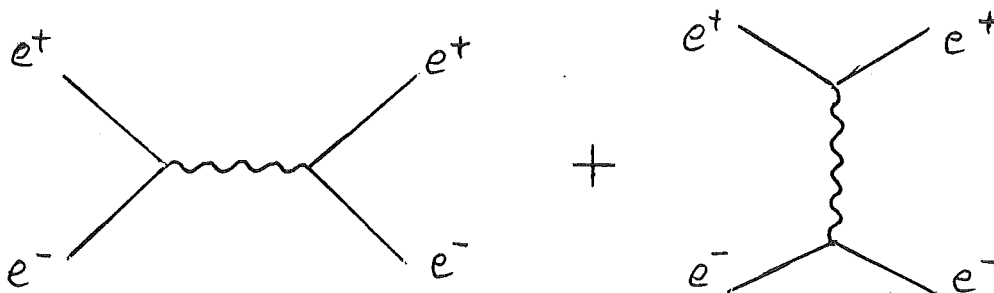
Bhabha scattering is used as a monitor reaction in e^+e^- collisions because it gives a large calculable cross section at small angles where the validity of QED is proven (low momentum transfer).

3. Hadron Production at Low Energies

The most important cross section in e^+e^- physics is, however, hadron production via the one-photon-channel:
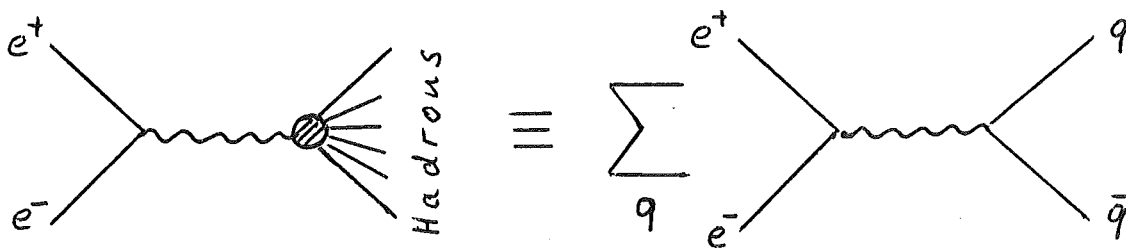
In the quark-parton model this process is simply described by the sum over all quark pair cross sections. It is, therefore, related to $\sigma_{\mu\mu}$ by the formula (assuming pointlike spin 1/2 massless coloured quarks)

$$R = \frac{\sigma_{had}}{\sigma_{\mu\mu}} = 3 \sum_q Q_q^2 \qquad q = \text{quark flavours} \qquad .$$

Thus R is just 3 times the sum over all quark charges squared where the sum runs over all quark flavours and the factor 3 takes care of the 3 colours. The expected values for R are summarized in table 4. This table also contains the expectation for R if we include QCD corrections in first order[18].

Near to a new flavour threshold bumps and peaks appear in the cross section. In addition also new leptons show up by their hadronic decay modes. Like in the case of $c\bar{c}$ and $\tau^+\tau^-$ production lepton and quark thresholds may (accidentally?) overlap. In the following I will

first talk about the asymptotic behaviour of the total cross section and then come back to the threshold region.

Table 4   Theoretical predictions for $R = \sigma_{had}/\sigma_{\mu\mu}$

Quark q	Charge Q_q	$R_{QPM} = 3 \Sigma Q_q^2$	R_{QCD}[+]
u	2/3		
d	- 1/3	2	~ 2.3 (E_{cm} = 3.6 GeV)
s	- 1/3		
c	2/3	3 1/3	~ 3.9 (E_{cm} = 5.0 GeV)

[+] Gluonic corrections in first order QCD:

$$R_{QCD} = R_{QPM}(1+\frac{\alpha_s}{\pi})$$
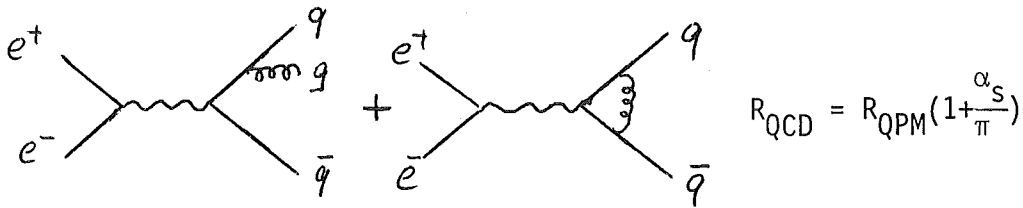
$$\alpha_s(E_{cm}) = \frac{12\pi}{(33 - 2N)\log \frac{E_{cm}^2}{\Lambda^2}} \quad ; \quad \begin{array}{l} \Lambda = 0.5 \text{ GeV} \\ N = \text{number of flavours} \end{array}$$

Measurement of σ_{had} below 5 GeV

The total hadronic cross section in e^+e^- reactions is measured according to

$$\sigma_{had} = \frac{N}{\varepsilon \cdot \int L \, dt}$$

where N is the number of events seen in the detector. ε is the acceptance

of the detector and $\int L \, dt$ is the integrated luminosity.

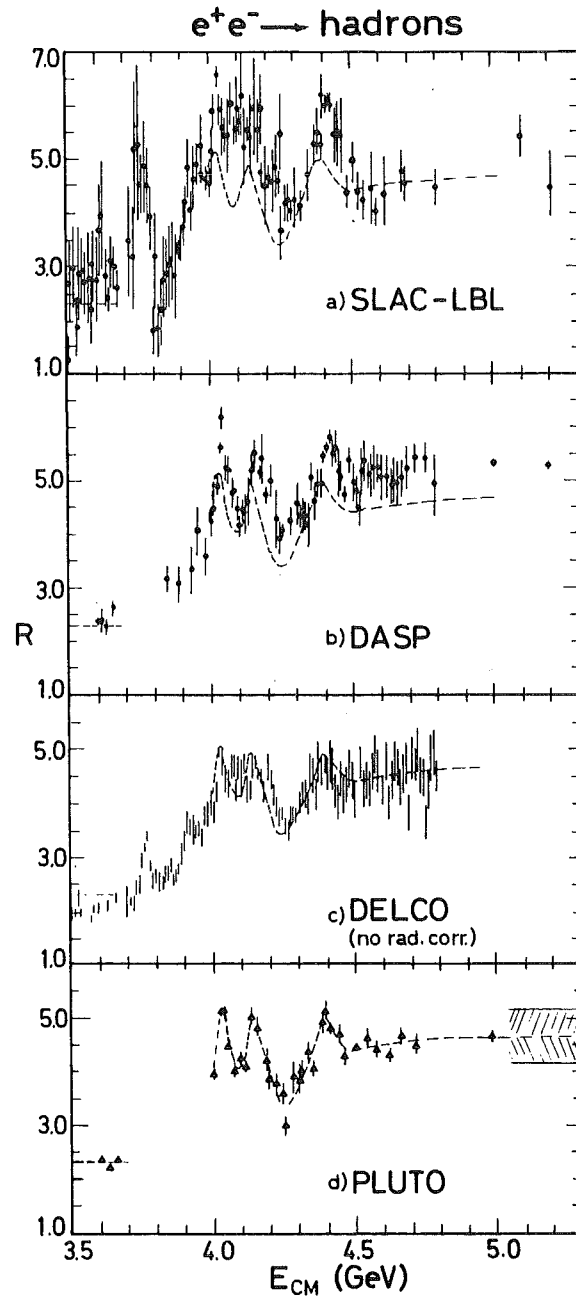Fig. 8 shows the results of the total cross section measurements

Fig. 8 Measurements of R as a function of energy
  a)   SLAC-LBL group[21]
  b)   DASP   group[22]
  c)   DELCO   group[23] (no radiative corrections)
  d)   PLUTO   group[19]
     Adopted from G. Feldman[20]

of the PLUTO collaboration[19] in terms of $R = \sigma_{had}/\sigma_{\mu\mu}$. The systematic error of ±15% is indicated in the figure. For comparison[26] also the results of three other experiments are shown: SLAC-LBL[21], DASP[22] and DELCO[23]. Below charm threshold around 3.5 GeV all data agree remarkably well. Also far above threshold in the asymptotic region around 5 GeV there is good agreement between all four experiments.

How well do these 'asymptotic' values above and below charm threshold reproduce the theoretical predictions? All measurements are higher than the simple quark-parton prediction. However, they agree well with the expectation of four quark flavours, heavy-lepton production (subtracted in fig. 8) and gluonic corrections. Since, however, both the gluonic corrections and the systematic errors are of the same level of 10 to 15% we cannot draw any definite conclusions about QCD contributions in the total cross section.

In the resonance region near charm threshold there are considerable differences between all four experiments, in width, height and also position of the resonances. All data agree about the dip in the cross section around 4.2 GeV which shows that charm production drops down to a very low level between the resonances even above threshold.

Charm

Since the discovery of the J/ψ resonance[6] in 1974 enormous progress has been achieved in the study of charmed particles and charmonium[24]. During the past year, however, the interest at DESY has rather moved to the higher energy region. Therefore, I will only give a very short summary of the situation of charm and charmonium in this lecture.

Our experimental knowledge on charm is schematically summarized in fig. 9. (Baryons are not included. Evidence for charmed baryon production in e^+e^- annihilation was reported recently[25].) The odd C-parity ^3S state ψ', and the ^3D state $\psi''(3.77)$ show up in the total e^+e^- cross section, the latter due to its mixing with the nearby ^3S state. The existence of the $\psi'(4.16)$ is somewhat controversial[20]. Quarkonium models would like it to be

a ^{3}D state[26].

The ^{3}P states are established, although their quantum number assignment is not rigorously proven[24].

The ^{1}S states were searched for in radiative decays of J/ψ and ψ'. Evidence for an X(2820) state based on a 5 standard deviation signal in J/ψ decays was reported by the DASP group[27]. Less significant signals χ(3.45) and χ(3.59 or 3.18) were seen by different groups in the cascade decays of ψ' $\rightarrow$ $\gamma\gamma$ J/ψ [28]. None of these states was confirmed in recent results from the crystal-ball experiment[29]. In particular the X(2820) was not seen, although resolution and sensitivity were superior to the DASP experiment. Instead, a new signal U(2976) showed up with 5 standard deviations in the inclusive γ spectrum of ψ' decays. It should be mentioned that this new signal fits much better into the charmonium model than the X(2820).

The upper part of fig. 9 indicates, how the production of D, D*, F and F* mesons comes in with increasing energy: D$\bar{D}$ at the ψ"(3.77), D$^+\bar{D}$ and D*D* at ψ'(4.o3) [24,3o], FF at ψ'(4.15) and F$^*\bar{F}$ and/or F*F* at ψ'(4.42) [31]. The evidence for F$\bar{F}$ production at the ψ'(4.16) is suggestive but not compelling, since it is only based on the inclusive η signal of the DASP group. No clear distinction between F$^*\bar{F}^*$ and F$^*\bar{F}$ production at the ψ'(4.42) can be made.

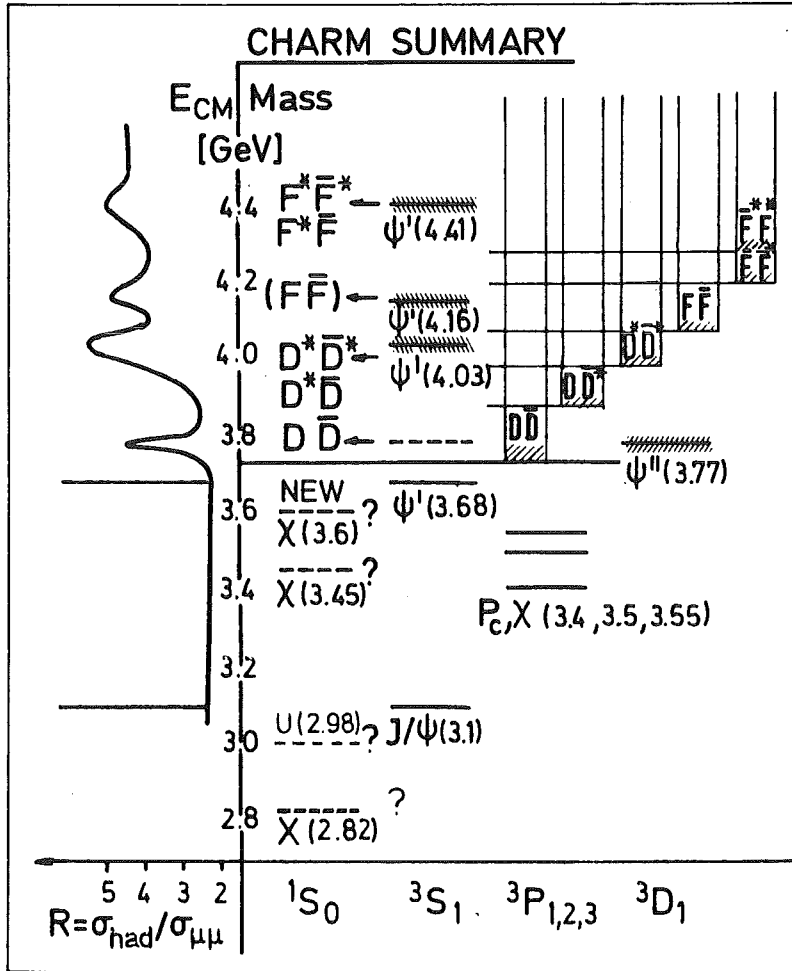Fig. 9   Schematic summary of the experimental situation of CHARM

II.   THIRD GENERATION OF QUARKS AND LEPTONS

Since the discovery of a new lepton τ in 1975 and of a new quark b in 1977 much work has been devoted to a study of the third generation of quarks and leptons:

Generation	1	2	3
Quarks	u d	c s	t b
Leptons	ν_e e^-	ν_μ μ^-	ν_τ τ^-

In this chapter I will, therefore, briefly summarize the achievements which have been obtained in the study of heavy leptons and Ypsilon particles during the last years.

1.   The Heavy Lepton τ

Table 5 gives a summary[32] of the experimental knowledge on τ [33], which is now clearly established as a new heavy lepton with the mass[34] $M_\tau = 1.782 {}^{+.003}_{-.004}$ GeV. All properties of this new particle are as expected for a sequential left-handed lepton with conventional weak coupling to its own massless neutrino. It should be noted, however, that the orthoelectron hypothesis (the neutrino being of the ν_e type) as well as pure V or pure A coupling cannot firmly be excluded. Direct evidence for the τ neutrino is still missing.

2.   The Bottom Quark b

Fig. 10 shows the status of the Υ particles at the Tokyo Conference in 1978, one year after the discovery by the Columbia-Fermilab-Stony Brook collaboration[40]. Two distinct narrow resonances (Υ and Υ') had

Table 5 Summary of τ parameters. World averages or best values are given (ref. 32 with further references)

Parameter	Units	Prediction[38]	Exp. Value	Experiments
Mass	GeV/c²	-	$1.782^{+.003}_{-.004}$	PLUTO, SLACL-LBL, DASP, DESY-Heidelberg, DELCO[34]
Neutrino mass	MeV/c²	0	<250 (95% C.L.)	SLAC-LBL, PLUTO, DELCO[35]
Spin		1/2	1/2	PLUTO, DASP, DELCO[35], DESY-Heidelberg
Lifetime	10^{-13}s	2.8	<14 (95% C.L.)⁺	PLUTO, SLAC-LBL, DELCO, TASSO[37]
Michel parameter ρ		0.75 ⁺⁺	0.72 ±.15	DELCO[35]
Leptonic branching ratios				
B_e: $\tau^- \to \nu_\tau e^- \bar{\nu}_e$)$B_e = B_\mu$ B_μ: $\tau^- \to \nu_\tau \mu^- \bar{\nu}_\mu$)	.973%	16.8	(17.1 ±1.0 (17.5 ±1.2⁺⁺⁺	SLAC-LBL, PLUTO, Lead-Glass-Wall Ironball, MPPS, DASP, DELCO
B_μ/B_e		.97	.99± .20 1.13± .16⁺⁺⁺	SLAC-LBL, PLUTO, DASP
Semihadronic BR				
$\tau^- \to \nu_\tau \pi^-$	%	9.5	9.8 ±1.4	PLUTO, SLAC-LBL, DELCO, MARKII
$\tau^- \to \nu_\tau \rho^-$	%	25.3	21.5 ±3.4	DASP, MARKII
$\tau^- \to \nu_\tau A_1^-$	%	8.1	10.8 ±3.4	PLUTO, SLAC-LBL
$\tau^- \to \nu_\tau + \geq 3$ prongs	%	~26	32 ±4 30.6 ±3.0⁺⁺⁺	PLUTO, DASP, DELCO
$\tau^- \to K^-.../\tau^- \to \pi^-...$		.05	.07± .06	DASP
$\tau^- \to \nu_\tau K^-$	%	1.0+0.2	1.26+0.5	MARK II

⁺In conjunction with upper limits on $\nu_\mu \to \tau$ production[39] this value excludes $\nu_\tau \equiv \nu_\mu$. Similar limits on $\nu_e \to \tau$ do not exists to exclude $\nu_\tau \equiv \nu_e$ (ortho electron hypothesis).

⁺⁺V-A prediction. ρ(V+A) = 0 is excluded, ρ(V or A) = 0.375 desfavoured by the data[35].

⁺⁺⁺From ref. 36.

then clearly been established at the upgraded DORIS[41-45]. Table 6 and 7 give a summary of the T and T' parameters[47].

From these data two main questions remained to be answered experimentally:

- The total width was only known to be within the limits 25 keV < Γ_{tot} < 8 MeV, where the upper limit is given by the energy spread of the colliding beams.

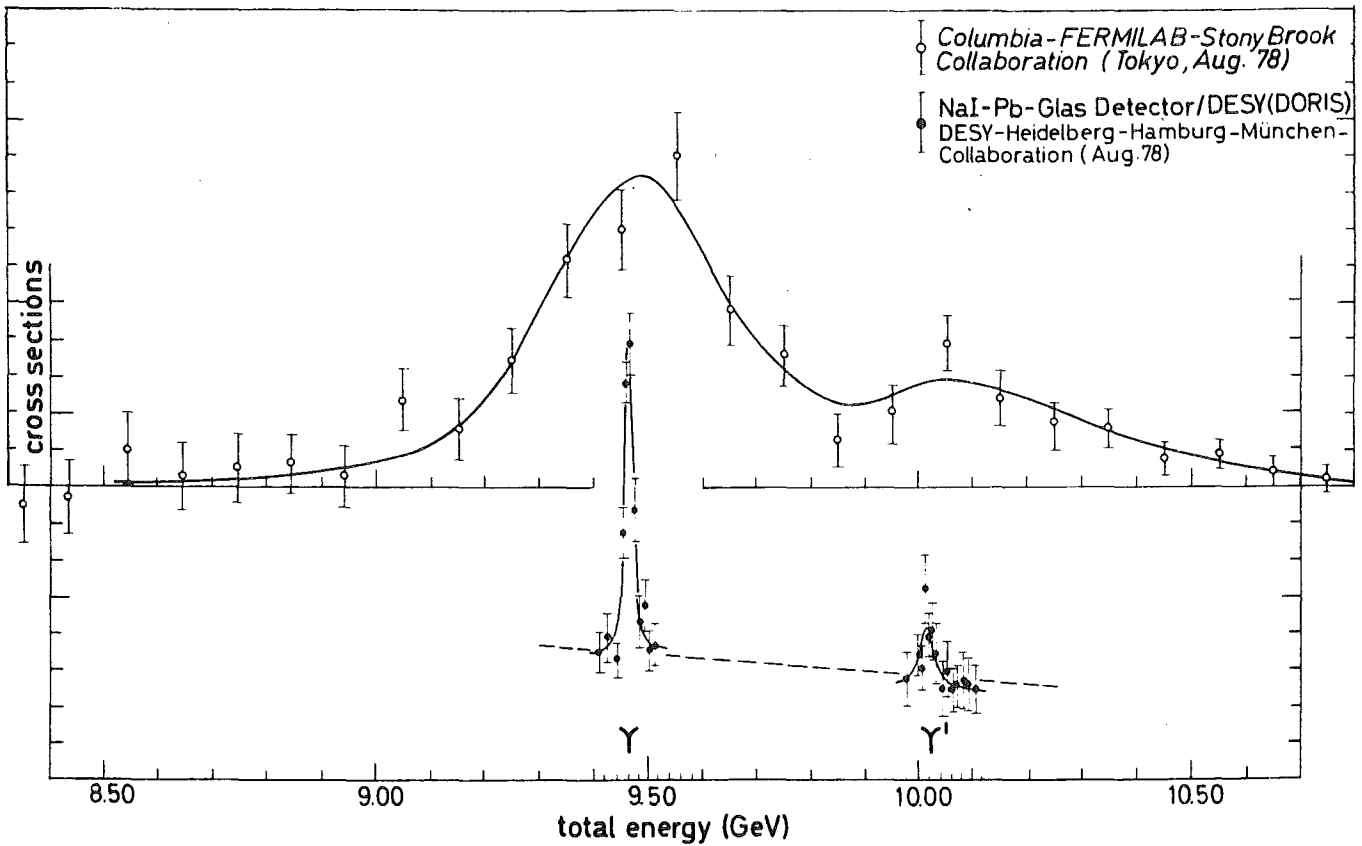- The FNAL data suggested a third resonance. In particular, taking the

Fig. 10 Columbia-Fermilab-Stony Brook and DESY-Hamburg-Heidelberg-München Collaborations: The T family in hadronic and e^+e^- reactions.

mass difference of $558\pm1o$ MeV between the T and T' they predicted a mass of $M(T") = 1o.41\pm0.o5$ GeV [48].

New data relevant to these two problems have become available in the last few months.

Table 6   Results on T(9.46)

	M(T) (GeV)	Exp. Width (MeV)	$\Gamma_{ee}(T)$ (keV)	$B_{\mu\mu}$ (%)	Γ_{tot} (keV)
PLUTO	9.46±0.o1	17.2±0.2	1.33±0.14	2.2±2.o	>23(2s.d.)
DASP2	9.46±0.o1	18 ±2	1.5 ±0.4	2.5±2.1	>2o(2s.d.)
NaJ-L.G.[46]	9.46±0.o1	17 ±2	1.o4±0.28	$1.o^{+3.4}_{-1.o}$	>15(2s.d.)

Mean Values: Γ = (1.32±0.o9) keV *

$B_{\mu\mu}$ = (2.3 ±1.4) %

Γ_{tot} > 25 keV (95% c.l.)

Table 7   Results on T'(10.o2)

	M(T') (GeV)	M(T')-M(T) (MeV)	$\Gamma_{ee}(T')$ (keV)	$\dfrac{\Gamma_{ee}(T)}{\Gamma_{ee}(T')}$
DASP2	10.o12±0.o2o	555±11	0.35±0.14	4.3±1.5
NaJ-L.G.	10.o2 ±0.o2o	56o±1o	0.32±0.13	3.3±0.9
Mean	10.o16±0.o2o	558±10	o.33±0.1o	3.6±0.6

---

* The quadratic treatment of errors applied here may be inadequate since errors are largely systematic. A linear treatment yields Γ_{ee} = (1.3±0.3) keV.

Total width

Only recently a refined analysis of the e^+e^- channel in the T region was completed by the PLUTO group[49]. The data on resonance displayed in fig. 11 show a deviation from the QED expectation at large angles, which can only be attributed to the decay $T \rightarrow e^+e^-$. The data are well described assuming a branching ratio

$$B_{ee} = (5.1 \pm 3.0) \%.$$

If one combines this with the parameters $B_{\mu\mu}$ and Γ_{ee} given in table 6 (assuming again μ-e universality) one obtains

$$\Gamma_{tot} = 45^{+38}_{-14} \text{ keV}$$

The DASP2 group[50] could increase their statistics in a recent data taking on the T resonance. Combining all their statistics available they obtain a value of

$$\Gamma_{tot} = 47^{+37}_{-15} \text{ keV}$$

in agreement with the PLUTO data.

T'' at CESR

The christmas mail last year contained the announcement of the discovery of the third resonance T'' in e^+e^- annihilations at CESR. Fig. 12 shows the measurement of the CLEO group. The results are summarized in table 8.
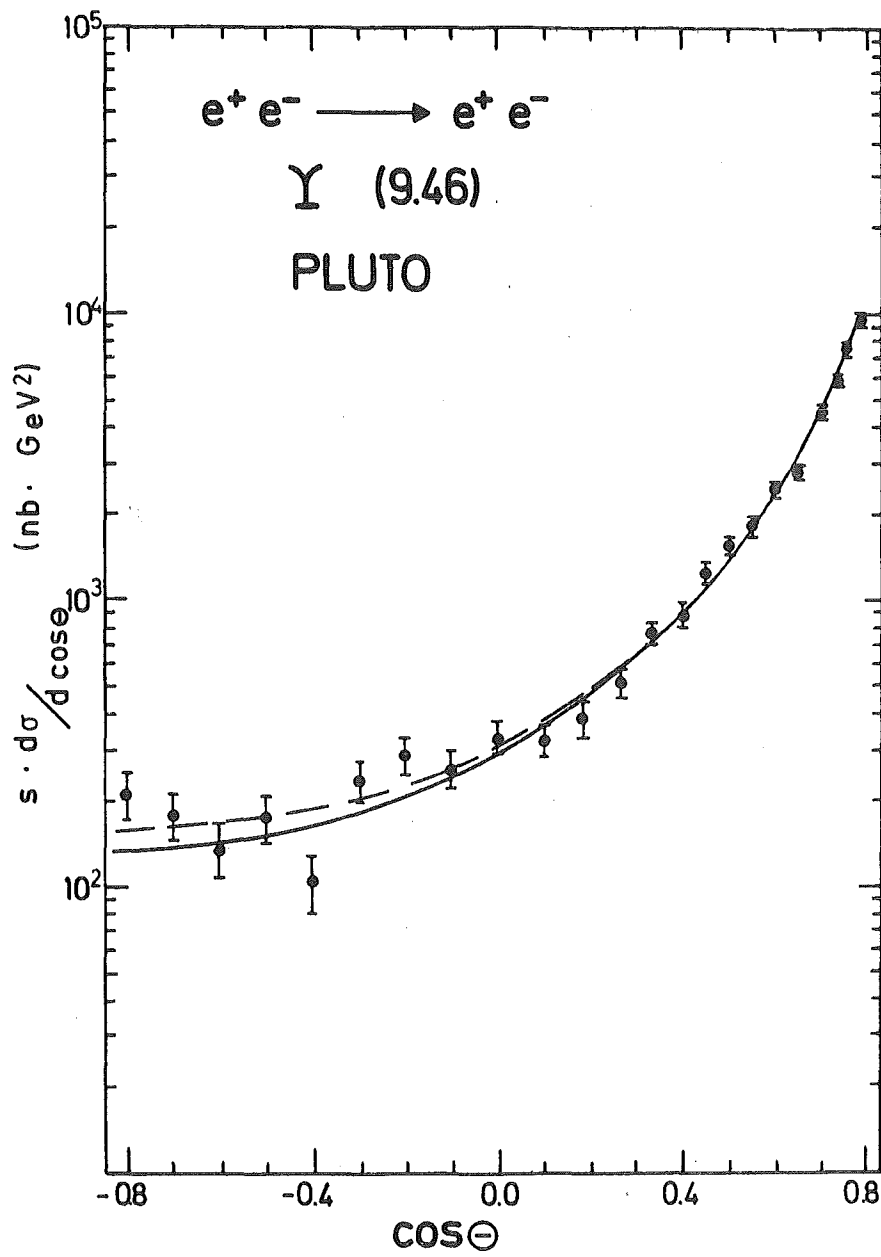
PLUTO: Differential cross section for the reaction $e^+e^- \to e^+e^-$ on the Υ resonance. The full curve shows the pure QED prediction, the dashed one includes the effect of Υ decays.
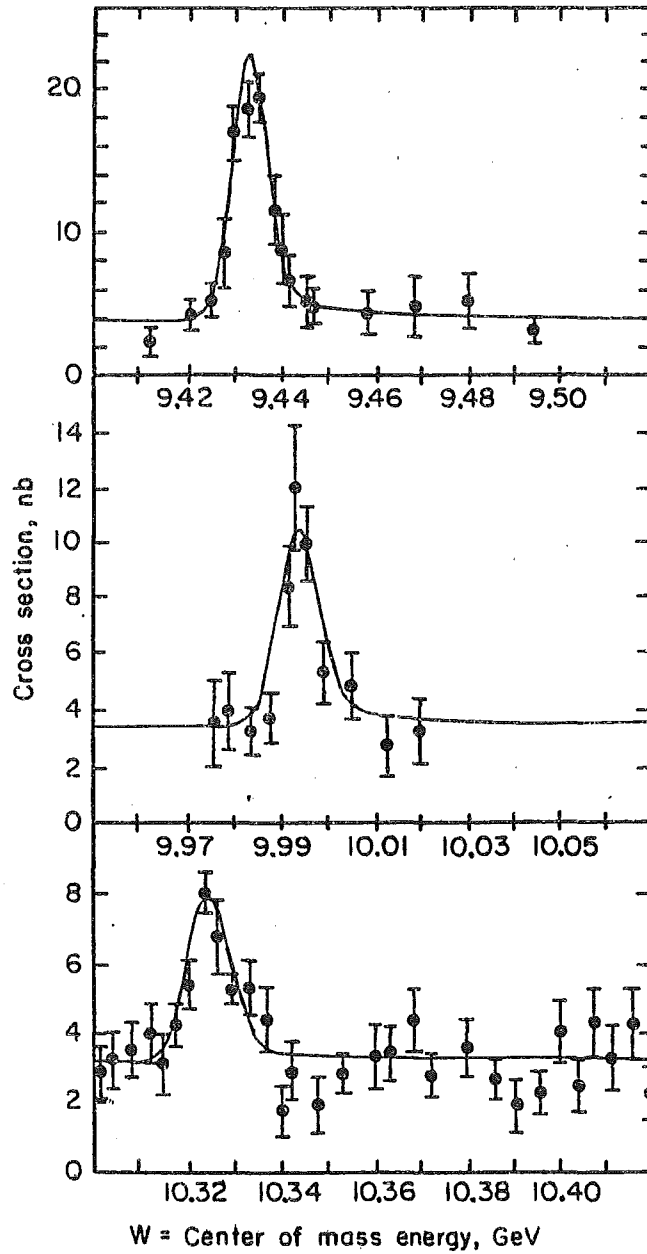
Fig. 12   CLEO: Cross section in the region of the three T resonances
(without radiative corrections). Systematic uncertainties
are ±20% on the cross section and 30 MeV on the energy cali-
bration.

Table 8   Level spacing and leptonic width of the T"

	$\dfrac{\Delta M(T-T")}{MeV}$	$\Gamma_{ee}(T")/\Gamma_{ee}(T)$
FNAL [48]	95o ±5o	
CLEO [51]	891.1±0.7±3.0	0.35±0.o4±0.o3
CUSB [52]	889 ±1.o±5.o	0.32±0.o4

The existence of three narrow resonances and their leptonic width confirm
theoretical predictions based on potential models[53,54]. Looking at fig.
13 one would expect the next resonance to be above threshold, which im-
plies a much larger width. In fact some preliminary indications of a
(probably broad) state at M ≃ 10.55 GeV were recently reported by the two
CESR groups [55].
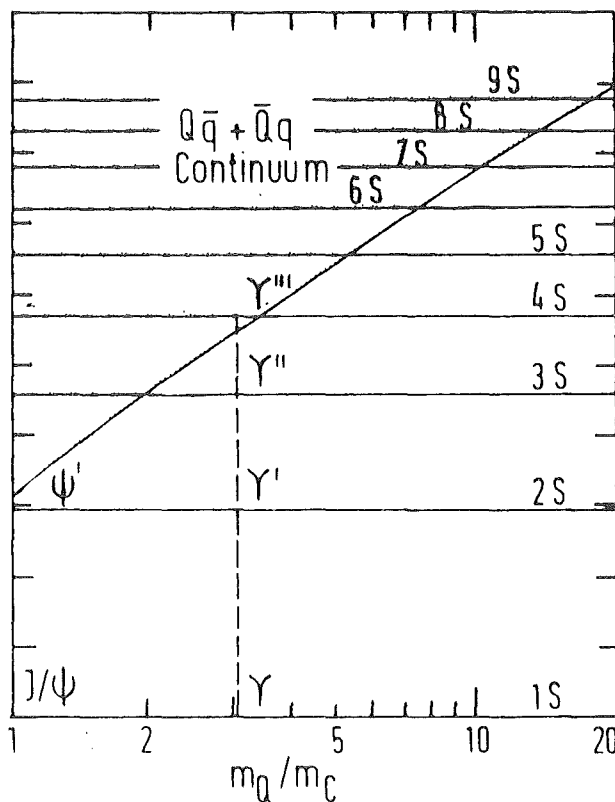
Fig. 13   Number of bound states in the bottonium system (Quigg and Rosner[53])

III.   LEPTONIC PROCESSES

1.   Test of QED

I will first concentrate on the QED process

$$e^+e^- \rightarrow e^+e^- \quad .$$

The cross section for Bhabha scattering is given by
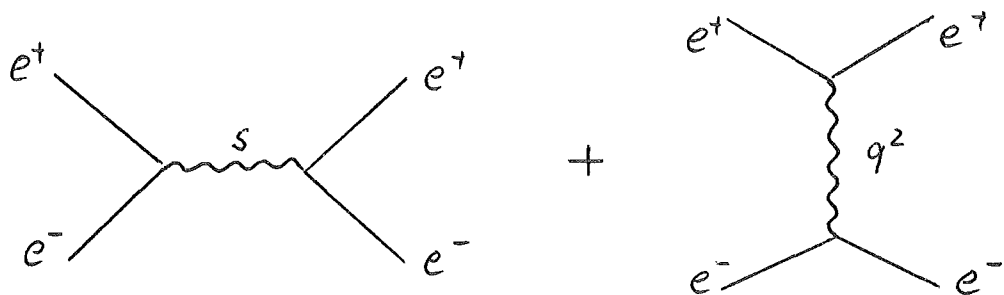
$$\frac{d\sigma}{d\Omega} = \frac{\alpha^2}{2s}\{\frac{q'^4+s^2}{q^4} + \frac{2q'^4}{q^2s} + \frac{q'^4+q^4}{s^2}\} \quad , \quad \begin{array}{l} q^2 = -s\,\sin^2\Theta/2 \\ q'^2 = -s\,\cos^2\Theta/2 \end{array}$$

QED Check

To quantify possible deviations from QED we introduce formfactors in the differential cross section for e^+e^- scattering[56].

$$\frac{d\sigma}{d\Omega} = \frac{\alpha^2}{2s}\{\frac{q'^4+s^2}{q^4}\,|F(q^2)|^2 + \frac{2q'^4}{q^2s}\,\text{Re}(F(q^2)\,F^+(q'^2)) + \frac{q^4+q'^4}{s^2}|F(q'^2)|^2\}$$

$$F(q^2) = 1 \mp q^2/(q^2-\Lambda_\pm^2)$$

(Timelike and spacelike formfactors are assumed to be equal.)

There are different ways of introducing deviations from QED. Accordingly the exact defintion and physical interpretation of Λ is model dependent.

All four experiments[57-60] at PETRA have made an attempt to determine
the cut-off parameters from their Bhabha scattering data. Table 9 summa-
rizes the results. For comparison also the best values previously known
from SLAC[61] are given. The values were obtained fitting the experimental
data with the above parametrization of the cross section and taking into
account radiative corrections[62]. The angular distribution of the JADE data
(ref. 6o) is shown in fig. 14, together with the reaction $e^+e^- \to \gamma\gamma$. All
data agree with QED predictions.

In conclusion we can say that QED holds up to the highest PETRA ener-
gies. Thus the cut-off parameter can be pushed as high as about 1oo GeV.
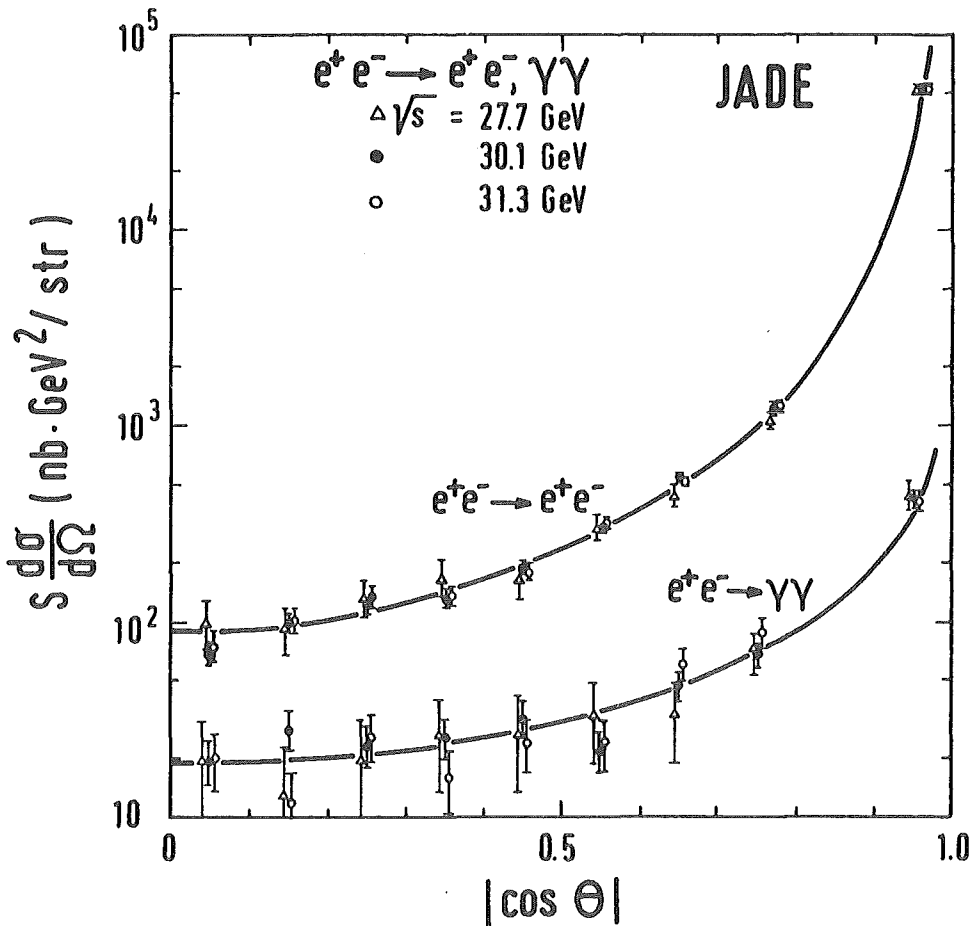
Fig. 14   JADE: angular distribution of the reactions $e^+e^- \to e^+e^-, \gamma\gamma$.
The solid curve is the QED prediction.

Table 9 QED cut-off parameters for the reaction $e^+e^- \to e^+e^-$ assuming
equal timelike and spacelike formfactors

$$F(q^2) = 1 \mp q^2/(q^2-\Lambda_\pm^2)^*$$

95% C.L. lower limits for Λ_+ and Λ_- are given.

Experiment		Λ_+ (GeV)	Λ_- (GeV)	Ref.
SLAC	1974 (rev. 1978)	22.6	16.1	61
	1975*	15	19	61
	1976	33.8	38.o	61
MARK J		74	95	57
PLUTO*		79**	23o**	58
JADE		87	1o4	6o
TASSO	(preliminary)	43	49	59

* In the limit $\Lambda^2 \gg q^2$ this parametrization equals

$$F(q^2) = 1 \pm q^2/\Lambda_\pm^2 \quad \text{(a)} \quad \text{or} \quad F(q^2) = 1/(1 \mp q^2/\Lambda_\pm^2) \quad \text{(b)} \quad .$$

These parametrizations have been applied to the data of the MARK I
(a) and PLUTO (b) detector.

** These values include $e^+e^- \to \mu^+\mu^-$ data at 9.4 GeV. Their effect on Λ
is small, however.

2. Pointlike Structure of Leptons

The above results can be interpreted as a test of the pointlike
structure of the electron. The values of table 9 set an upper limit on
its charge radius

$$r_e \lesssim \hbar c/\Lambda = 2 \cdot 10^{-16} \text{ cm} \quad .$$

Similarly, the pointlike structure of the other two leptons μ and τ can

be tested in the processes

$$e^+e^- \rightarrow \mu^+\mu^-$$

$$e^+e^- \rightarrow \tau^+\tau^-$$

by introducing formfactors F_{μ}, in the total cross section.
τ

$$\sigma_{\mu\mu} = \sigma_{\mu\mu} (QED) \cdot |F_{\mu}(s)|^2 \quad .$$
$\tau\tau \quad\quad \tau\tau \quad\quad\quad\quad \tau$

Figs. 15 and 16 show the energy dependence of these cross sections measured at PETRA. The data agree perfectly well with the QED prediction indicated in the figure. To quantify this statement, a formfactor

$$F_{\mu}(s) = 1 \pm \frac{s}{s - \Lambda_{\pm}^2}$$
τ

was defined. The upper limits on $\Lambda_{\pm}$ are shown in tables 1o and 11. They correspond to:

$$r_{\mu} \lesssim 3 \cdot 10^{-16} \text{ cm} \quad\quad\quad\quad r_{\tau} \lesssim 3 \cdot 10^{-16} \text{ cm} \quad .$$

Table 10   QED cut-off parameters for the reaction $e^+e^- \rightarrow \mu^+\mu^-$ for the formfactor $F(s) = 1 \pm s/(s - \Lambda_{\pm}^2)$.95 % C.L. lower limits for Λ_+ and Λ_- are given.

Experiment	Λ_+ (GeV)	Λ_- (GeV)	Ref.
MARK J	71	97	57

Table 11   QED cut-off parameters for the reaction $e^+e^- \to \tau^+\tau^-$
Λ is defined as in table 1o.

Experiment	Λ_+ (GeV)	Λ_- (GeV)	Ref.
MARK J	47	53	57
TASSO	65	74	37
PLUTO (preliminary)	67	74	63
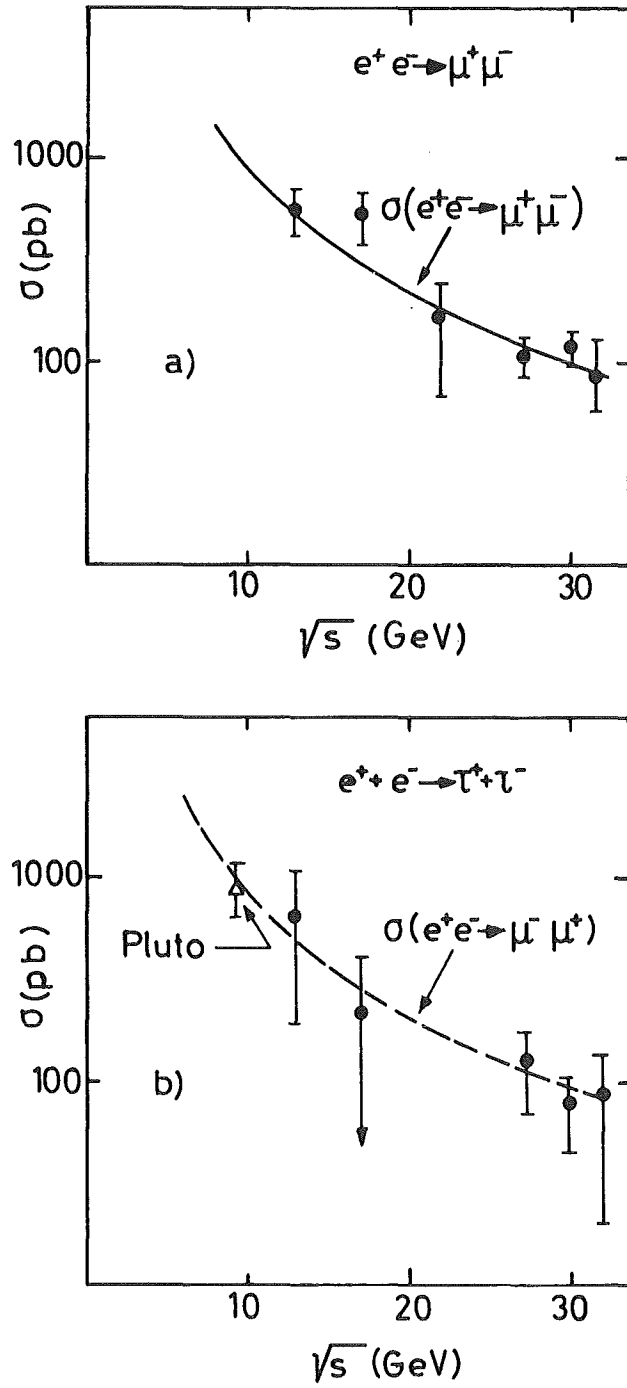
Fig. 15 MARK J: Test of e μ τ universality.
a) the reaction $e^+e^- \to \mu^+\mu^-$ compared to the QED expectation.
b) the reaction $e^+e^- \to \tau^+\tau^-$ compared to QED.

$$\sigma_{QED} = \frac{4\pi\alpha^2}{3s}$$

$e^+e^- \longrightarrow \tau^+\tau^-$
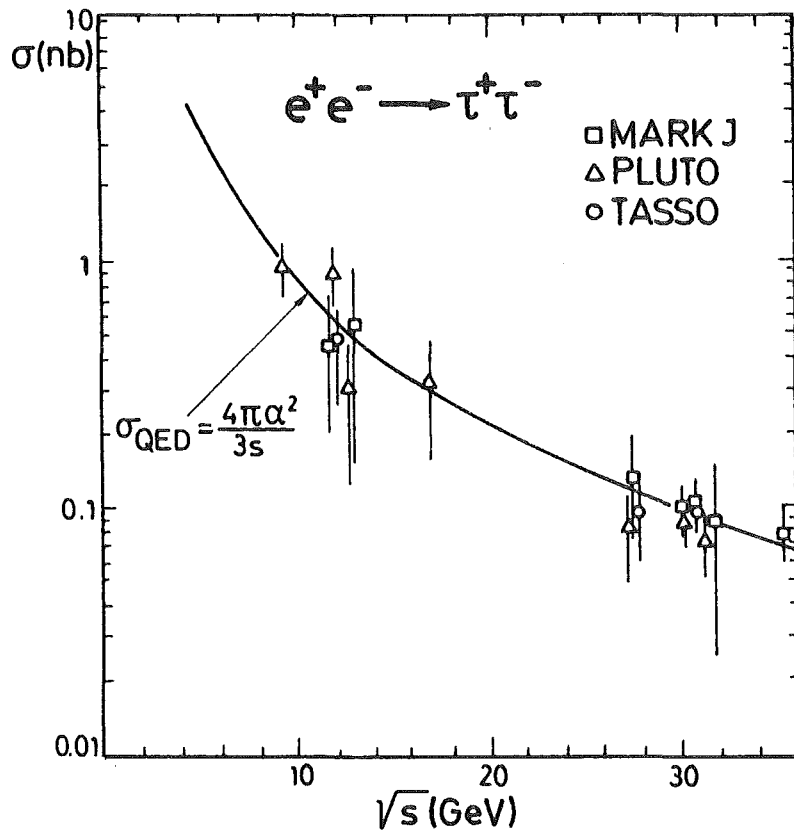
□ MARK J
△ PLUTO
○ TASSO

Fig. 16   PLUTO, MARK J, TASSO: Energy dependence of the cross section
für τ pair production. The curve shows the QED prediction.

IV. HIGH ENERGY HADRON PRODUCTION

1. Total Cross Section

Entering a new region of energy the PLUTO, MARK J, TASSO and JADE groups made an attempt to measure the total cross section[64-67]. It has been emphazised already in the first chapter why this quantity is of particular interest in e^+e^- reactions. Any increase in $R = \sigma_{had}/\sigma_{\mu\mu}$ would indicate new flavours. To determine R the theoretical value of $\sigma_{\mu\mu}$ is taken while σ_{had} is measured experimentally:

$$\sigma_{had} = \frac{N}{\varepsilon \cdot \int L \, dt} \quad .$$

The total number of observed hadronic events N has been normalized to the integrated luminosity derived from small angle Bhabha scattering.

The event acceptance ε is obtained by Monte Carlo studies. Events are generated according to the Feynman-Field parametrization and passed through a realistic model of the detector. Of course, the larger the acceptance the less does ε depend on details of the model. The typical acceptance of the three detectors is of the order of 80%. The systematic erros of the total cross section measurements are mainly due to acceptance and luminosity uncertainties.

The number of hadronic events N has to be separated from a background of cosmic rays, QED events of the e and μ type, beam gas, beam losses, synchrotron radiation and so on. This background is about 6 to 7 orders of magnitude higher than the event rate of a few events per hour under the typical PETRA running conditions. The event selection criteria are based on a combination of energy and track requirements. In the PLUTO detector[64] for example at least 2 charged particles and a total energy deposition of more than $0.4 \times E_{CM}$ was required. Fig. 17 demonstrates the quality of this event selection. It shows that after the energy cut only very little background remains in the sample. - Fig. 18 shows a hadronic event from the PLUTO detector.
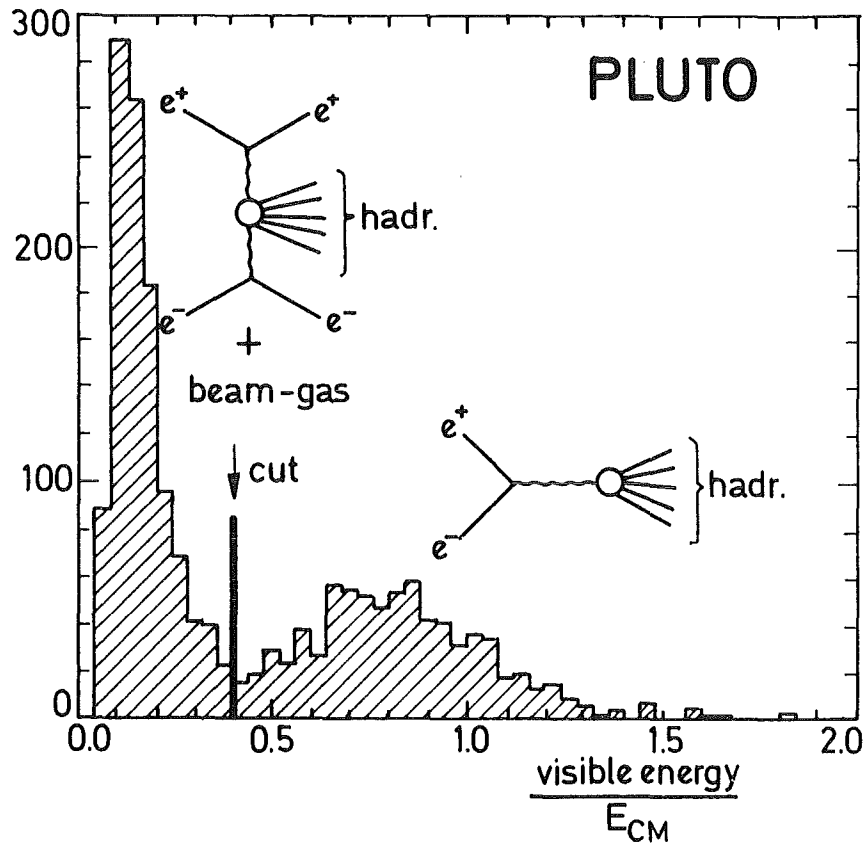
Fig. 17 PLUTO: Distribution of the visible energy after all except
the energy cut. The different sources of background are indi-
cated in the figure.

Measurements

The energy range up to 31.6 GeV was scanned in large steps: 13,
17, 22, 27.4, 27.7, 30 and 31.6 GeV. The values of R are plotted in
fig. 19 together with low energy data. Only statistical errors are
shown. The systematic error is of the order of 10-15%.

The experiments agree on the measurement of R within their stati-
stical errors. Since there are no obvious correlations between the four
experiments, the systematic errors are probably smaller than assumed.

We can draw the following conclusions:

- Since the relative systematic error between different energies are
  small compared to the statistical error we can exclude an increase as

20453
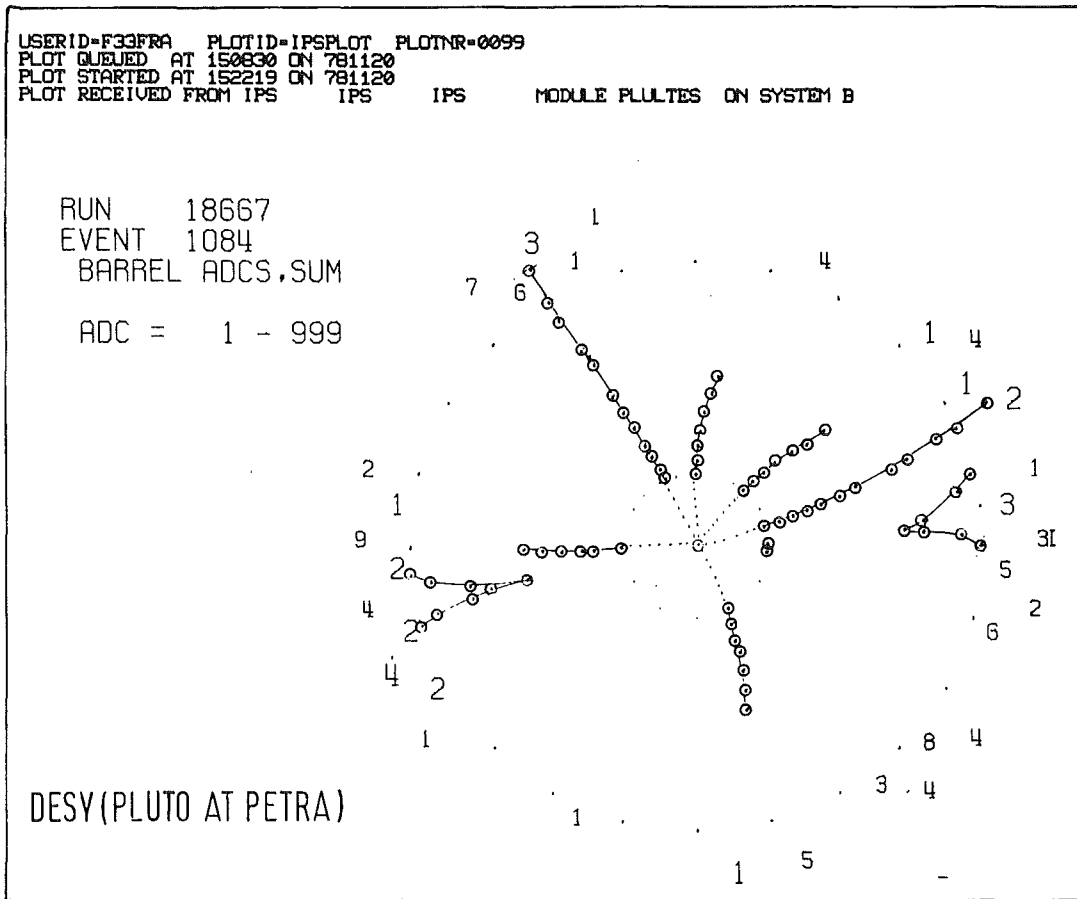
Fig. 18   PLUTO: first hadronic event seen at PETRA

expected from a new t quark.

- The absolute value of R is well compatible with the expectation of the
quark model for 5 flavours (u,d,s,c,b):

$$R = 3 \Sigma Q_q^2 = 3.7 \quad .$$

The agreement is even better, if QCD corrections are included:

$$R(udscb + QCD) \simeq 4.o \quad .$$
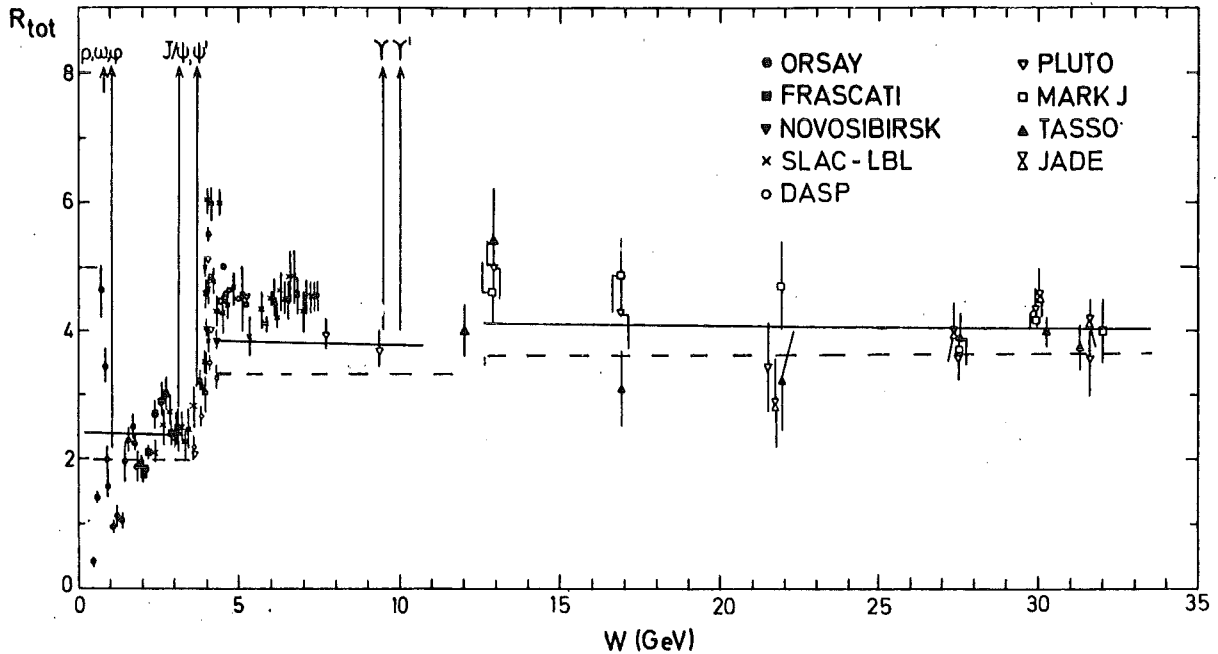
<u>Fig. 19</u> PETRA: The relative total hadronic cross section $R = \sigma_{had}/\sigma_{\mu\mu}$ as a function of energy. The expected values for udscb without (--) and with QCD (-) are indicated.

2. Jets in $e^+e^- \to$ hadrons

We have seen that the asymptotic behaviour of R is in good agreement with the simple description of the quark-parton model. Let us, therefore, assume that quark-pair production really governs the process

$$e^+e^- \to \text{hadrons}.$$

In this picture the two quarks should fragment to form two back-to-back jets of particles (fig. 2o).

What are these jets like? In the quark-parton model jets are described in a phenomenological way by a fragmentation of quarks with limited transverse momentum with respect to the original quark axis. On the other hand QCD tells us that jets are broadened by gluon bremsstrah-
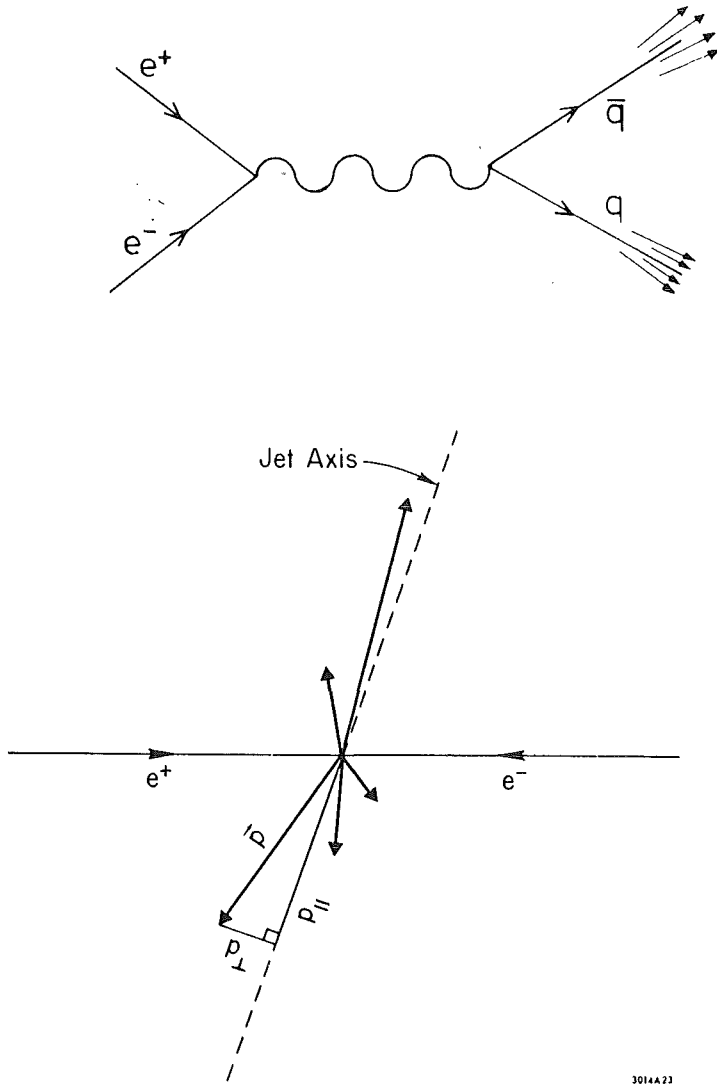
Definition of quantities used in the jet analysis.

lung in the framework of perturbative QCD[68]. Since in this process the transverse momentum increases with energy it will eventually win over the quark-parton process once the energy is high enough[69]. (These effects will be discussed quantitatively in chapter VI).)

In 1975 first evidence for a two jet structure was reported at SLAC[70]. At the upgraded DORIS the phenomenon was confirmed by the PLUTO group[71].

Fig. 21 shows a very clean jetlike event from the PLUTO detector. Two
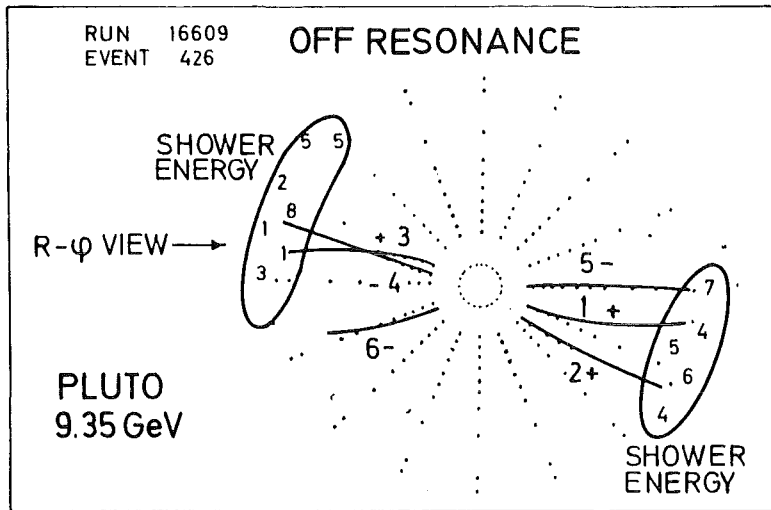
<u>Fig. 21</u>   PLUTO: a non-typical nice jetlike event of E_{CM} = 9.35 GeV.

distinct back-to-back bunches of particles are clearly visible. Also
the neutral energy of the two jets is clustered and follows the charged
energy. At these energies of about 9.4 GeV only few events show a jet
structure in such a nice way. At high PETRA energies however the two
jet structure gets a prominent feature of the data. Fig. 22 shows an
example from the JADE detector.

<u>Jet Measures</u>

Several quantities have been proposed to measure jets. I will only
use two of them here, namely spericity[72]

$$S = \frac{3}{2} \min \frac{\sum p_{Ti}^2}{\sum_i p_i^2}$$

and thrust[73]

$$T = \max \frac{\sum_i |p_{Li}|}{\sum |p_i|} \quad .$$
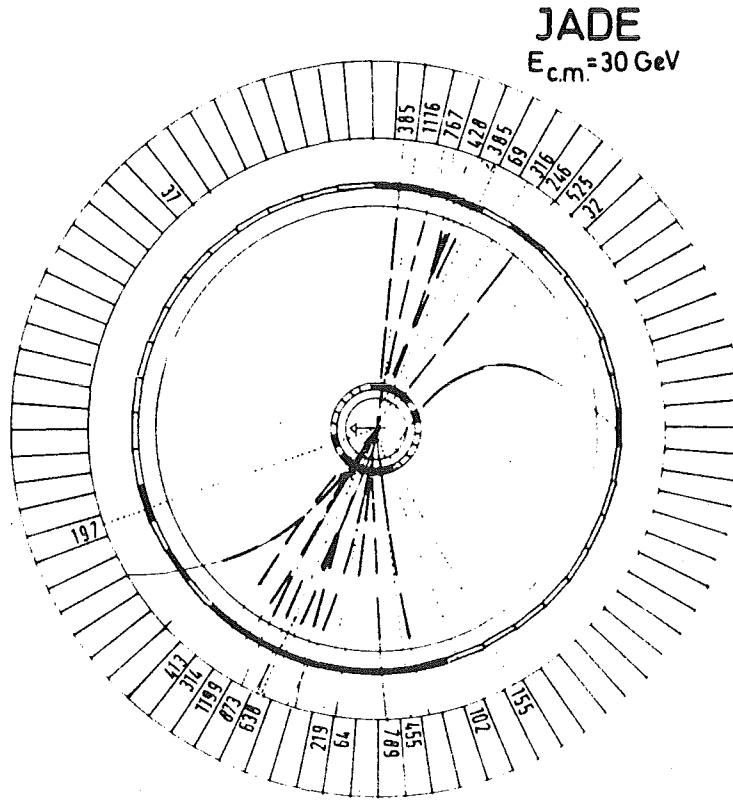
Fig. 22   JADE: A typical multihadron event detected in the central part of the JADE detector. Trajectories of charged and neutral particles are represented by full and dotted lines, respectively. The energy deposited in the shower counters is shown in MeV.

(This definition is slightly different from the original one, were the sum for p_L runs over one hemisphere only.)

Both quantities simultaneously define the jet axis and give a measure for the topological structure of the event. The axis is found in a variational method by either minimizing the sum of the transverse momentum squared (p_T^2) or maximizing the sum of the absolute longitudinal momentum component ($|p_L|$) with respect to a given axis (fig. 2o). Extreme values of the two quantities for isotropic or ideally jetlike events are summarized in table 12.

Table 12   Values for S and T in extreme topologies

Events		S	T
isotropic		$\to 1$	$\to 1/2$
ideally jetlike		$\to 0$	$\to 1$
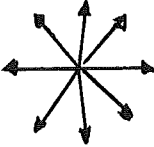
If we assume that p_T is about constant the quantities $<S>$ or $<1-T>$ will both fall with increasing energy (assuming that the multiplicity is only slowly varying).

Measurements

Fig. 23 shows the mean longitudinal and transverse momentum of charged particles with respect to the thrust axis as measured in the PLUTO and TASSO group[64,66]. The tendency at lower energies prevails. p_L increases whereas p_T stays small, i.e. the jet structure is getting more and more pronounced.

The energy dependence of (1 - mean thrust) (fig. 24) quantifies this observation. The figure includes data from PLUTO, TASSO and MARK J (ref. 64-66). Whereas the TASSO group uses charged particles only, neutrals are included in the PLUTO measurement at PETRA.

The angular dependence of the thrust axis[74] is shown in fig. 25 (PLUTO data). It exhibits a $1+\alpha \cos^2\theta$ behaviour, with $\alpha = 1.2\pm0.3$. This is exactly as expected for a pair production of spin 1/2 objects.

Thus all measurements are in quantitative agreement with the expectations of the quark-parton model, where $e^+e^- \to$ hadrons proceeds though the production of a spin 1/2 quark pair.
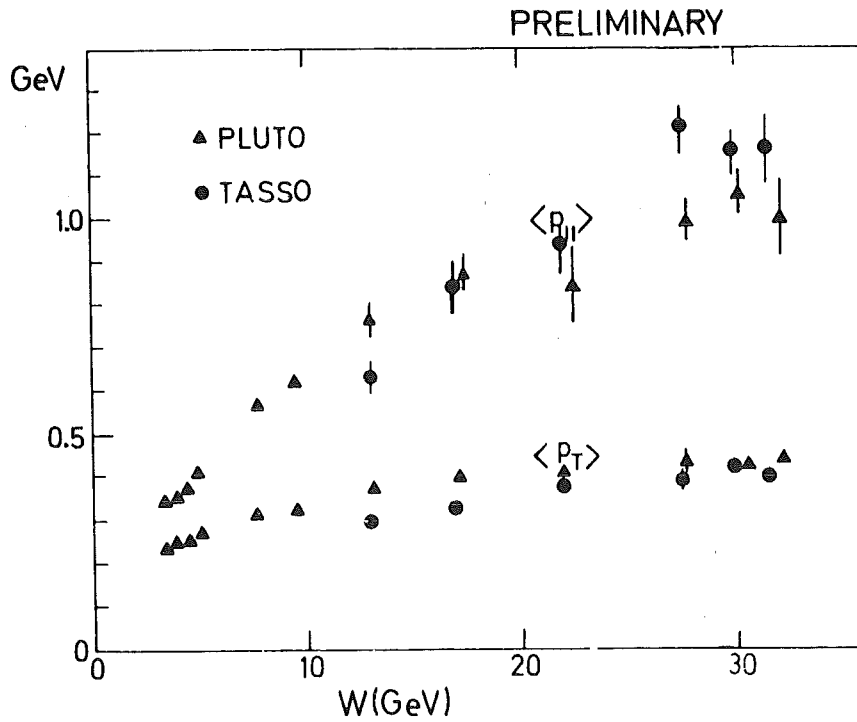
PRELIMINARY

Fig. 23 PLUTO and TASSO: mean transverse $<p_T>$ and mean longitudinal $<p_L>$ momentum as a function of energy. $<p_T>$ and $<p_L>$ are calculated for charged particles with respect to the event thrust axis.
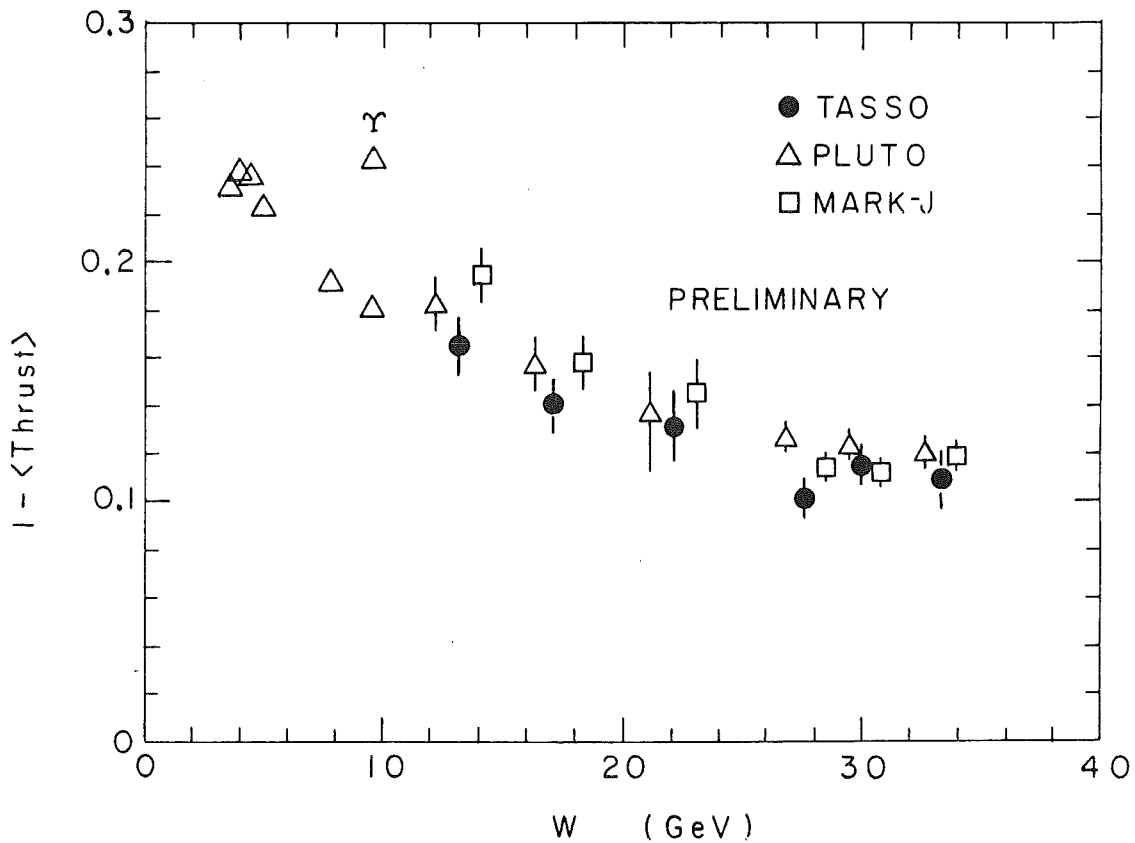

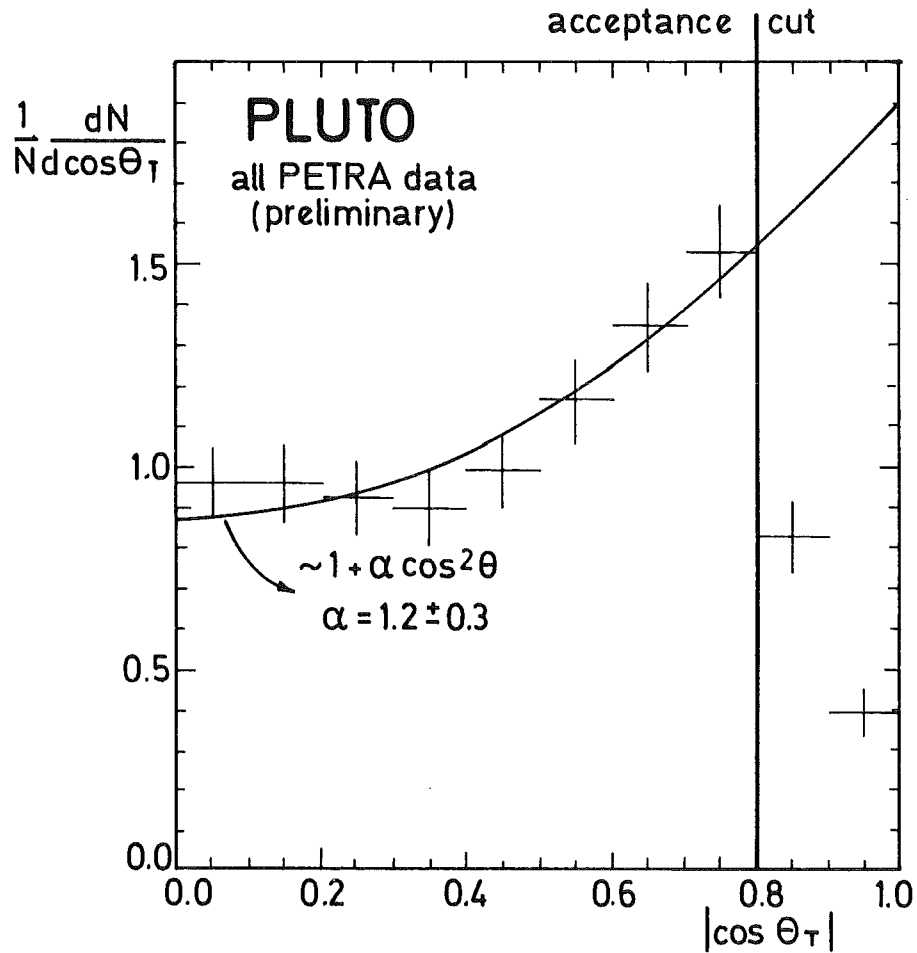Fig. 24 TASSO, PLUTO and MARK J (preliminary): 1-$<T>$ as a function of energy

Fig. 25 PLUTO (preliminary): angular distribution of the thrust axis

3. Topology of Heavy Quark Decays

We have seen in section 1 that the measurement of the total anni-
hilation cross section is not very sensitive to new quark flavours,
since statistical and systematic erros are relatively large. Even for
Q_Q = 2/3 the increase in R is expected to be of the order of 25% only,
thus large statistics is required for clear effects.

There is, however, a topological effect, which may help to detect
new heavy quarks. The basic idea is very simple[69,75]. Near threshold,
a pair of heavy slow quarks will tend to decay nearly isotropically.
Thus, the events will reveal themselves by large values of sphericity

(or small thrust). Since the mean sphericity of the "background" jets decreases, this method will be exceedingly sensitive at higher energies. The mean sphericity will change to

$$\langle S \rangle = \frac{\langle S_Q \rangle R_Q + \langle S_q \rangle R_q}{R_Q + R_q}$$

where $S_{q,Q}$ and $R_{q,Q}$ are the contributions from the light quarks q and the new heavy quark Q. In contrast to R, not only the mean value but also the distribution of S may be used. This will increase the sentitivity of the analysis.

Model of weak heavy quark decays

The applicability of this method has been studied by Ali, Körner, Kramer and Willrodt[75] at DESY. They based their model on the Kobayashi-Maskawa scheme (KM)[76]. KM assumes three quark doublets with a weak current of the form

$$J^{weak}_{hadron} = (\bar{u} \ \bar{c} \ \bar{t}) \gamma_\mu (1 - \gamma_5) \upsilon \begin{pmatrix} d \\ s \\ b \end{pmatrix}$$

where υ is a unitary matrix that describes the mixing within d, s and b.

$$\upsilon = \begin{pmatrix} C_1 & -S_1 C_3 & -S_1 S_3 \\ S_1 C_2 & C_1 C_2 C_3 - S_2 S_3 e^{i\delta} & C_1 C_2 S_3 + S_2 C_3 e^{i\delta} \\ S_1 S_2 & C_1 S_2 C_3 + C_2 S_3 e^{i\delta} & C_1 S_2 S_3 - C_2 C_3 e^{i\delta} \end{pmatrix} ,$$

where $C_i = \cos \theta_i$, $S_i = \sin \theta_i$.

υ is an extension of the Cabibbo mixing matrix in the GIM scheme. θ_i are the Euler angles of a 3 dimensional rotation, δ is a free phase. Phenomenological limits on their values are[77]:

$$\theta_1 \quad \simeq \quad 13^0 \quad \text{Cabibbo angle}$$

$$\theta_2, \theta_3 \quad \leq \quad 30^0$$

$$\theta_2 \cdot \theta_3 \quad \neq \quad 0$$

$$\delta \quad > \quad 0.3^0 \quad \text{CP violation phase} \qquad .$$

If we assume now that θ_i are small but non zero, all decays involving $\sin \theta_i$ will be suppressed. The situation can be visualized in the following scheme[78]:
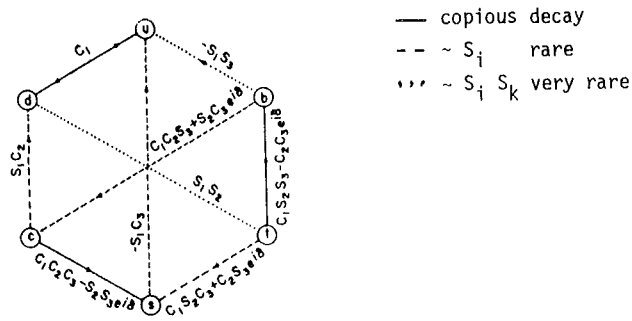

Fig. 26 illustrates the application of KM to the production of a pair of heavy b quarks. The b quarks fragment down to form a B meson. b in B decays weakly into c which again fragments to form a D meson.
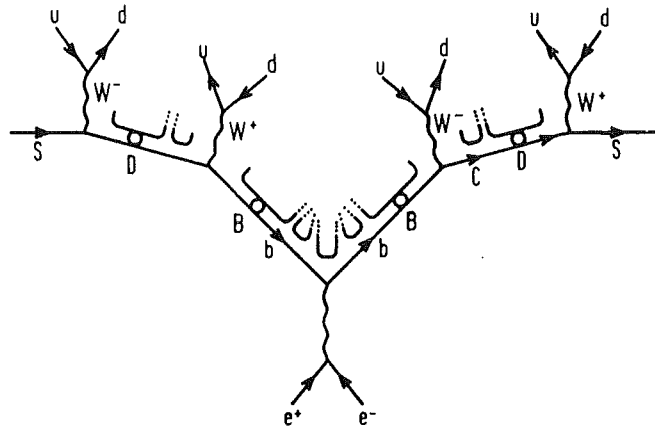
Fig. 26   A model for the production of heavy quark pairs in e^+e^- annihilation.

The assumptions of the model are

- t, b, c follow the dominant weak decay chain of the KM scheme with 30% leptonic branching ratio.

- The fragmentation of the heavy quark b is given by $D_b{}^B(z) \sim z$, the same for t.

- The charm quark fragments like $D_c{}^D(z) \sim (1-z)$.

- Light quarks are treated à la Feynman-Field[79].

In some of the model calculations used later a constant fragmentation function is used for c, b and t. The results depend very little on this choice[75].

The reason for this weak dependence on the model can be easily understood e.g. for thrust: Since momenta enter linearly, T depends only on the jet mass (at fixed energy and if all secondaries are measured).

Fig. 27 shows the result of the model calculations for the c, b and t threshold, assuming $M_{t\bar{t}}$ = 30 GeV. The effect is as large as naively expected. It is particularly impressive for the top quark.

Measurements

Let us return to fig. 22. It shows a smooth variation of thrust up to highest PETRA energies, without any prominent structure. Comparing with the theoretical expectation (fig. 27), a b threshold is not suggested but compatible with the data. There is no sign of a top quark contribution.

The effect due to a top quark should be even clearer in the differential distributions. They are shown in fig. 28 and 29 for the PLUTO and MARK J detector. The PLUTO data are well accounted for by udscb quark calculations (full curves), whereas additional top quark contributions (dashed curves) are excluded. The evidence against top quark production is not very strong at 31.6 GeV. 8 events are seen with T < 0.8 whereas 18.9 are expected from the (udscbt) model at this energy.
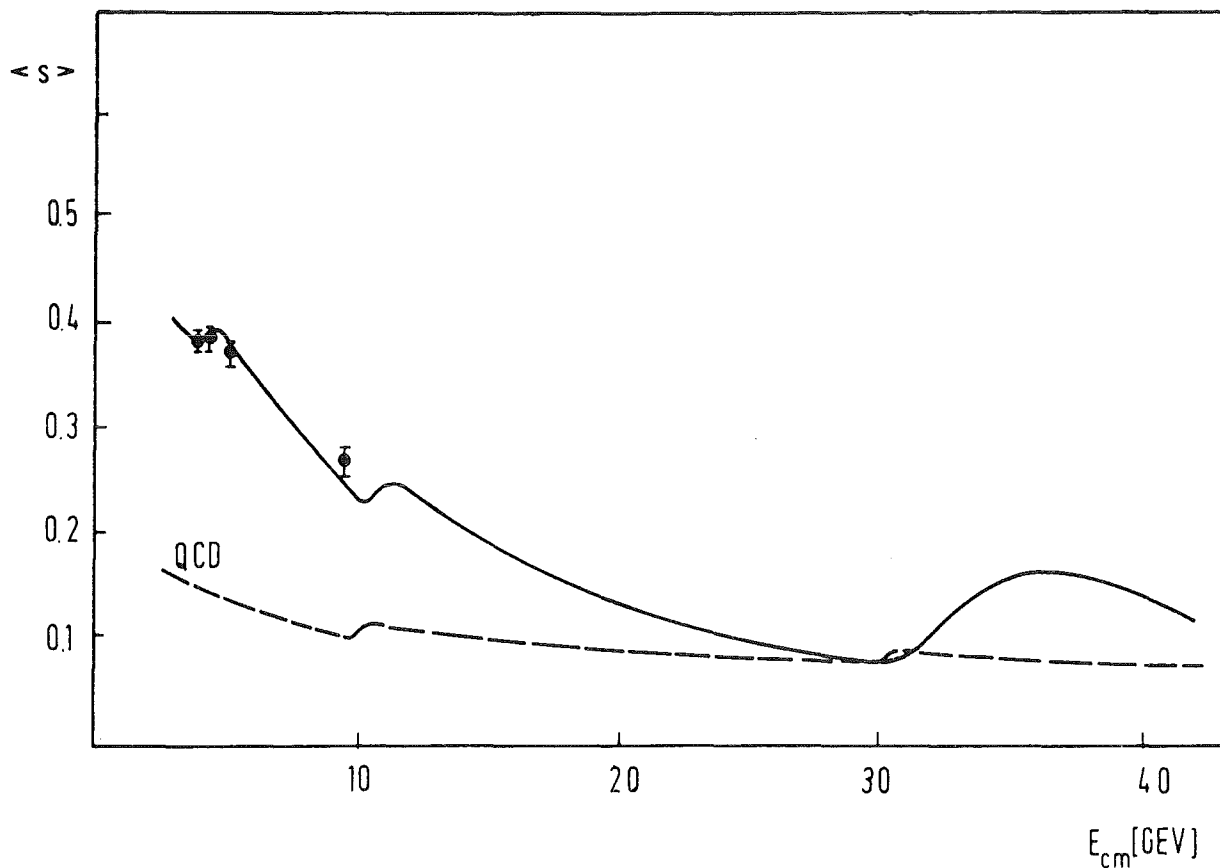
Predicted change of sphericity above t threshold: Mean spheri-
city as a function of energy.

The MARK J data up to 30 GeV [65] are well accounted for by the
(udscb) model (full line). At 31.6 GeV neither the udscb nor the udscbt
model fits the data. I will come back to this point in the next chapter.
As far as the top quark is concerned, the data do not show any evidence
for it.

Whereas thrust is the appropriate variable to describe PLUTO (in-
cluding neutrals) and MARK J data, the TASSO experiment was mainly ana-
lyzed in terms of sphericity. Fig. 30 shows the mean sphericity as mea-
sured by the PLUTO and TASSO group[64,66]. Differential distributions (TASSO)
are given in fig. 31. Again a top quark contribution (dash-dotted line)
is clearly ruled out.
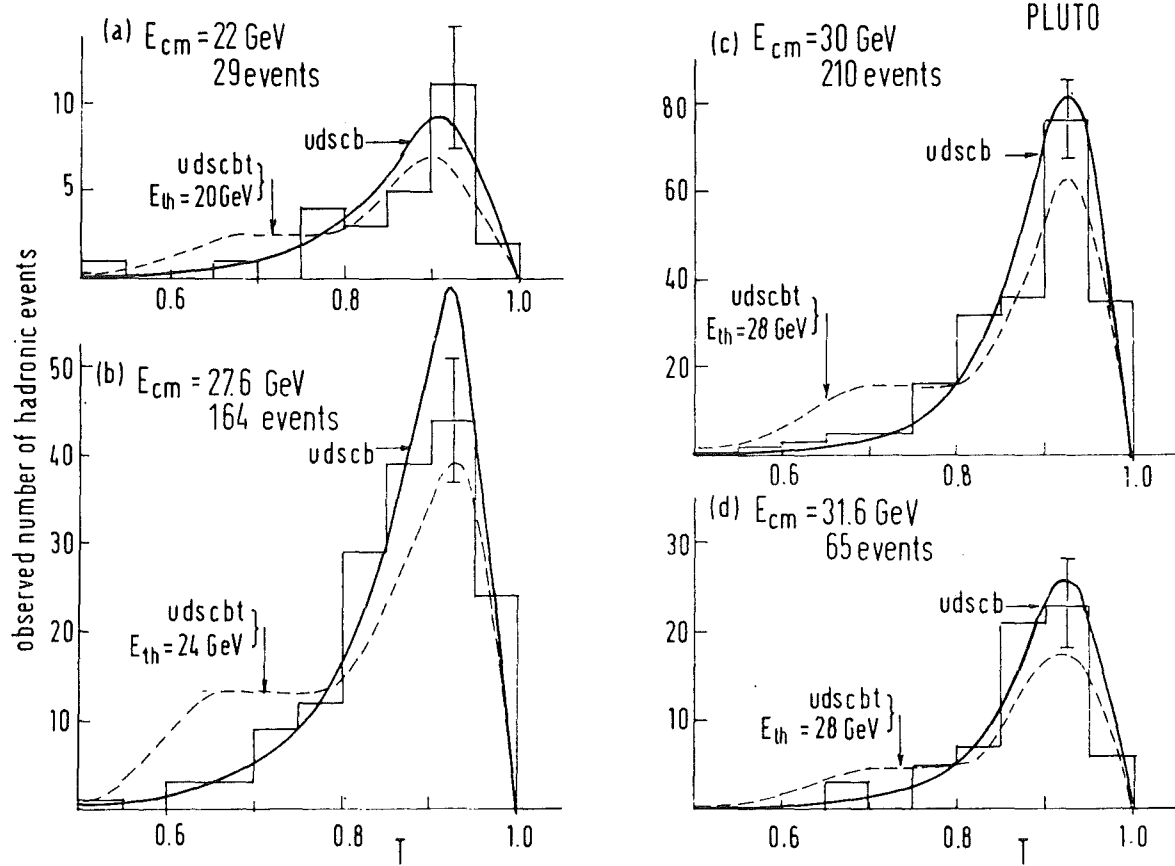
Fig. 28   PLUTO: thrust distribution at different energies. Thrust is cal-
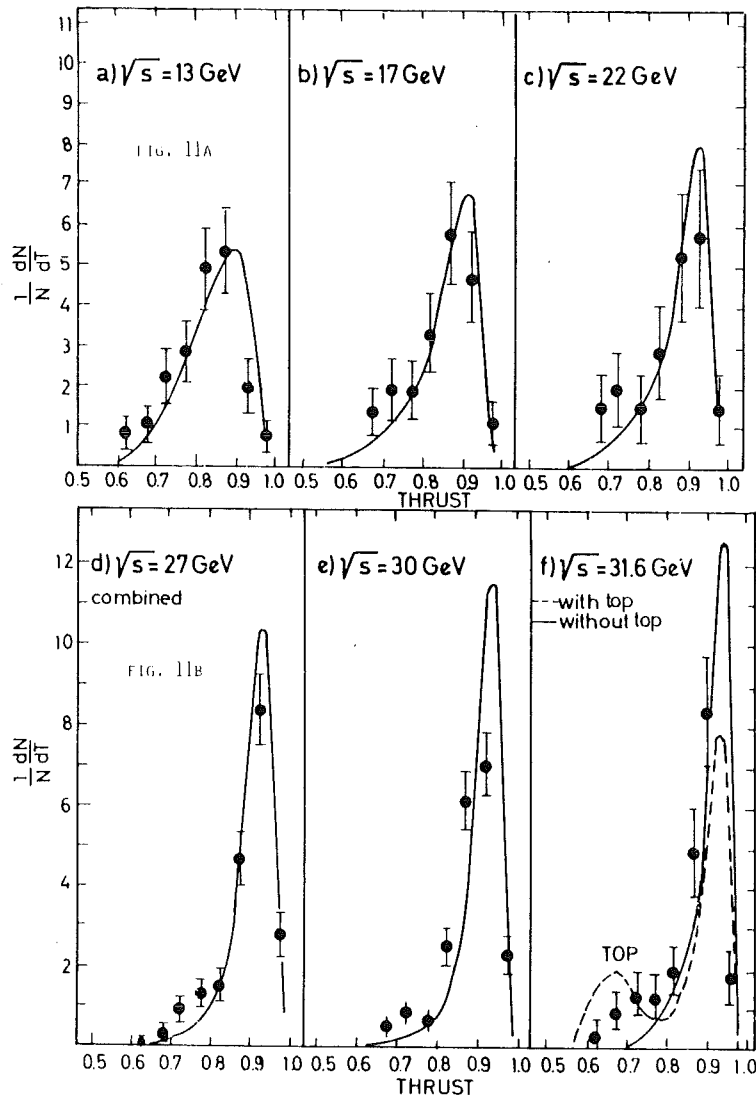culated from charged and neutral particles..

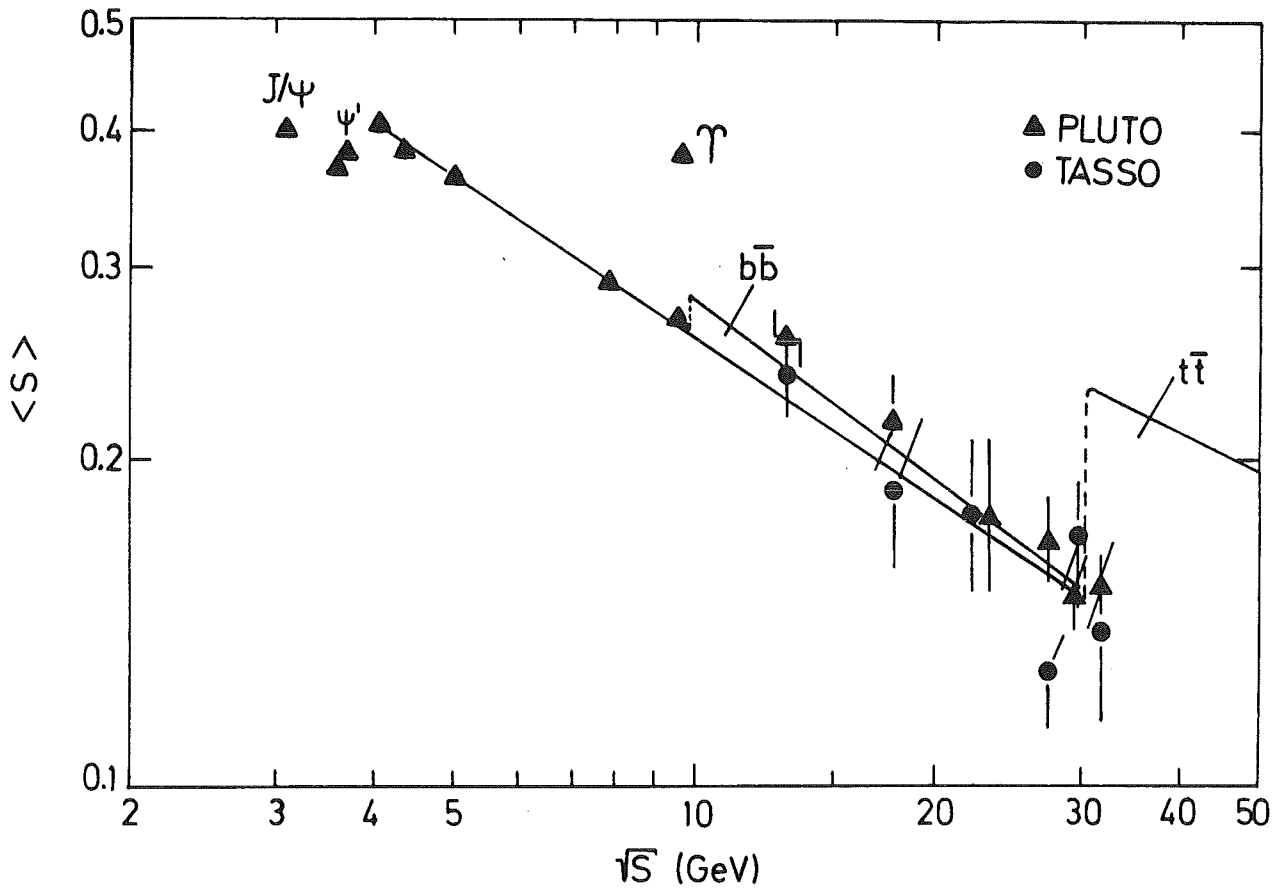Fig. 29   MARK J: Thrust distribution at different energies

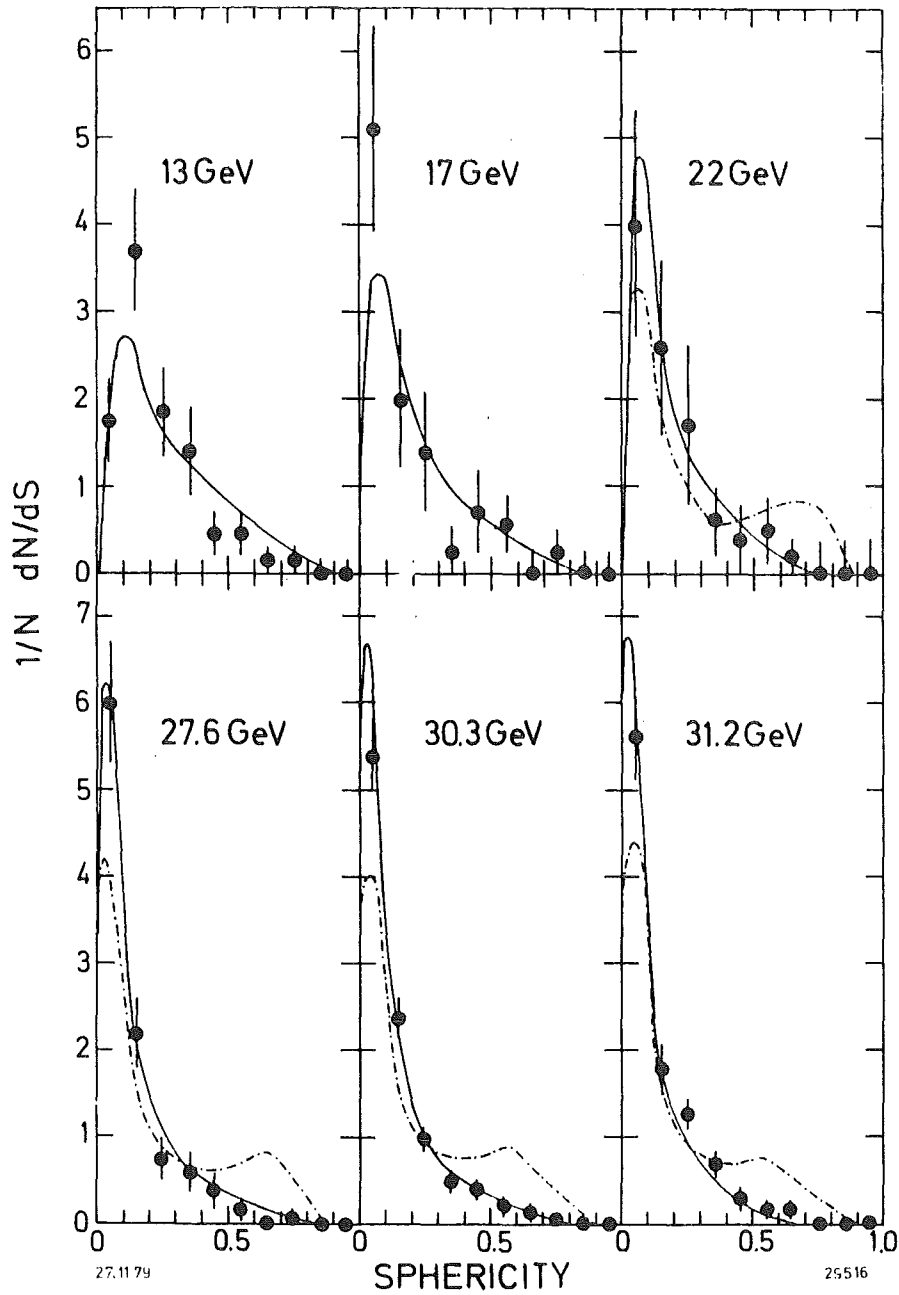Fig. 30   PLUTO and TASSO: mean sphericity as a function of energy

Fig. 31 TASSO: sphericity distributions for different
energies. The curves show predictions of the quark model udscb
plus gluon corrections (—) and with top quark (-.-).

Note that contrary to the measurements of R, these results are in-
dependent of normalization erros. In this respect the results are safer
than the ones reported in the previous section.

4. Search for Toponium

Although the data described in the previous section did not reveal any sign of top quark production, the experimenters did not give in. The reason can best be explained looking at fig. 32. Remember, that only a course scan was made up to 31.6 GeV. What if the last data point or points were to lie in between two resonances or in a "valley" above threshold?
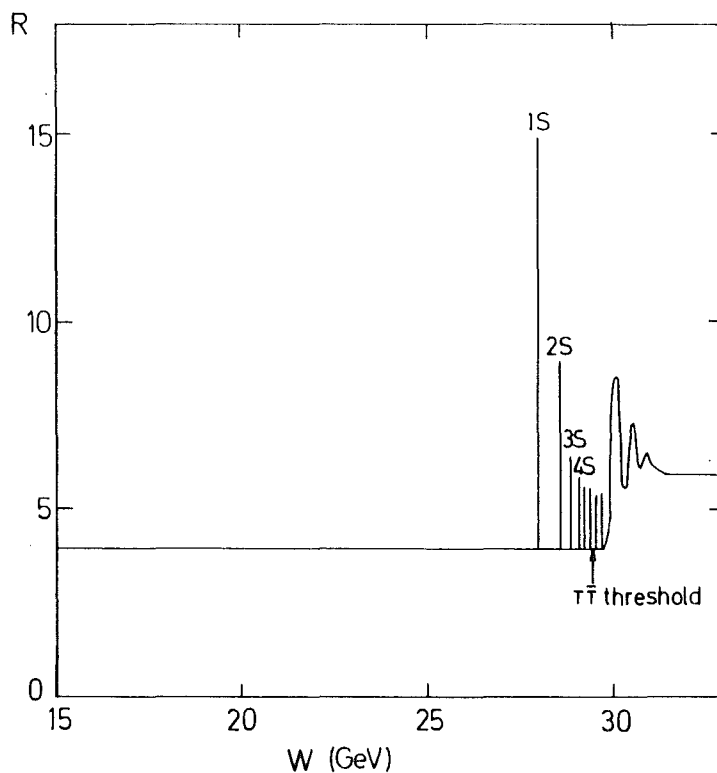
Fig. 32 Predicted variation of the cross section $e^+e^- \to$ hadrons near to a hypothetical $t\bar{t}$ threshold.

To answer this question a fine scan in steps of the machine resolution ($\sim$ 20 MeV) was applied to look for resonance structure within the last 1 1/2 GeV of CM energy.

To get an estimate of the relative height of the resonance (σ_p) compared to the continuum (σ_c) we can scale the relative cross sections from the T region to the toponium region (assuming $M_{t\bar{t}}$ = 30 GeV):

$$\sigma(e^+e^- \to V \to \text{hadrons}) \quad = \quad \frac{\pi}{s} (2J+1) \; \frac{\Gamma_{ee} \, \Gamma_{had}}{(M-E)^2 + \Gamma^2/4} \quad \text{(Breit-Wigner)}$$

With $J(V) = 1$ and $\Gamma_{had} \simeq \Gamma$ this yields:

$$\sigma_{peak} \quad = \quad \frac{12\pi}{M_{t\bar{t}}^2} \; \frac{\Gamma_{ee} \, \Gamma_{had}}{\Gamma^2} \qquad \frac{12\pi}{M_{t\bar{t}}^2} \; \frac{\Gamma_{ee}}{\Gamma}$$

Since the resolution of PETRA is $\Delta W \gg \Gamma$ the peak cross section will scale like

$$\sigma_p \quad = \quad \sigma_{peak} \quad \sim \quad \frac{1}{M_{t\bar{t}}^2} \cdot \frac{\Gamma_{ee}}{\Delta W}$$

whereas the continuum scales like

$$\sigma_c \quad = \quad \sigma_{cont} \quad \frac{1}{E^2} \qquad .$$

Therefore, we can write the following relationship between the Υ data measured at DORIS and toponium search at PETRA:

PETRA $\hspace{9cm}$ DORIS

$$\left(\frac{\sigma_p}{\sigma_c} \right)_{t\bar{t}} \quad \simeq \quad \left(\frac{\sigma_p}{\sigma_c} \right)_{\Upsilon} \cdot \frac{\Delta W(9.4)}{\Delta W(30)} \cdot \frac{\Gamma_{ee}(t\bar{t})}{\Gamma_{ee}(b\bar{b})} \quad \simeq \quad 0.9 \cdot \left(\frac{\sigma_p}{\sigma_c} \right)_{\Upsilon}$$

Since the energy resolution ΔW will be about three times worse at the toponium and Γ_{ee} will scale like Q_q^2 the relative peak cross section at the toponium will be roughly as large as the Υ. Therefore, from a total cross section measurement the toponium could be found if it exists in the PETRA energy region.

Measurements

The energy scan was performed in steps of 20 MeV between E_{CM} = 29.9 and 31.6 GeV. About 20 nb^{-1} were taken at each energy. All four experiments (ref. 80) found a flat energy dependence of R. The combined result of the JADE and TASSO measurements is shown in fig. 33.

From their data, the four groups determined upper limits on the production of narrow resonances in this region. The results for the leptonic width times the hadronic branching ratio $\Gamma_{ee} \cdot B_h$ is given in table. 13

Table 13   Upper limits on leptonic width times hadronic branching in the range E_{CM} = 29.9 to 31.6 GeV

Experiment	$\Gamma_{ee} \cdot B_h$ (keV)	C.L.
TASSO	< 1.6	95%
JADE	< 1.5	95%
PLUTO	< 1.5	95%
MARK J	< 1.3	90%

Since the theoretical expectation for narrow bound states of charge 2/3 e quarks is about 4 keV, the production of such resonances can be safely excluded from the data. A bound state built out of charge 1/3 e quarks is unlikely.

Very recent data

After the shutdown in fall 1979 new data were taken at PETRA, now upgraded to reach 2×18 GeV. The MARK J group[80] has analyzed their data up to E_{CM} = 35.6 GeV. They find no indication of a change in cross section or topology indicative of new flavour production. The thrust distribution they find at E_{CM} = 35 GeV is shown in fig. 34. Production of t quarks is clearly excluded.
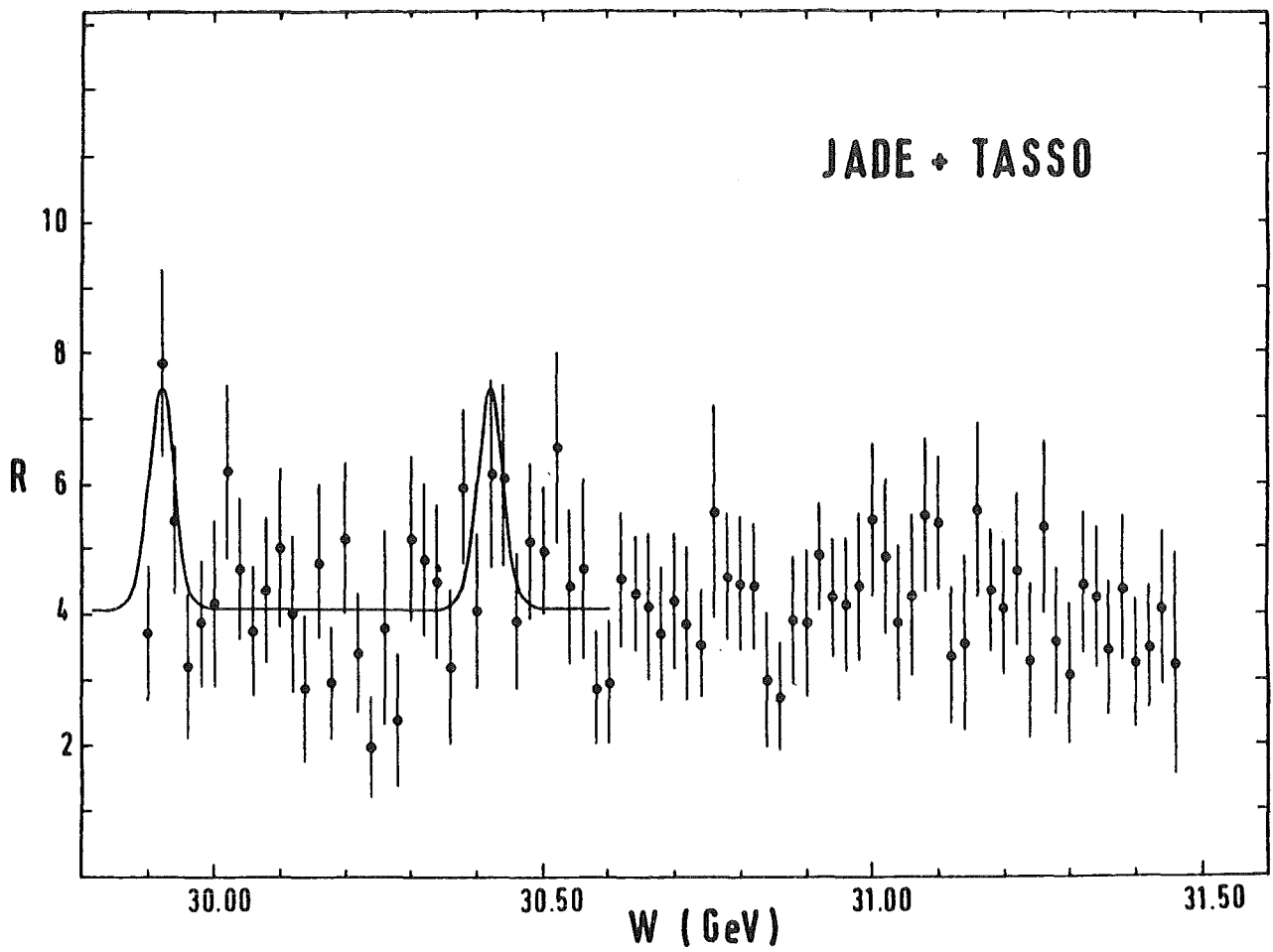
Fig. 33   JADE and TASSO: fine scan of the hadronic cross section between
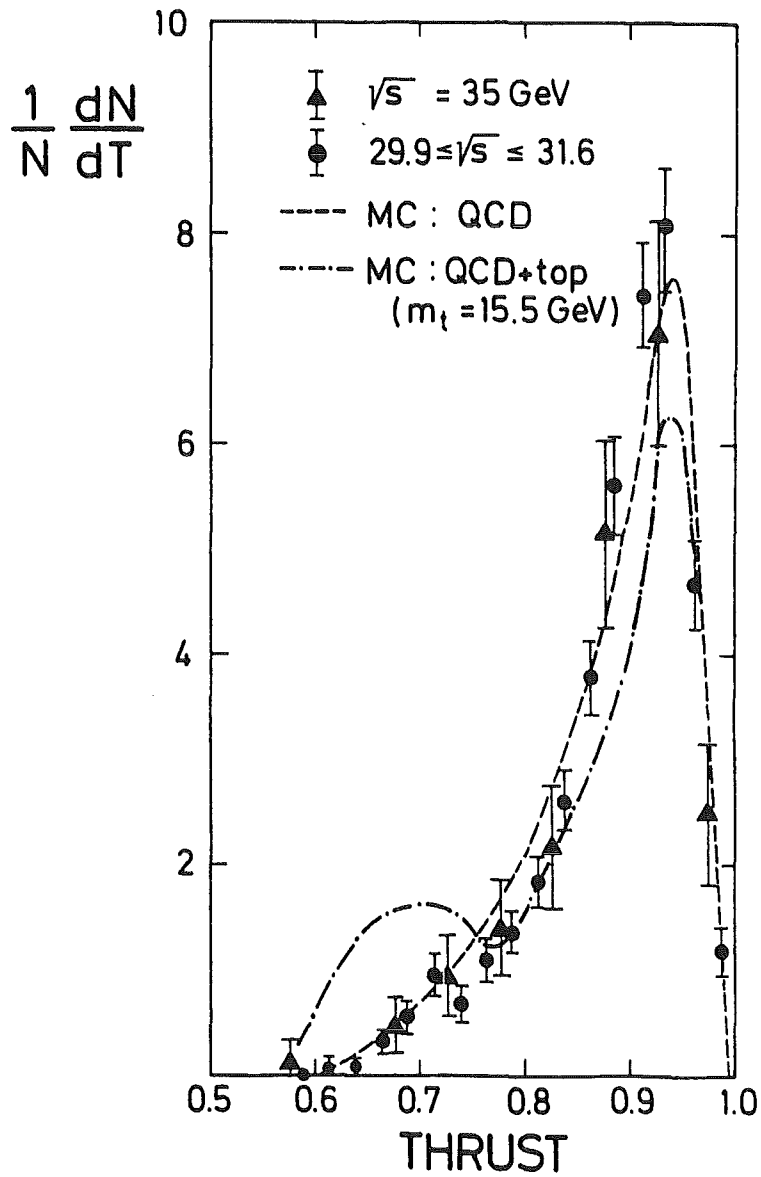29.9 and 31.6 GeV (CM). Combined data of the two groups.

Fig. 34   MARK J: thrust distributions at E_{CM} = 35 GeV and 29.9 < E_{CM} < 31.6 GeV compared to model predictions: five quarks and gluons (--) and additional top quark (-•-).

V.   QCD IN QUARKONIA

1.   Branching Ratios

Bound vector states of heavy quarks (quarkonia) can decay through the one photon channel. The corresponding term in e^+e^- annihilation, a quark loop correction to the one photon channel, is often called vacuum polarisation. Its contribution to the hadronic decay channel is simply given by

$$\Gamma_{q\bar{q}} = \Gamma_{ee} \, \Sigma \, Q_q^2 = \Gamma_{ee} \, R$$
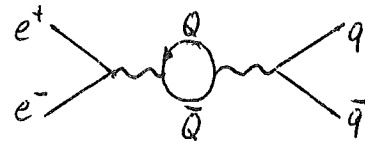
where

$$\Gamma_{ee} = 16 \, \pi \, \frac{\alpha^2 \, Q_q^2}{M^2} \, |\psi(0)|^2$$

is known from QED.

Quantum chromo dynamics[81] (QCD) is the only theory that offers a prediction for the direct decay of quarkonia into hadrons. In this approach, the direct decay width is given by the coupling of the quark pair to more than 2 gluons (1 gluon is forbidden by colour, 2 by C parity). The lowest order contribution (3 gluons) is then (e.g. ref. 26)

$$\Gamma_{ggg} = \frac{160 \, (\pi^2 - 9) \, \alpha_s^3}{81M^2} \, |\psi(0)|^2$$
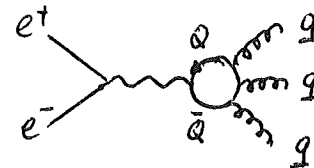
where α_s is the strong coupling constant.

The total width (for given Γ_{ee})

$$\Gamma = \Gamma_{q\bar{q}} + \Gamma_{ggg} = R \, \Gamma_{ee} \, (1 + \frac{\Gamma_{ggg}}{\Gamma_{q\bar{q}}})$$

is independent of the wavefunction of the quarks, since $|\psi(0)|$ drops out in

$$\frac{\Gamma_{ggg}}{\Gamma_{q\bar{q}}} = \frac{10 \ (\pi^2 - 9) \ \alpha_s^3}{81 \ \pi \ \alpha^2 \ Q_q^2 \ R} \quad .$$

If we apply this formula to the $c\bar{c}$ ground state J/ψ with Γ_h = 57 keV, Γ_{ee} = 4.8 keV, R = 2.3 and Q_c = 2/3 we get

$$\alpha_s = 0.19 \quad (J/\psi) \ .$$

If we scale this value from J/ψ to Υ taking the formula

$$\alpha_s(E) = \frac{12 \ \pi}{(33-2N_f) \ \ln E^2/\Lambda^2} \ ; \quad N_f = \text{number of flavours}$$

we get

$$\alpha_s \simeq 0.17 \quad (\Upsilon) \ .$$

With R = 4, Q_b = -1/3 and Γ_{ee} = 1.3 keV this yields

$$\Gamma_{tot} = \Gamma + 3 \ \Gamma_{ee} \simeq 50 \text{ keV}$$

in agreement with the measured value (section II.2).

Since these numbers look like good agreement with theory, a word of caution is in order: Other determinations of α_s from ν-data, J/ψ radiative decays and charmonium models yield values of $\alpha_s \simeq 0.3 \ ./. \ 0.4$ for J/ψ energies. There is no generally excepted explanation for this discrepancy; higher order radiative corrections[*] and difficulties in defining α_s in the potential picture may cause the trouble.

Though, whatever the absolute value of α_s is, the J/ψ and Υ resonance parameters given above fit into a consistent picture with the right (small) energy dependence predicted by QCD.

[*] R. Barbieri et al. (Nucl.Phys. B154 (1979) 535) point out that higher order corrections to radiative transitions in charmonium may be very large.

2. T Decay Topology

In first order of QCD a $q\bar{q}$ bound state couples to three gluons. Once the energy of the $q\bar{q}$ state is high enough a fragmentation of these three gluons into jets will become the preferred decay mode[18].
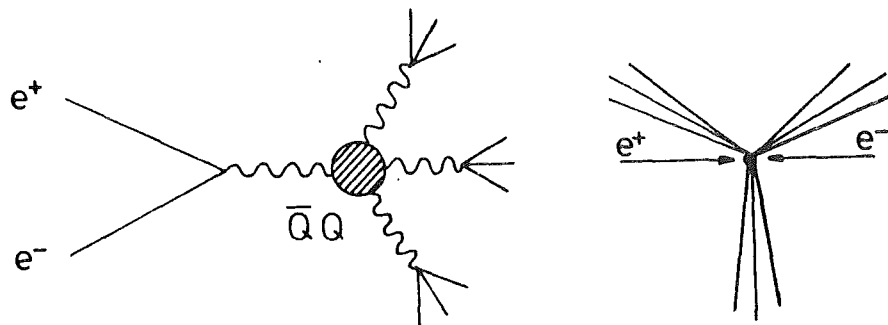
The observation of a three jet structure in the T decay would therefore be a decisive test on the existence of gluons and the validity of QCD[82,83]. This conjecture leads to the following predictions.

(1) Topological quantities like sphericity and thrust change drastically as one passes through the resonance.

(2) A three jet structure would of course lead to a planar configuration of the events.

(3) Eventually three separated jets may be visible.

Although a possible observation of (1) and (2) may be indicative only (3) could be really decisive. Unfortunately it turns out that an asymmetric partition of energy among the three jets is preferred[82] which leads to a nearly back-to-back structure of the events instead of a symmetric three star structure (fig. 35). In addition at the present stage of theory and analysis any interpretation of the data suffers from the following problems :
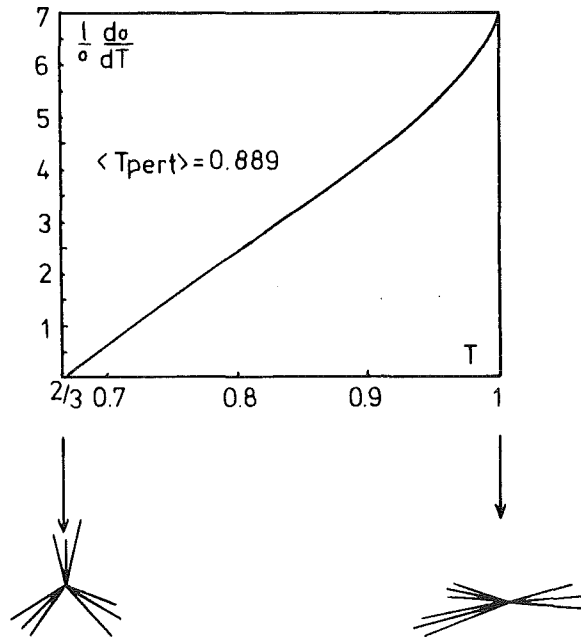
<u>Fig. 35</u>   Relative cross section for symmetric and asymmetric three-gluon
          events.

- The fragmentation of gluons is not known and theoretical predictions are
  rather vague and controversial[84].
- At the Υ resonance the energy of the proposed gluon jets is still very
  low (about 3 GeV/jet).
- Resonance events can only be separated statistically from the continuum.

<u>Measurements</u>

      Data are available from three groups: The NaJ-lead glass[85] experiment,
the DASP2[86] and the PLUTO[87] collaboration. I will restrict myself to a
short discussion of the PLUTO results. The analysis proceeds in three
steps.

- Isolate the direct decay mode.
- Define models.
- Compare the data with these models.

Data were compared with three models:

(1) a phase space model,

(2) the two-jet Feynman-Field model, and

(3) a three-gluon jet model.

In this latter model the gluons fragment like quarks[82]. The two ingredients of the model are:

- A three-gluon matrix element[82,88] for the production of three massless gluons through an intermediate virtual photon.

- A fragmentation of the gluons with limited p_T. The mean p_T is adjusted to fit the two-jet data at 9.4 GeV below the resonance (at comparable jet energies). The charged multiplicity and neutral energy is adjusted to the T data.

Fig. 36 shows the mean observed thrust in the T region compared to lower energy data. T data are given before and after subtraction of the continuum value (T direct). We observe a drastic change of topology as one passes through the resonance (see also insert in fig. 36). The predictions for the two jet model and phase space are indicated in the figure. The three gluon model[89] (not shown in the figure) coincides exactly with the T direct data point.

From this and similar analyses we can certainly exclude the two jet decay mode as a major contribution to the T decay. Data are in excellent agreement with the three gluon model. The phase space description is, however, only disfavoured by about two standard deviations.

Three Jets?

In the proposed three-jet structure of T decays the mean jet energy would be $\sim$ 3 GeV. We know from the corresponding two-jet data at 6 GeV that a jet structure is very difficult to reveal. The identification of a three-jet-structure is even more difficult since the average relative jet angles are smaller than in the two-jet case. Nevertheless, two methods have been tried: the triplicity and the energy flow analysis.
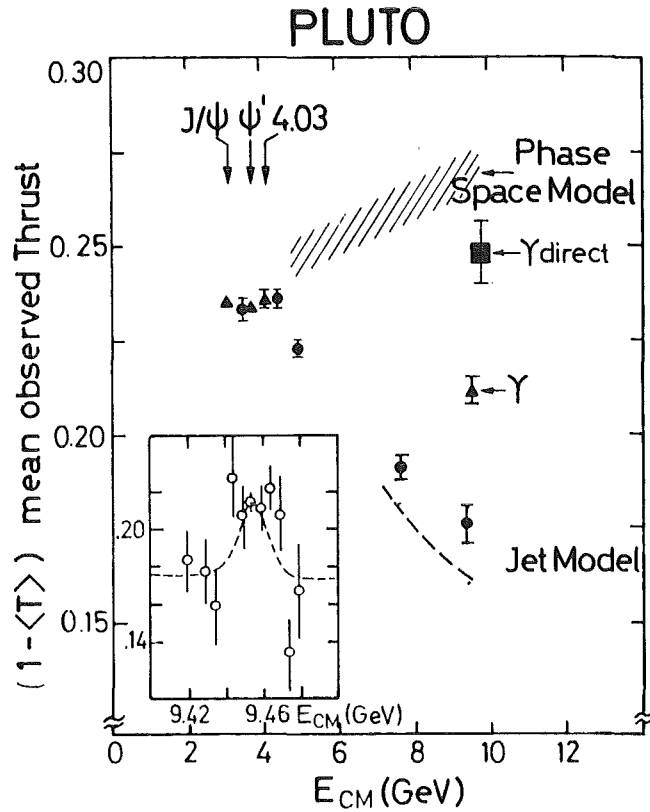
Fig. 36   PLUTO: observed mean thrust for charged particles including the
          Ypsilon. Data are compared to different model predictions: phase
          space and two jets. The three-gluon prediction coincides with
   the T direct data point.

Triplicity

Brandt and Dahmen[90] have extended the two jet quantity thrust to the case of three jets. For each event they form three classes of particles C_1, C_2 and C_3 with $\vec{P}_k = \sum_{i \in C_k} \vec{p}_i$ such that $\sum_1^3 |\vec{P}_k|$ is maximized. The triplicity of an event is then given by

$$T_3 = \frac{1}{\sum |p_i|} \max \{ | \sum_{i \in C_1} \vec{p}_i | + | \sum_{i \in C_2} \vec{p}_i | + | \sum_{i \in C_2} \vec{p}_i | \}$$

P_k are ordered: $P_1 \geq P_2 \geq P_3$. The values for T_3 range from $T_3 = 1$ for a perfect three-jet event to $T_3 = 3 \sqrt{3}/8$ for a spherical event. The procedure defines a three fold structure of each event with three axes and relative

angles as defined below.
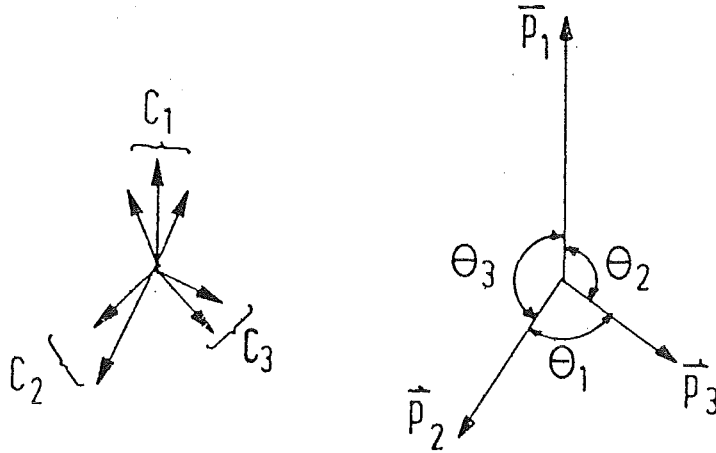
Figs. 37 and 38 show a comparison of the on and off resonance data with the predictions of the three models defined above[91]. The data are in excellent agreement with the two-jet model off resonance and the three-gluon prediction on resonance. Phase space does not describe the data.

As in the discussion of sphericity and thrust distributions, one may argue that modifications of the phase space model may yield better agreement. Let us, therefore, go one step further and study the relative angles defined by the triplicity method. These angles have the virtue of depending very weakly on the details of the gluon fragmentation.

Fig. 39 shows the distributions of the angles θ_1 and θ_3 opposite to the largest and smallest jet momentum. The agreement with the three-gluon model and the complete disagreement with the phase space are presently our best evidence for the decay of Ypsilon into three gluons.

Energy flow

De Rujula, Ellis, Floratos and Gaillard[69] have proposed another method to detect possible three-jet structures in quarkonium decays. The events are oriented along two perpendicular axes which are defined by the largest and second largest momentum flow. All events are then super-
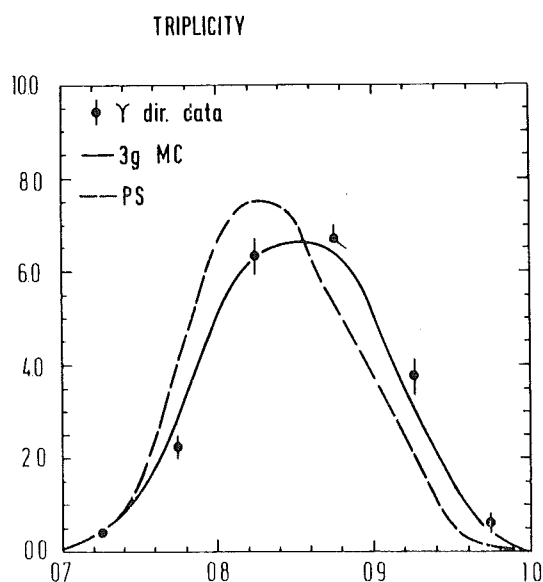
TRIPLICITY

PLUTO (preliminary): distribution of triplicity for events from the T-resonance. The data disagree with expectations from a phase-space model (--) or a two-jet model. They agree with a three-jet model (—).
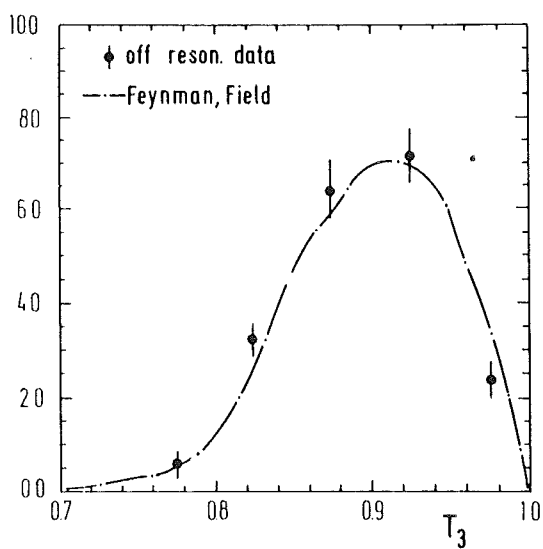

Fig. 38 PLUTO (preliminary): distribution of triplicity T_3 for events outside the T resonance. They show a two-jet structure and agree with the prediction from a Feynman-Field two jet model.
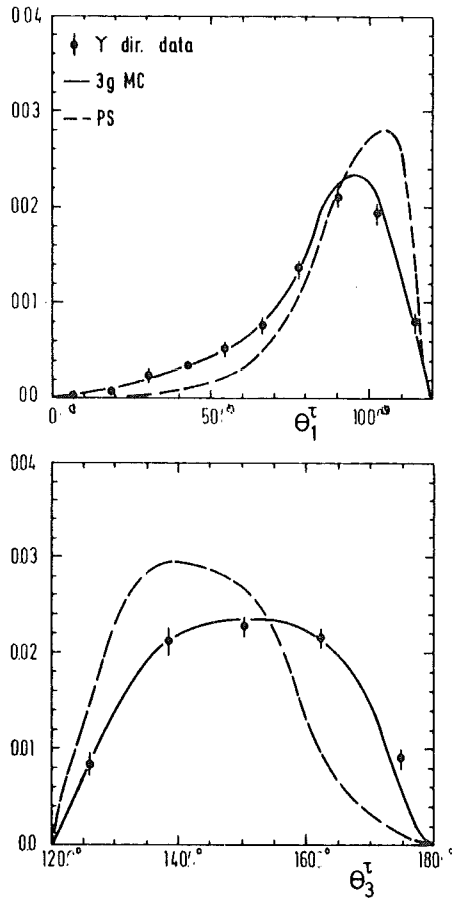
Fig. 39 PLUTO (preliminary): distribution of the angles θ_1 and θ_3 be-tween gluon jets (see text) for events from the Υ resonance. The distributions agree with a three gluon jet model, they disagree with phase space.

imposed and the total momentum flow in the plane defined by the two axes is studied. This analysis has been applied to the PLUTO data[92]. Several procedures have been tried to define the event plane. Excellent agreement between data and the three-gluon model was found. However, the discrimination against phase space turns out to be rather weak. In particular, the energy flow at fixed thrust is nearly model independent, i.e. the method does not add much information in addition to a simple thrust analysis. The method could have its virtues with higher statistics (and higher energies), since it is sensitive to the details of the jet fragmentation.

Angular distribution

The alignment of the fastest jet with respect to the beam axis strongly depends on the gluon spin. If we accept the 3 gluon hypothesis for Υ decays, we can therefore perform a sensitive test on the spin of the gluons.

Fig. 4o shows the angular distribution of the sphericity axis in direct Υ decays as measured by the PLUTO group[87]. The data are compared with the predictions for spin 1 (full curve)[82] and spin 0 (dashed curve) (ref. 93).

The data are in good agreement with the vector gluon prediction. A fit with $1 + \alpha \cos^2\theta$ yields $\alpha = 0.83\pm0.23$, which excludes scalar gluons.

Conclusions

The event shape encountered in Ypsilon decays strongly deviates from the two-jet structure found in the continuum. All topological quantities studied are in agreement with a three-gluon jet model. A simple phase-space model cannot explain the details of the data, in particular the three-jet angular distributions: QCD is the only model that offers a satisfactory ex-
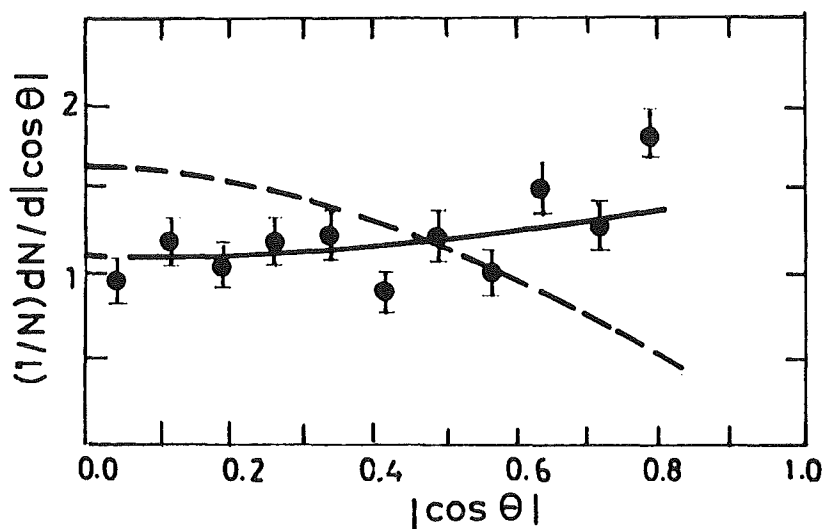

Fig. 40   PLUTO: angular distribution of the sphericity axis on resonance. The full curve is proportional to $1 + 0.39 \cos^2\theta$, the dashed curve to $1 - 0.995 \cos^2\theta$.

planation of all experimental aspects of Ypsilon decays. If we accept the three-gluon picture, we can exclude scalar gluons.

VI. QCD IN HIGH ENERGY JETS

1. Quark-Parton Model and QCD

Quark-Parton Model (QPM)

The simple quark-parton model has lead us throughout most of the pre-ceeding discussions. In this picture electrons and positrons annihilate into a pair of quarks which fragment into jets. The basic assumptions of this model are:

- Quarks behave like leptons with fractional charges at the $\gamma q \bar{q}$ vertex, i.e. the process $e^+e^- \rightarrow q\bar{q}$ can be calculated from QED.
- The hadronic nature of quarks is introduced ad hoc: the quarks fragment with limited p_T and thus produce jets.
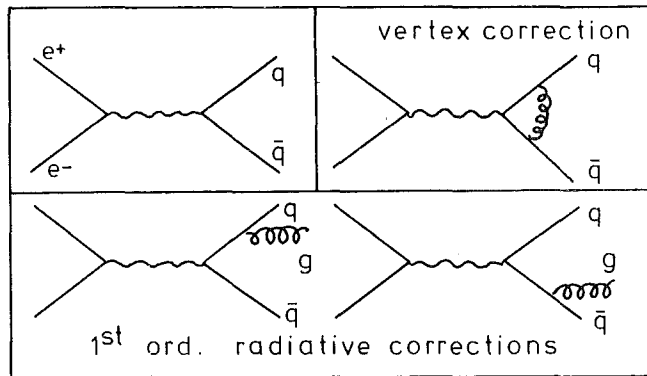
The predictions of this model are:

$$R = 3 \sum_q Q_q^2 \qquad\qquad q = \text{quark flavours}$$

$$\langle p_T \rangle \simeq \text{const} \simeq 320 \text{ MeV}$$

$$\langle S \rangle \simeq \frac{\langle n(E) \rangle \langle p_T \rangle}{E^2} \sim \frac{\ln E}{E^2}$$

$$\langle 1-T \rangle \simeq \frac{\langle n(E) \rangle \langle p_T \rangle}{E} \sim \frac{\ln E}{E}$$

where we assume a logarithmic increase of the mean multiplicity $n(E)$ with energy.

First Order Perturbative QCD

QCD[81] tells us that quark pair production is only the 0th order in a perturbation expansion. In 1st order radiative gluon corrections and a vertex correction term[94] have to be added. Like in QED the infrared divergences in the $q\bar{q}g$ terms cancel against those arising from the interference between the vertex correction and the Born term.

The process of gluon emission is governed by the strong coupling constant α_s. Once α_s is known, QCD predicts quantitatively where the quark-parton model is a valid approximation and how large the radiative terms are. In this order of QCD the problem of fragmentation is of course not solved. Again both the quark and the gluon fragmentation have to be introduced heuristically. Thus the QPM assumptions change in the following way:

- Including first order gluonic corrections the annihilation process $e^+e^- \rightarrow$ hadrons can be calculated in QCD with only one free parameter, α_s.
- Quarks fragment like in the QPM. The fragmentation of gluons is probably softer due to the three-gluon vertex which exists in a non-abelian gauge theory like QCD[95].
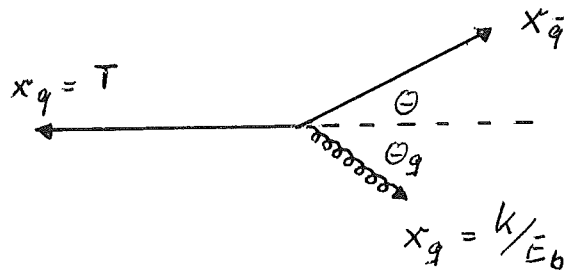
Characteristics of Gluon Emission

The QCD cross section for gluon emission in the process

$$e^+e^- \rightarrow q\,\bar{q}\,g$$

in first order α_s and integrated over all orientations of the $\bar{q}qg$ plane with respect to the beams reads[94]:

$$\frac{1}{\sigma_{q\bar{q}}}\,\frac{d\sigma(q\bar{q}g)}{dx_q\,dx_{\bar{q}}} = \frac{2}{3}\,\frac{\alpha_s}{\pi}\,\frac{x_q^2 + x_{\bar{q}}^2}{(1-x_q)(1-x_{\bar{q}})} \qquad (a)$$

where $x_i = E_i/E_b$ are the scaled energies of the quarks and the gluon (Feynman x; E_b = beam energy).

For simplicity we assume that the quark q carries the largest momentum. We can easily see that without fragmentation the thrust of a $q\bar{q}g$ event is $T = x_q$. Since $x_q + x_{\bar{q}} + x_g = 2$ we can rewrite (a):

$$\frac{1}{\sigma_{q\bar{q}}}\,\frac{d\sigma(q\bar{q}g)}{dT\,dx_{\bar{q}}} = \frac{2}{3}\,\frac{\alpha_s}{\pi}\,\frac{x_q^2 + x_{\bar{q}}^2}{(1-T)(1-x_{\bar{q}})}$$

$$= \frac{2}{3}\,\frac{\alpha_s}{\pi}\,\frac{x_q^2 + x_{\bar{q}}^2}{(1-T)(T-1+x_g)} \qquad (b)$$

The expression has a singularity for $T \rightarrow 1$ when the two quarks are lined up (colinear singularity). In the small angle limit $T \rightarrow 1$ and for small gluon

momenta $(x_g \ll 1)$ (b) reads:

$$\frac{1}{\sigma_{q\bar{q}}} \frac{d\sigma(q\bar{q}g)}{dT\ dx_{\bar{q}}} = \frac{2}{3} \frac{\alpha_s}{\pi} \frac{T^2 + (2-T-x_g)^2}{(1-T)(T-1+x_g)}$$

$$\simeq \frac{4}{3} \frac{\alpha_s}{\pi} \frac{1}{1-T} \frac{E_b}{k}$$

(c)

Formula (c) demonstrates the $1/k$ behaviour of the gluon brems-spectrum. A soft gluon singularity occurs for $k \to 0$.

Transverse Momentum

If we integrate over T we get

$$\frac{1}{\sigma_{q\bar{q}}} \frac{d\sigma}{dx_T} = \frac{1}{\sigma_{q\bar{q}}} \int dT \frac{d\sigma(q\bar{q}g)}{dx_T\ dT}$$

(d)

where we have introduced

$$x_T = x_{\bar{q}} \sin \theta \quad .$$

(d) diverges for $x_T \to 0$. If we take moments, however,

$$\langle x_T^n \rangle = \frac{1}{\sigma_{q\bar{q}}} \int dx_T \int dT\ x_T^n \frac{d\sigma(q\bar{q}g)}{dT\ dx_T}$$

we get finite solutions of the type

$$\langle x_T^n \rangle = \alpha_s(E) \cdot f(x_q, x_{\bar{q}}) \quad .$$

$f(x_q, x_{\bar{q}})$ does not depend on the beam energy. Therefore we get

$$\langle x_T^n \rangle \sim \alpha_s(E) \sim 1/\ln (E/\Lambda)^2.$$

i.e. $<x_T^n>$ varies only slowly with energy. Consequently the moments of the transverse momenta increase with powers of the energy

$$<p_T^n> \; \sim \; E^n/\ln \, (E/\Lambda)^2$$

in particular we get a linear or quadratic increase of the first two moments

$$<p_T> \; \sim \; E/\ln \, (E/\Lambda)^2$$

$$<p_T^2> \; \sim \; E^2/\ln(E/\Lambda)^2 \quad .$$

This is a dramatic deviation from the QPM prediction[69,96,97,98].

Fixed Angle Jets

At high energies, the gluon emission with increasing p_T will eventually win over the fragmentation. The broadening of the "jet" consisting of a quark and a gluon in 1st order QCD is then given by an opening angle

$$<\theta> \; \simeq \; \frac{<p_T>}{E_b} \; \sim \; \alpha_s(E) \; \sim \; 1/\ln(E/\Lambda)^2 \quad .$$

Thus the width of the jet will only depend slightly on energy, a phenomenon being denoted as: "fixed angle jets"[68].

Simple Tests of QCD

From the above considerations a number of conceptually simple tests can be derived (table 14):

Table 14 Additional contributions expected in 1st order QCD
         compared to the simple QPM predictions

Quantity	QPM ($q\bar{q}$)	+ 1st order QCD ($q\bar{q}g$)
R	$3\ \Sigma\ Q_q^2$	$3\ \Sigma\ Q_q^2\ \dfrac{\alpha_s}{\pi}$
$<p_T>$	const.	$\sim \alpha_s\ E \quad \sim E/\ln\ (E/\Lambda)^2$
$<p_T^n>$	const.	$\sim \alpha_s\ E^n \sim E^n/\ln(E/\Lambda)^2$
$<S>$	$\sim \ln E/E^2$	$\sim \alpha_s \quad \sim 1/\ln\ (E/\Lambda)^2$
$<1-T>$	$\sim \ln E/E$	$\sim \alpha_s \quad \sim 1/\ln\ (E/\Lambda)^2$

R should be higher than predicted in the QPM. The effect is of the or-
der of 10% to 15% and has been discussed in the previous chapters. The data
agrees with the expected increase. For a decisive test, however, an accura-
cy of at least 5% would be needed on the absolute value of the total cross
section. The precision is not yet reached and seems hard to achieve.

Rising $<p_T>$ would influence the energy dependence of S and 1-T. Visi-
ble effects are predicted somewhere between 10 GeV [69] and 3o GeV[98] CM ener-
gy. In this context I want to recall deviations from the expected two-jet
behaviour in the topological quantities which have already been mentioned
in chapter IV in connection with the top search (fig. 41). Neither the
udscb nor the udscbt prediction gave a good description of the data. If
gluon radiation is introduced (dashed-dotted line in fig. 41) the agreement
with the data becomes much better.

2. $q\bar{q}g$ Event Generator

The effects in the data are small and call for a quantitative des-
cription before any significance can be attributed to them. To this end
a model based on the QCD prediction (a) was constructed by Hoyer et al.
(ref. 98). The two main problems for such a model are (i) the infrared
singularities in (a) and (ii) the fragmentation of quarks and gluons.
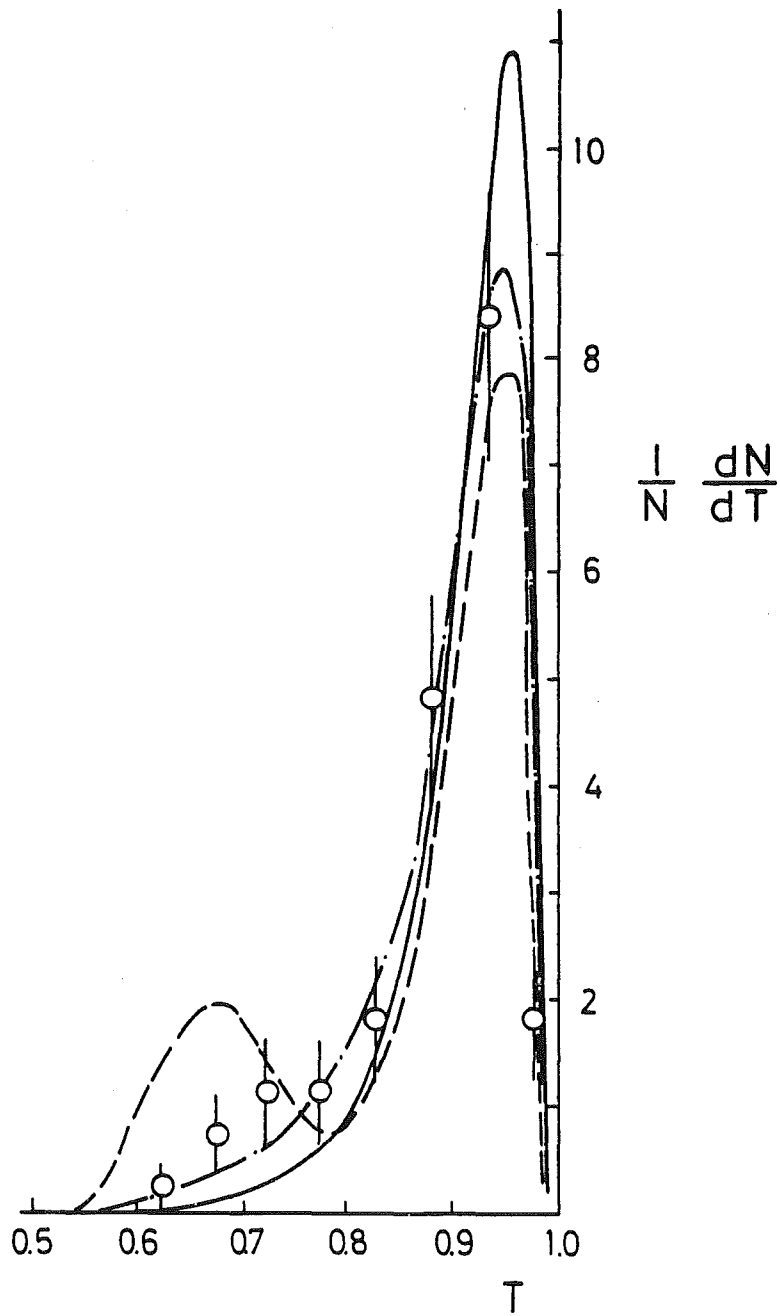
MARK J: thrust distribution at E_{cm} = 31.6 GeV. The curves are MC predictions for udscb (—), udscbt (--) and udscb + gluons (-•-).

(i) Infrared Singularities

We have seen in the previous section that (b) diverges for T → 1. On the other hand, non-perturbative effects will dominate this region anyway. In fig. 42 the thrust distributions of the 1st order QCD calculation (without fragmentation) and the non-perturbative effects of quark fragmentation are compared. The model proceeds like this:

A cutoff value T_o for thrust is defined. For $2/3 \le T \le T_o$ q$\bar{q}$g events are generated according to the QCD cross section (a). Only uds and c quarks participate in the gluon emission process. The remaining interval $T_o < T<1$ is assumed to be dominated by fragmentation. Therefore, σ(q$\bar{q}$g) is set to zero and q$\bar{q}$ events are generated such that σ(q$\bar{q}$g) + σ(q$\bar{q}$) = 3 Σ Q_q^2(1 + α_s/π) accounts for the total cross section expected in QCD.

T_o is somewhat arbitrarily defined as the maximum of the non-perturbative distribution.

(ii) Fragmentation

The fragmentation of quarks is done according to Field-Feynman for uds and Ali et al. for c and b quarks. Gluons are assumed to decay into u$\bar{u}$, d$\bar{d}$ and s$\bar{s}$ pairs with a relative abundance of 2 : 2 : 1 (mass suppression of s$\bar{s}$).

The magnitude of the effects depends linearly on the absolute value of α_s. For Λ = 5oo MeV in

$$\alpha_s = \frac{12 \pi}{(33 - 2 N_f) \ln (E/\Lambda)^2}$$

one gets the values of table 15.

At 30 GeV about 30% of the events will be generated according to q$\bar{q}$g. Of course, most of the gluons will be either colinear or very low

Table 15   Energy dependence of QCD contributions

E_{CM} (GeV)	T_0	$q\bar{q}g/q\bar{q}$
15	0.92	0.17
3o	0.95	0.29
9o	0.98	0.49

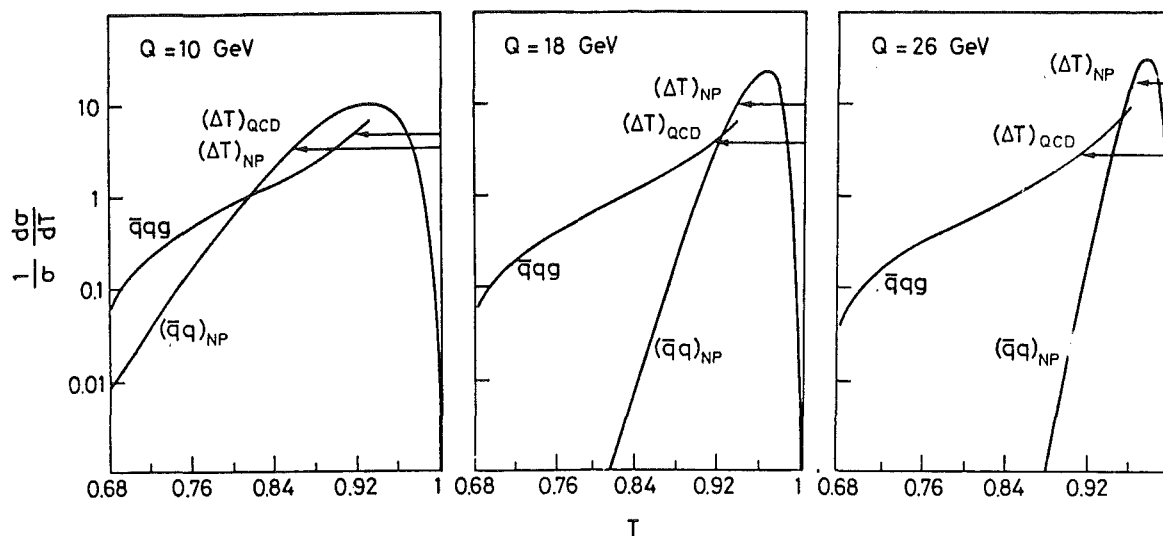Fig. 42   QCD predictions for the thrust distribution at different
energies (1st order q$\bar{q}$g) compared to the non-perturbative
jet fragmentation (q$\bar{q}$)$_{NP}$ (the mean values ΔT defined in
ref. 69 are not used here).

energy. Above 30 GeV the QCD effects get too large to be considered in first approximation. Therefore, the model is not applicable for $E_{CM} \simeq$ 100 GeV in this form.

3. Experimental Results

After preliminary results had been reported by the TASSO collaboration[99] at the CERN conference in June 1979, evidence for QCD effects in e^+e^- annihilation was published by the MARKJ[100], TASSO[101], and PLUTO[102] groups in September 1979 and by the JADE group[103]. In this section I will give a short summary of their analysis.

Like in the previous chapters in general observed quantities will be shown and compared with various model calculations. Only some of the distributions are corrected (or partially corrected) for detector effects. At this point some remarks are in order to explain, why these ·corrections are generally difficult and problematic (and, therefore, not yet applied to the data).

Corrections are usually estimated from a comparison of Monte Carlo generated events before and after having passed the detector. Even if the detector simulation is perfect the following principle problems remain:

- The corrections will be model dependent. Before applying them one has to make sure that they are independent of the different models one wants to compare with.
- There are different effects one may want to correct for: detector efficiency and resolution, neutral particles (if only charged are seen) or even the fragmentation process. This has to be matched to the model under consideration.
- Model calculations often predict distributions which are taken with respect to the original quark axis. In such a case the correction to the data has to take this into account. Of course this increases the model dependence.

In summary, corrections have to be consistent with the specific model one wants to compare with. This may be difficult, if several models are to be tested.

a) Rising Transverse Momentum

The mean transverse and parallel momentum with respect to the thrust axis as a function of energy is shown in figs. 43 and 44 for the experiments TASSO and PLUTO. The TASSO group has determined the thrust axis from charged particles only, whereas the PLUTO data are evaluated with respect to the common thrust axis of charged and neutral momentum. In both figures, the mean transverse momentum $<p_T>$ and the mean parallel momentum $<p_L>$ are calculated from charged tracks only. Apart from the gross features of the data - bounded $<p_T>$ and rising $<p_L>$ - both figures indicate a slight increase of $<p_T>$ with energy. This increase becomes dramatic if we plot the second moment $<p_T^2>$, which gives more weight to high momentum particles.

Only a small part of this increase can be accounted for by detector effects. This can be checked by comparing the data with the Feynman-Field model for uds quarks, which has no inherent energy dependence of $<p_T^2>$. The TASSO data (fig. 43) are corrected for this effect. The uds expectation would then be a constant $<p_T^2>$.

An increase in p_T is expected from new heavy quark production. In fact, including detector effects and c and b quarks, the energy depcn-dence is quite strong, accounting for roughly half of the increase in the PLUTO data (dashed line in fig. 44). Still the models do not account for the full effect.

In summary, $<p_T^2>$ increases roughly by a factor of 2 between 1o and 3o GeV. This effect cannot fully be explained by detector effects and new quark flavours. Fig. 45 shows a comparison of the p_T^2 distributions at low and high PETRA energies. To account for the data the parameter σ_q in
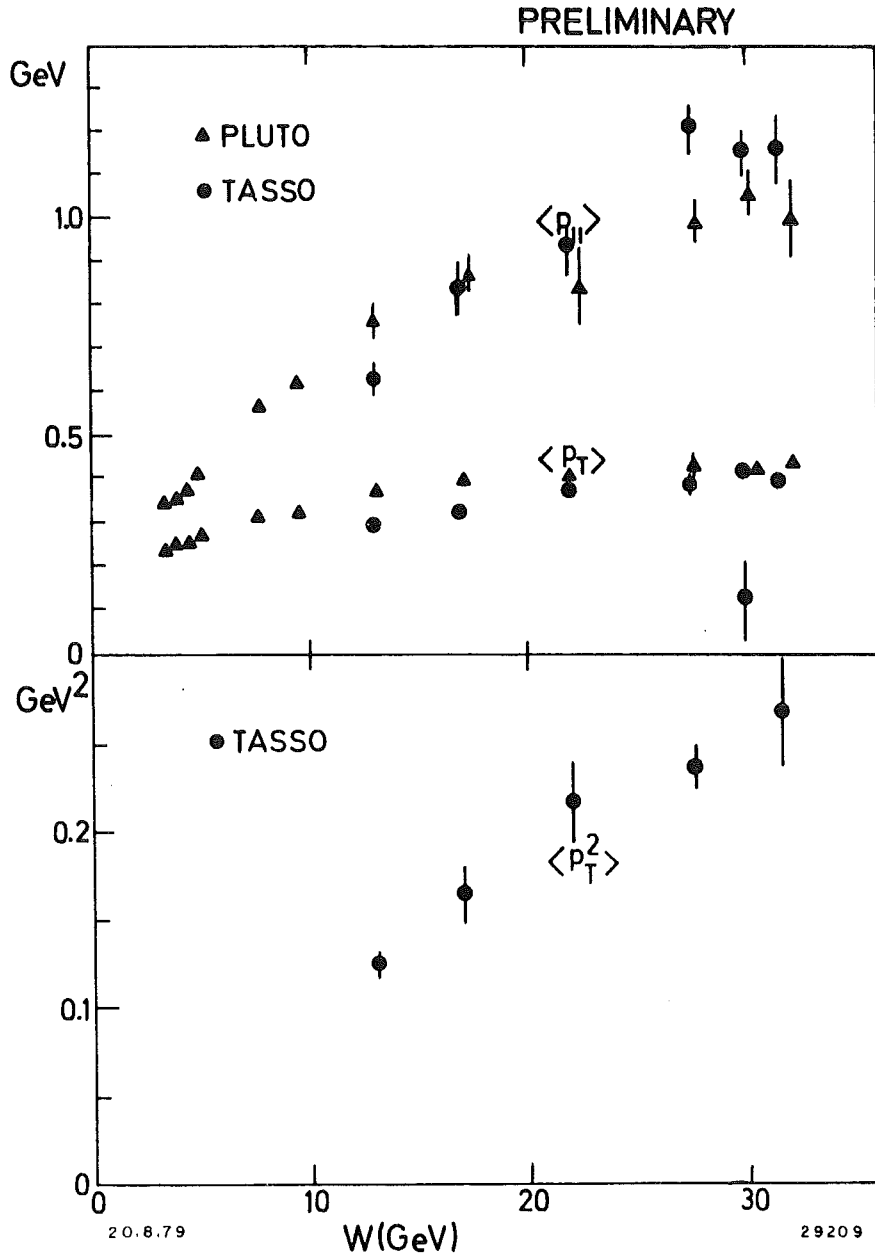
Fig. 43   TASSO (preliminary): mean momentum components $<p_T>$, $<p_L>$ and $<p_L^2>$ for charged particles with respect to the thrust axis. Some PLUTO data are shown for comparison.

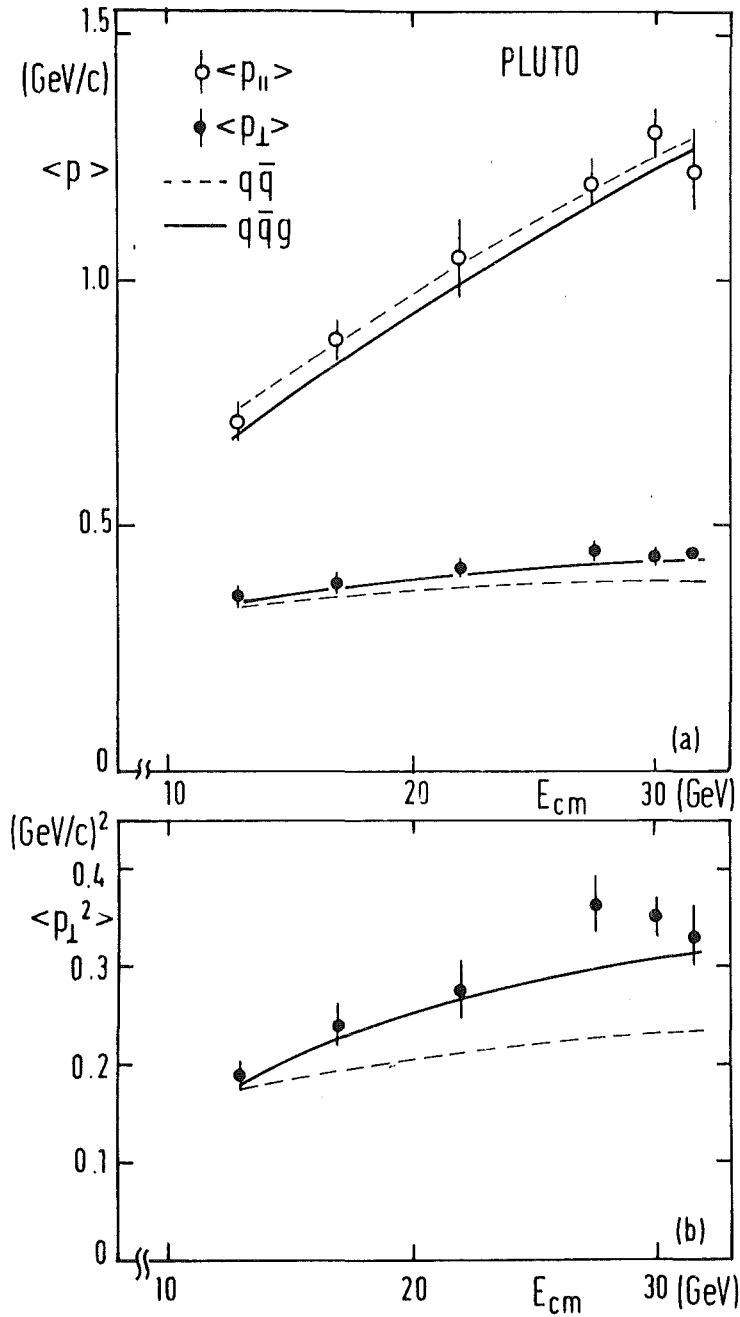Fig. 44   PLUTO: energy dependence of the mean momentum components
$<p_T>$, $<p_L>$ and $<p_T^2>$ compared to the models of quark pair
production with (——) and without (--) gluons.

$$d\sigma/dp_T^2 \sim e^{-p_T^2/2\sigma_q^2}$$

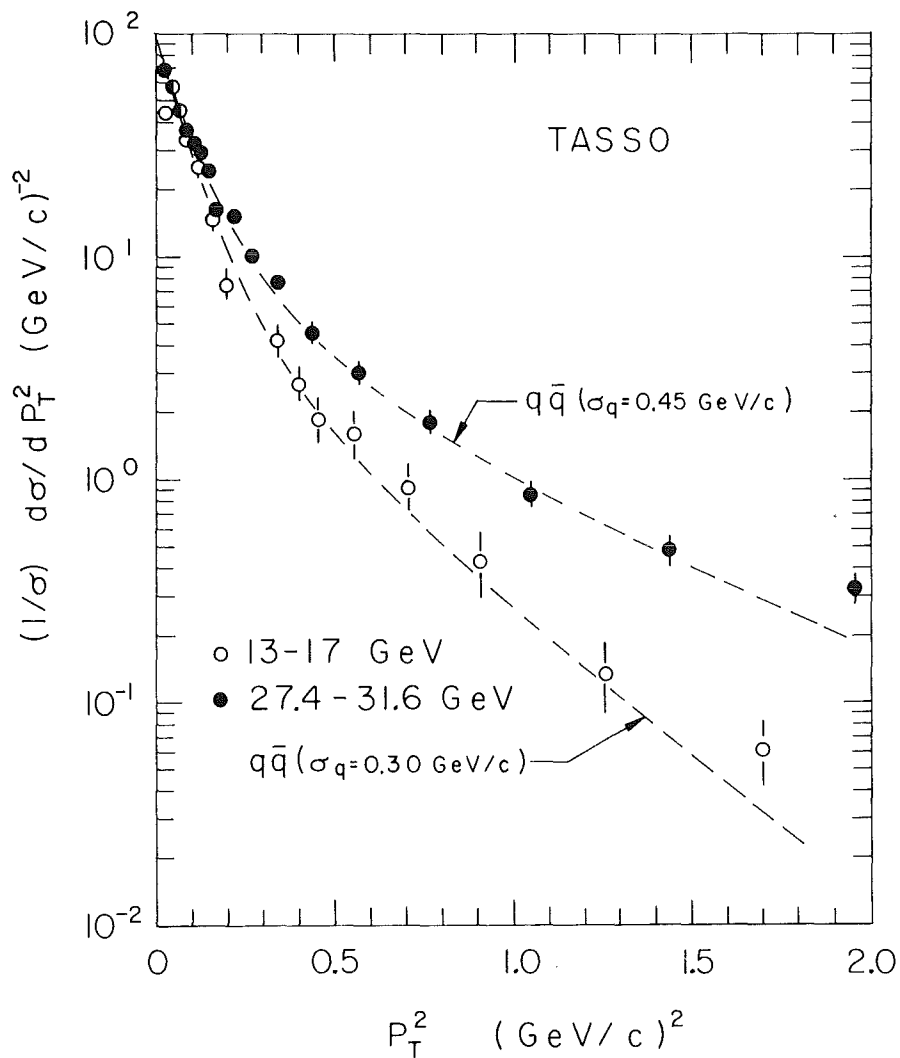which describes the transverse spread of the momentum distribution in

Fig. 45 TASSO: distributions of the square of the transverse momen-
tum with respect to the thrust axis. Data at low (13 + 17
GeV) and high (27.4 - 31.6 GeV) energies are compared with
different parametrisations in the qq̄ model.

the Feynman-Field model has to be increased from σ_q = 0.3 GeV at 13
and 17 GeV to σ_q = 0.45 GeV in the 27 - 32 GeV range.

A possible explanation is offered by QCD. In fact, model calcula-
tions coincide perfectly well with the observed energy dependence of
the data (fig. 44).

Seagull effect

What could one do to enhance the signal? If the effect is due to gluon emission, the fast hadrons from the gluon fragmentation should carry the best memory of the gluon transverse momentum. The same holds for the
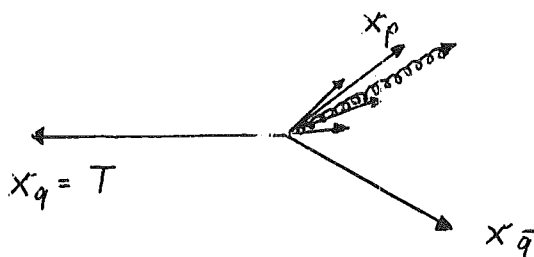
fragmentation particles of the quark from which the gluon is radiated. The effect first predicted by Kramer and Schierholz[97] is shown in fig. 46. The energy dependence $\langle p_T^2 \rangle$ is growing with $x_p = 2\, p/E_{CM}$, the scaled hadron momentum. Since all curves drop to zero in the kinematical limit $x_p \to 1$, intermediate values of x_p will be the best place to look for QCD effects. (Fig. 46 is often called a "seagull" plot.)

Asymmetry of the Seagull Effect

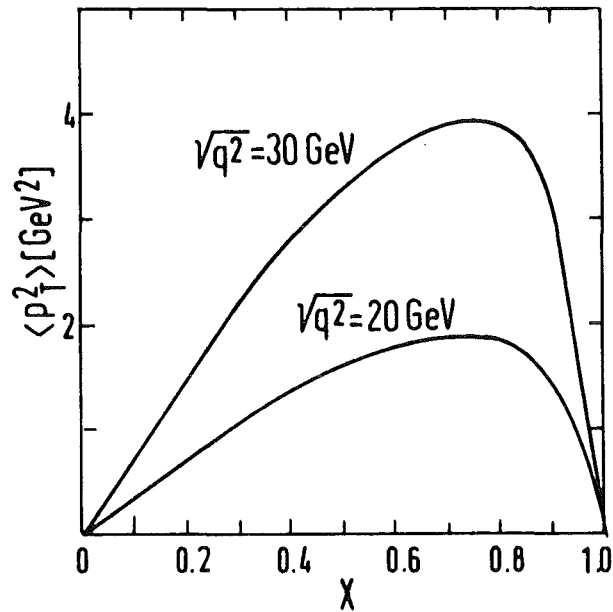Let us go one step further and consider the gluon radiation process in more detail
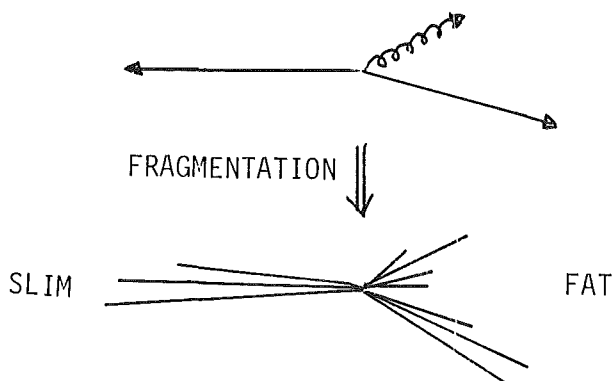
Fig. 46   Predicted energy dependence of the seagull effect in first order
           QCD. $<p_T^2>$ is shown as a function of Feynman x (Kramer and
           Schierholz[97]).

The fragmentation of quarks and gluons will in general lead to an asym-
metric two-jet structure. Let the events be oriented along their thrust axis
in such a way that the "slim" jet always points to the same (say left) side.
A seagull plot, carried out separately over the left (slim) and right (fat)
jet will then reflect this asymmetry. The effect predicted[98] in QCD is shown
in fig. 47. Besides the striking asymmetry also the increase in the fat jet
is stronger than for non oriented events.

Such an analysis has been carried out by the TASSO and PLUTO groups.
Their results are shown in figs. 48 and 49. The seagull effect increases
drastically with energy in the "fat" jet, whereas it stays small and roughly
constant in the "slim" jet. Data are in good agreement with the QCD predic-
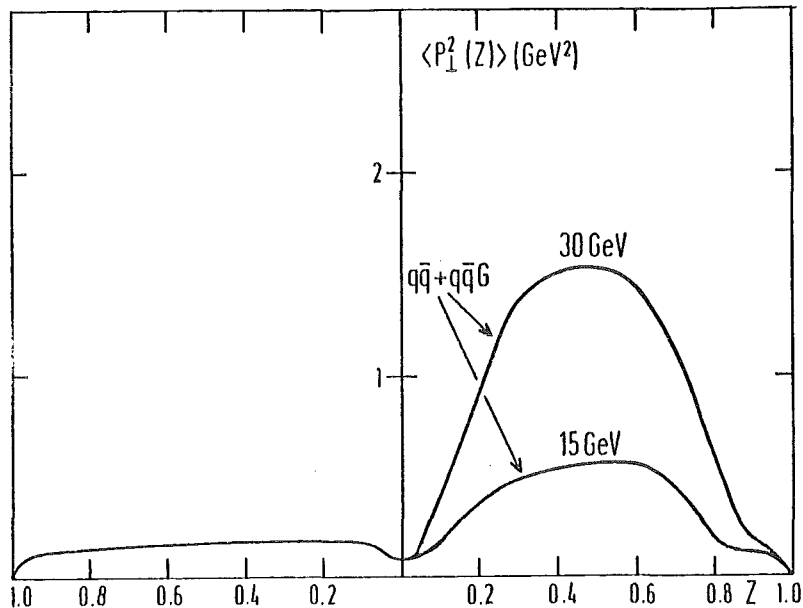tion (fig. 49,full curve).

Fig. 47   Monte Carlo simulation of the asymmetry in $<p_T^2>$ for the "slim" and "fat" jets in $e^+e^- \to q\bar{q} + q\bar{q}g$ (Hoyer et al. [98]).

Given the increase in $<p_T^2>$ which had already been realized in the previous discussion, we have to ask how much new information is really contained in figs. 48 and 49. The answer is given by the dashed curve in fig. 48 and the dash-dotted line in fig. 49. The change in σ_q needed to describe the p_T distribution accounts well for the increasing asymmetry, i.e. statistical fluctuations in conjunction with the slim-fat selection method introduce a sufficiently strong effect already.

We have seen so far that the mean transverse momentum rises with energy. The increase is in good agreement with the prediction of QCD. Though it has to be kept in mind that this is only a necessary but not sufficient condition for QCD to be proven. After all we do not have a reliable prediction for the quark fragmentation up to 3o GeV. There may be other sources
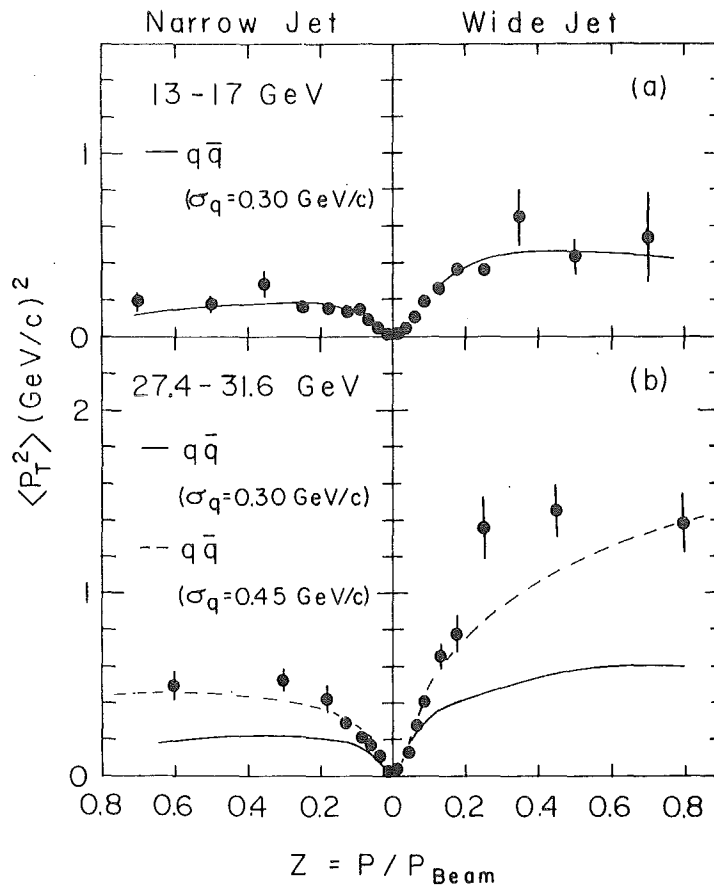
Fig. 48   TASSO: $<p_T^2>$ distributions as a function of $z = p/p_b$ for the "fat" and "slim" jet. Data are grouped in two energy bins. $q\bar{q}$ models with different σ_q are shown for comparison.

for jet broadening, some of which have been mentioned already.

b)   Planar Event Structure

The radiation of a gluon would induce a planar structure of the event. Two ways of analysing coplanar structures were applied to the TASSO and PLUTO data: the three eigenvalues of the sphericity tensor and the Q-parameters (first defined by G. Alexander[104]) and the triplicity (first defined by S. Brandt and H. Dahmen[90]). The MARK J group studied the energy flow in terms of "oblateness".
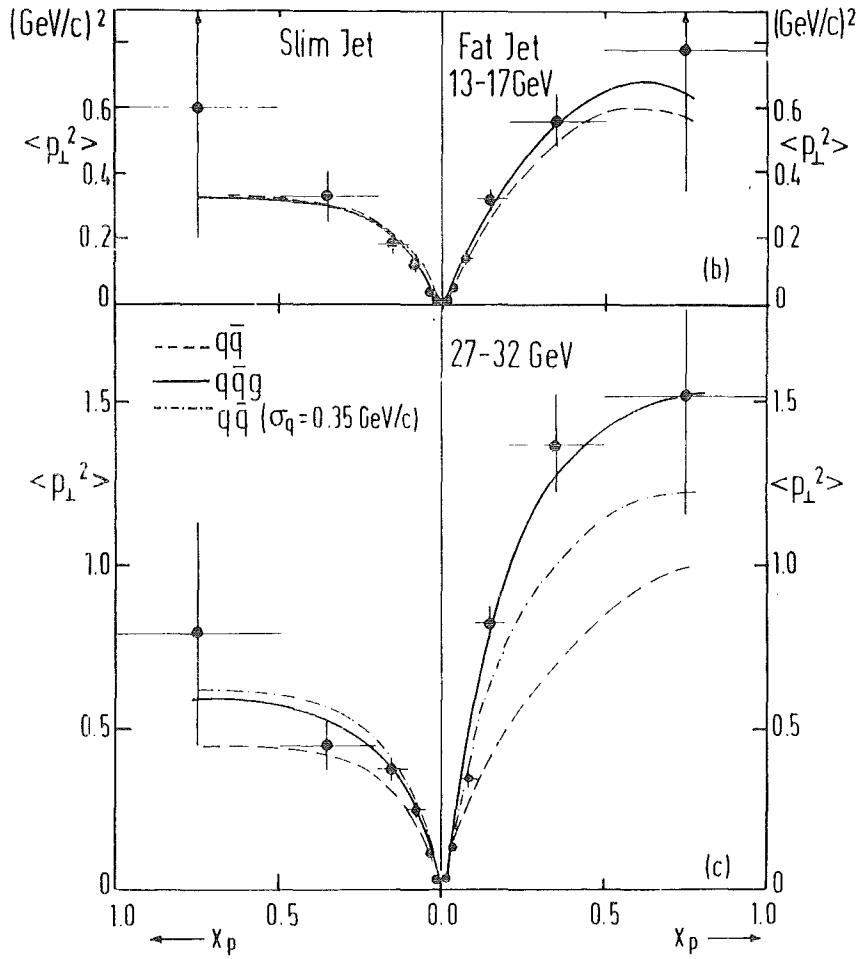
Fig. 49   PLUTO: $<p_\uparrow^2>$ distributions like in fig. 48. Data are compared
with different $q\bar{q}$ predictions for σ_q = 0.25 GeV (--) and σ_q
= 0.35 GeV (-•-). The full curve shows the QCD calculation.

Oblateness

In the MARKJ analysis thrust is defined by the maximum energy flow in
the detector

$$T = \max \frac{\sum\limits_i |\vec{E}^i \cdot \vec{e}_1|}{\sum\limits_i |E^i|} .$$

The Energy flow E^i is calculated for each detector hit. $\vec{e}_1$ is the di-
rection of maximum energy flow.

To investigate the energy distribution perpendicular to $\vec{e}_1$ a new quantity "Major" is defined in analogy to thrust

$$\text{Major} = \max \frac{\sum_i |\vec{E}^i \cdot \vec{e}_2|}{\sum_i |E^i|} \qquad \vec{e}_1 \cdot \vec{e}_2 = 0 \qquad .$$

$\vec{e}_2$ is the direction of largest energy flow in a plane perpendicular to $\vec{e}_1$.

To define the flatness of an event a third axis $\vec{e}_3$ orthogonal to both $\vec{e}_1$ and $\vec{e}_2$ is constructed. The normalized energy flow along this axis is called "Minor". The flatness is then measured by a quantity called "Oblateness".

$$O = \text{Oblateness} = \text{Major} - \text{Minor} \qquad .$$

Fig. 5o shows the energy dependence of the mean oblateness $<O>$ compared to a $q\bar{q}$ model and the QCD prediction $(q\bar{q}g)$. We realize that the $q\bar{q}$ model decreases much faster with energy than the data, whereas QCD gives a proper description of the observed energy dependence.

The distributions of oblateness at low and high PETRA energies are compared in fig. 51. Again, at high energies, data cannot be described by the $q\bar{q}$ model, even if $<p_T>$ is increased from 325 to 425 MeV (dashed and dash-dotted lines). All measurements are in very good agreement with the QCD predictions (full curves).

Eigenvalues of the Sphericity Tensor

Several methods are based on the generalized three-dimensional sphericity which is introduced in the following way[70]: let us look at the expression

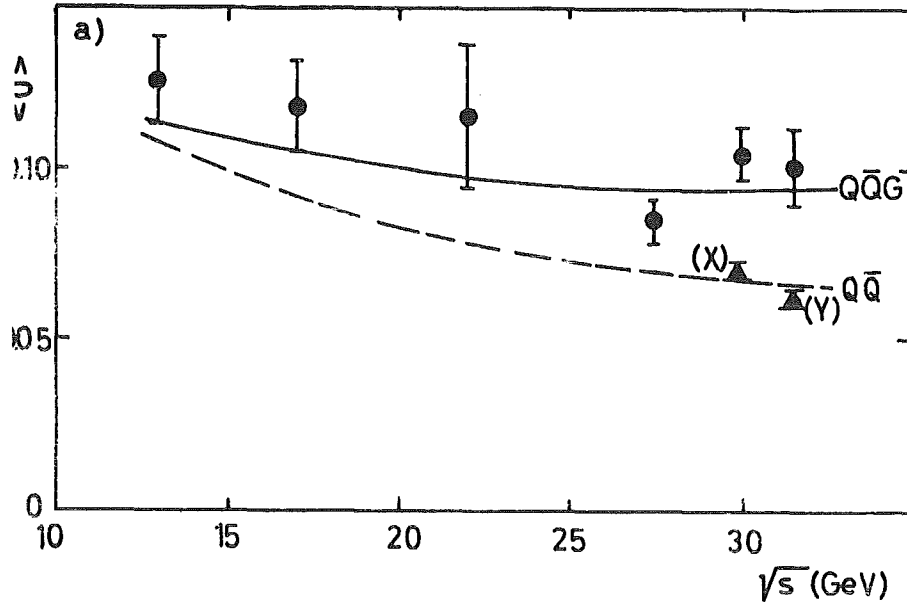$$T_{\alpha\beta} = \sum_i (\delta_{\alpha\beta} (p^i)^2 - p_\alpha^i p_\beta^i) \qquad \alpha,\beta = 1,2,3$$

Fig. 5o   MARK J: the mean oblateness <O> as a function of energy. Data
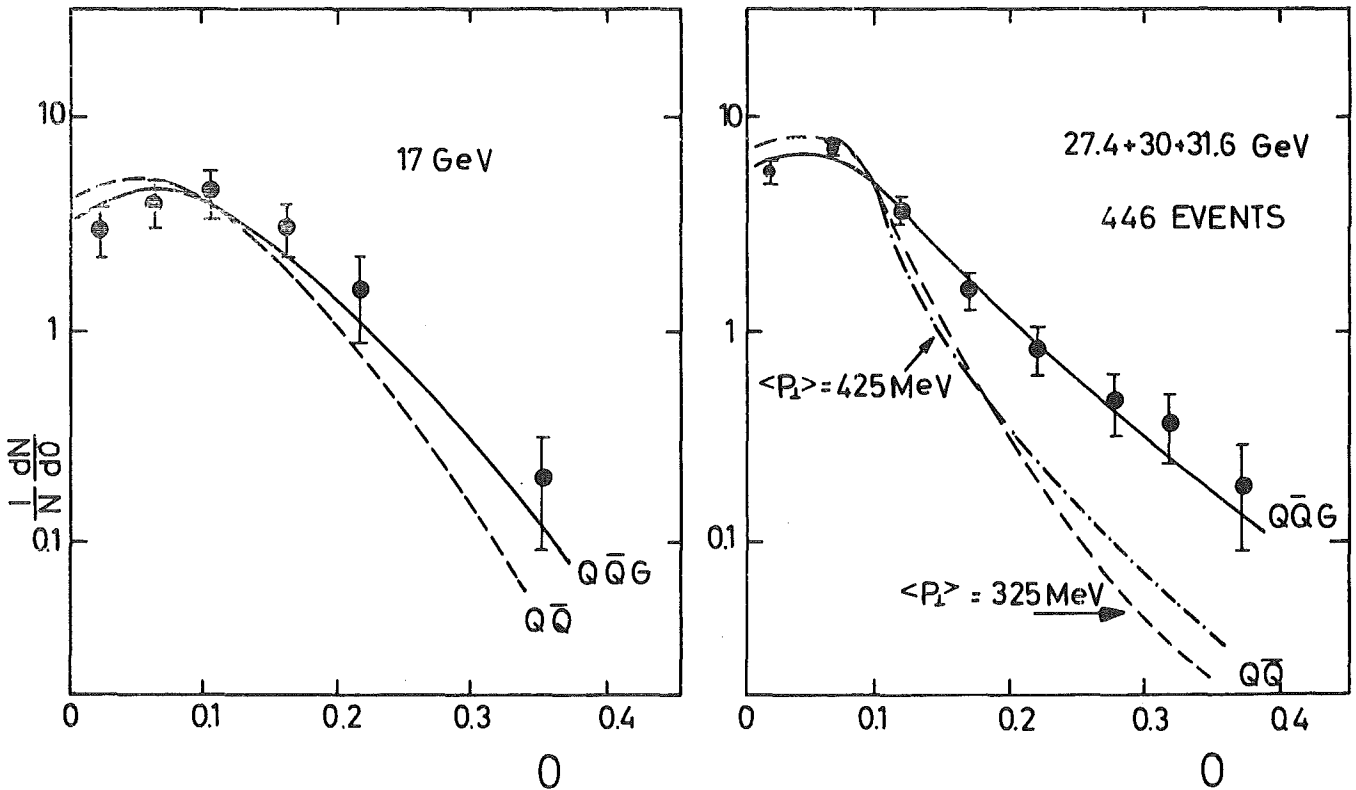   are compared with the q̄q and the q̄qg model.

Fig. 51   MARK J: oblateness distributions for two different energies
          (27.4 to 31.6 GeV are grouped together). Data are compared with
          q̄q predictions for <p_T> = 325 MeV (--) and <p_T> = 425 MeV (-•-)
          and the QCD model (—).

defined in analogy to the inertia tensor. If we diagonalize this expression we obtain the (normalised) Eigenvalues λ_k which correspond to the three main axes of the event in momentum space (fig. 52). If we order these Eigenvalues such that

$$\lambda_1 \geq \lambda_2 \geq \lambda_3$$

then λ_3 closely resembles our well known sphericity definition

$$\lambda_3 = \frac{\sum\limits_i (p_1^i)^2 + (p_2^i)^2}{\sum (p^i)^2} = \frac{\sum (p_T^i)^2}{\sum (p^i)^2} \quad ; \quad S = 3\lambda_3/(\lambda_1 + \lambda_2 + \lambda_3) \quad .$$

The physical meaning of λ_3 is again best understood from an analogy with the inertia tensor. λ_3 points into the direction of the smallest inertia moment in momentum space. To measure the flatness of events we have to study the other two Eigenvalues in particular λ_1 which points into the direction of the smallest extent of the event in momentum space.

It is convenient to define the following quantities[87,1o4] (fig. 52):

$$Q_k = 1 - \frac{2\lambda_k}{\lambda_1 + \lambda_2 + \lambda_3} = \frac{\sum\limits_i (p_k^i)^2}{\sum\limits_i (p^i)^2}$$

Q_k points into the same direction as λ_k, however, it measures the sum of the momentum components p_k parallel to the axis λ_k. Consequently the Q_k are ordered in a rising sequence
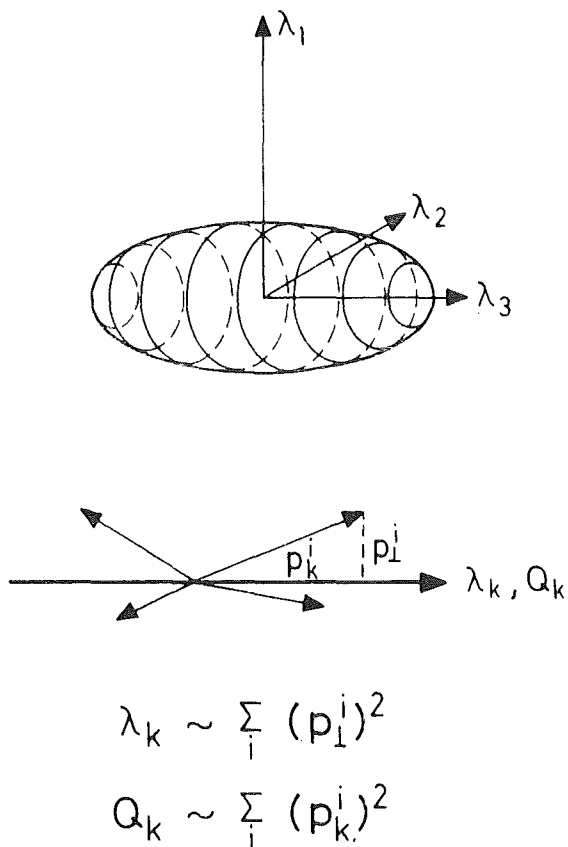
$$Q_1 \leq Q_2 \leq Q_3$$

for a falling sequence of λ_k.

$$\lambda_k \sim \sum_i (p_\perp^i)^2$$

$$Q_k \sim \sum_i (p_k^i)^2$$

Fig. 52   The sphericity tensor in analogy to the inertia tensor. De-
finition of λ_k, Q_k.

$<p_{in}>$ and $<p_{out}>$

We recall the eigenvalues of the sphericity tensor λ_k with $\lambda_1 \leq \lambda_2 \leq \lambda_3$ and introduce the corresponding eigenvectors $\vec{n}_1$, $\vec{n}_2$ and $\vec{n}_3$.

In a disklike structure, the normal to the event plane is given by $\vec{n}_1$. The vector $\vec{n}_2$ lies in the disk and is normal to the sphericity vector $\vec{n}_3$. The following quantities are defined[101]:

$$<p^2_{out}> = <(\vec{p}\,\vec{n}_1)^2>$$

measures the mean momentum component pointing out of the plane, whereas

$$\langle p^2_{in} \rangle \quad = \quad \langle (\vec{p} \ \vec{n}_2)^2 \rangle$$

gives the mean momentum component $\underline{in}$ the plane perpendicular to the main event axis $\vec{n}_3$.

Figs. 53-55 show the experimental distributions obtained by the PLUTO, TASSO, and JADE collaborations. We notice that, due to the method, the $\langle p^2_{out} \rangle$ distributions are narrower than the ones for $\langle p^2_{in} \rangle$. The width of the distributions increases with energy. Whereas all $\langle p^2_{out} \rangle$ plots and the $\langle p^2_{in} \rangle$ at low energies are well described by the conventional $q\bar{q}$ model (udscb), this model fails to describe the high energy data. Increasing σ_q to 45o MeV as suggested by the p_T distribution (fig. 45) gives a reasonable account of the TASSO data up to $\langle p^2_T \rangle \simeq 0.8$ GeV (fig. 54, dashed line). It does not explain the high momentum tail, however, This tail can be well explained by QCD, as demonstrated e.g. in the PLUTO data of fig. 53 (full curve). Note, however, that the distribution at intermediate $\langle p^2_{in} \rangle$ is not well reproduced by neither $q\bar{q}$ nor $q\bar{q}g$.
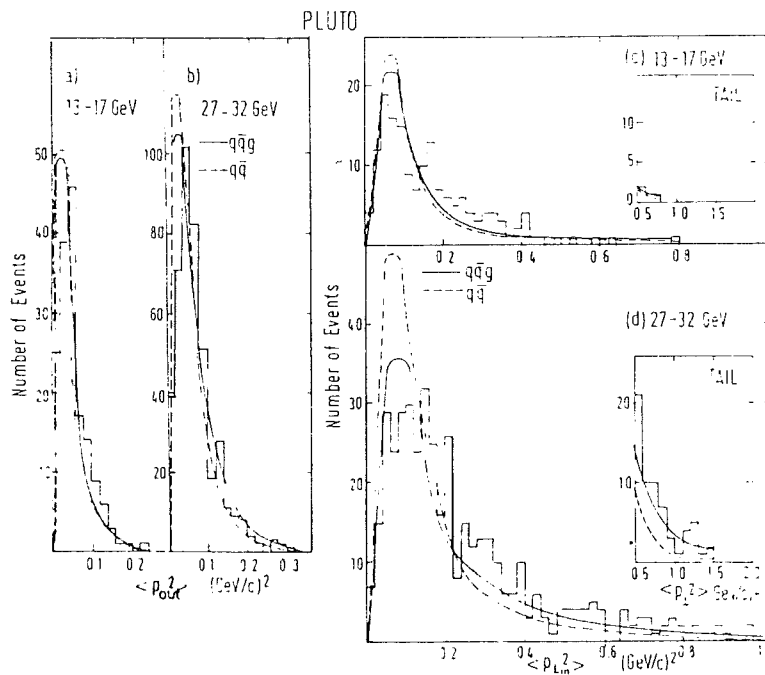

Fig. 53   PLUTO: mean transverse momentum squared in and normal to the event plane $\langle p^2_{T,in} \rangle \equiv \langle p^2_{in} \rangle$ (text). Model calculation for two jets (--) and QCD (—) are shown for comparison.
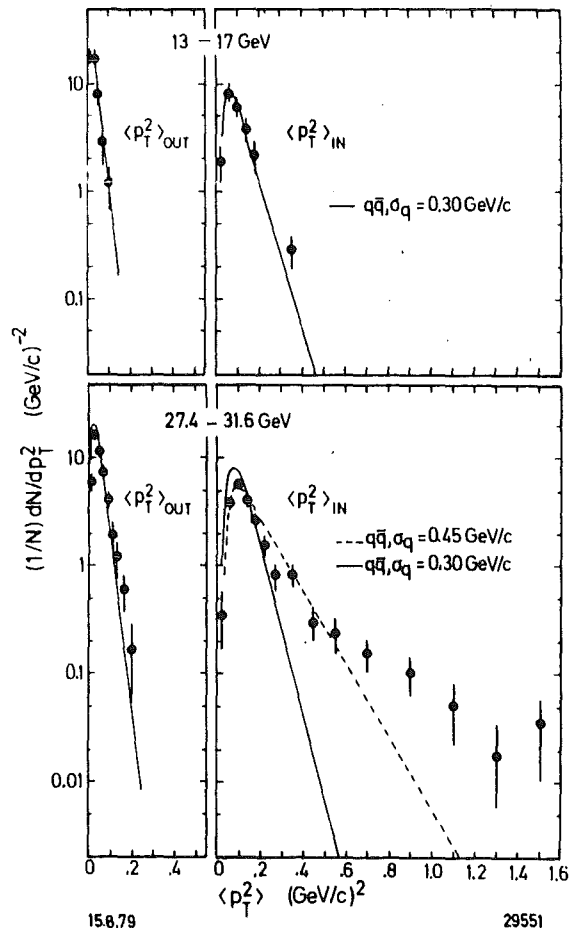
Fig. 54 TASSO: the mean transverse momentum squared in and normal to the event plane. $\langle p_T^2 \rangle_{in} \equiv \langle p_{in}^2 \rangle$ (text); $\langle p_T^2 \rangle_{out} \equiv \langle p_{out}^2 \rangle$ (text). Model calculations with $\sigma_q = 0.3$ GeV (——) and $\sigma_q = 0.45$ GeV (--).
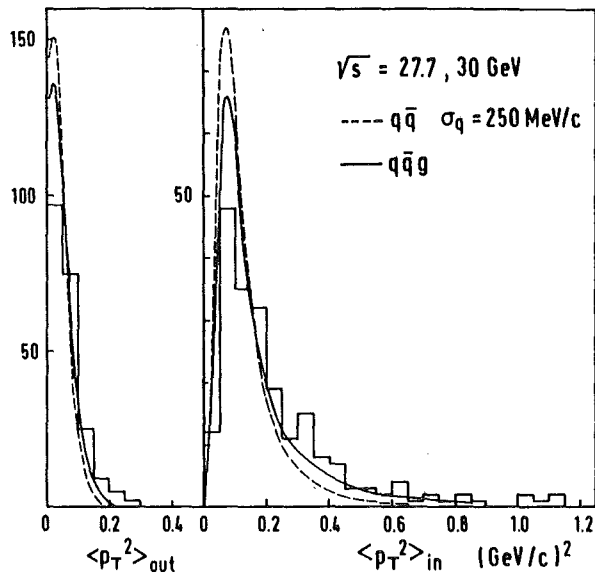

Fig. 55 JADE: the mean transverse momentum squared in and normal to the event plane. $\langle p^2_T \rangle_{out}$ and $\langle p_T^2 \rangle_{in}$ as in fig. 54. Model calculations for $q\bar{q}$ (--) and $q\bar{q}g$ (——).

Aplanarity

The normalized eigenvalues

$$Q_k = \frac{\Sigma \, (p_k^i)^2}{\Sigma \, (p^i)^2}$$

defined above   which measure the total momentum component along the axis $\vec{n}_k$ can be used to define a new variable

$$A = 3/2 \; Q_1 = 3/2 \; <p_{out}^2>/<p^2> \quad ,$$

the aplanarity[105]. In terms of Q_k the sphericity can be written as

$$S = 3/2 \; (Q_1 + Q_2) = 3/2 \; <p_T^2>/<p^2> \; .$$

Since $Q_1 + Q_2 + Q_3 = 1$, events can be plotted in a Dalitz-like tri-angle. The TASSO group has carried out such an analysis. Fig. 56 shows the result for the low and high energy data separately. At both energies, most events fall into the jet corner at low sphericity. Planar events would congregate along the triangle side of low aplanarity. If one eliminates the "background" of two-jet events with S < 0.25, the remaining sample may be subdivided into planar (A < 0.o4) and non-planar events (A > 0.o4). Table 16 gives the observed numers of coplanar events in the two energy regions together with the expectation of different models.

Table 16   Observed number of non-colinear (S > 0.25) coplanar (A < 0.o4) events compared to different predictions (TASSO collaboration)

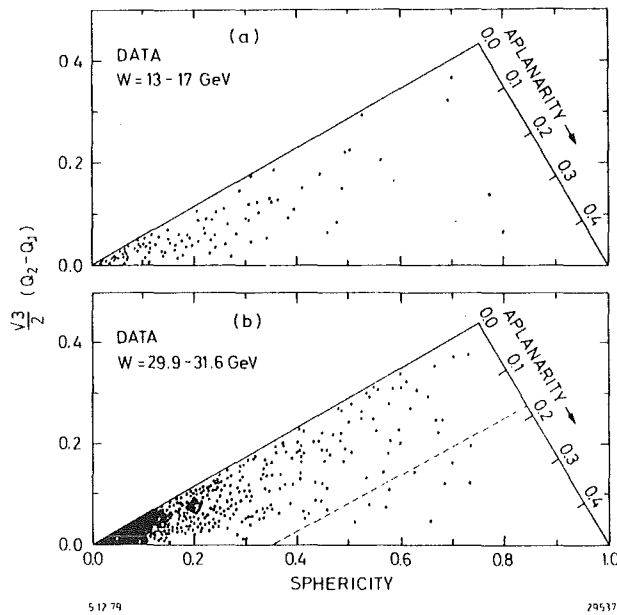| Energy (GeV)	observed events	$\sim q\bar{q}$ $\sigma_p = 0.3$	$q\bar{q}$ $\sigma_q = 0.45$	$q\bar{q}g$
13 - 17	6	3.5		
27.4 - 31.6	18	4.5	4.5	~17

Fig. 56   TASSO: distribution of events in a scatter plot of aplanarity
and sphericity. Data are grouped into low (a) and high (b)
energies.

At low energies, the observed number of events agrees with the pre-
diction of the $q\bar{q}$ model within statistical errors. In the high energy bin,
however, the effect of 18 events cannot be reproduced by the $q\bar{q}$ model,
even if the transverse momentum is increased (σ_q = 0.45).

A similar analysis based on a Dalitz plot of the high energy data was
performed by the JADE collaboration. Fig. 57 shows scatter plots for the
data and the $q\bar{q}$ and $q\bar{q}g$ model. A quantitative comparison is given in table
17. Again the $q\bar{q}g$ model is strongly favoured by the data.

Table 17   JADE: Observed number of events with $(Q_3-Q_2)/\sqrt{3} < 0.35$ and
$Q_1 < 0.o7$ compared to model predictions.

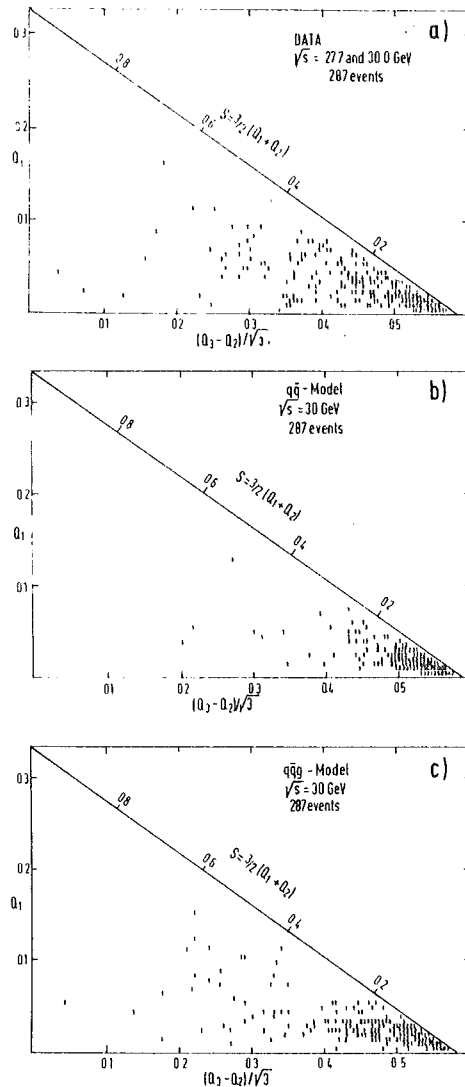| observed	expected	
27.7÷3o GeV	$q\bar{q}$ (σ_q = 25o MeV)	$q\bar{q}g$
23	6	22

Fig. 57 JADE: distribution of high energy events in a Dalitz plot of Q_1
vs. $(Q_3-Q_2)/\sqrt{3}$.
a) Data
b) $q\bar{q}$ model prediction
c) $q\bar{q}g$ model prediction

Triplicity

The PLUTO data have been analyzed in terms of triplicity T_3 and thrust
T. A correlation plot of the two quantities for the high energy sample
(27.4 - 31.6 GeV) is given in fig. 58. Two-jet events cluster in the corner
of large T and T_3 (two and three jet events cannot be distinguished at
large T). Let us look at the events with small T < 0.8 which are our three
jet candidates. In fact, if we plot the angles θ_i found by the triplicity
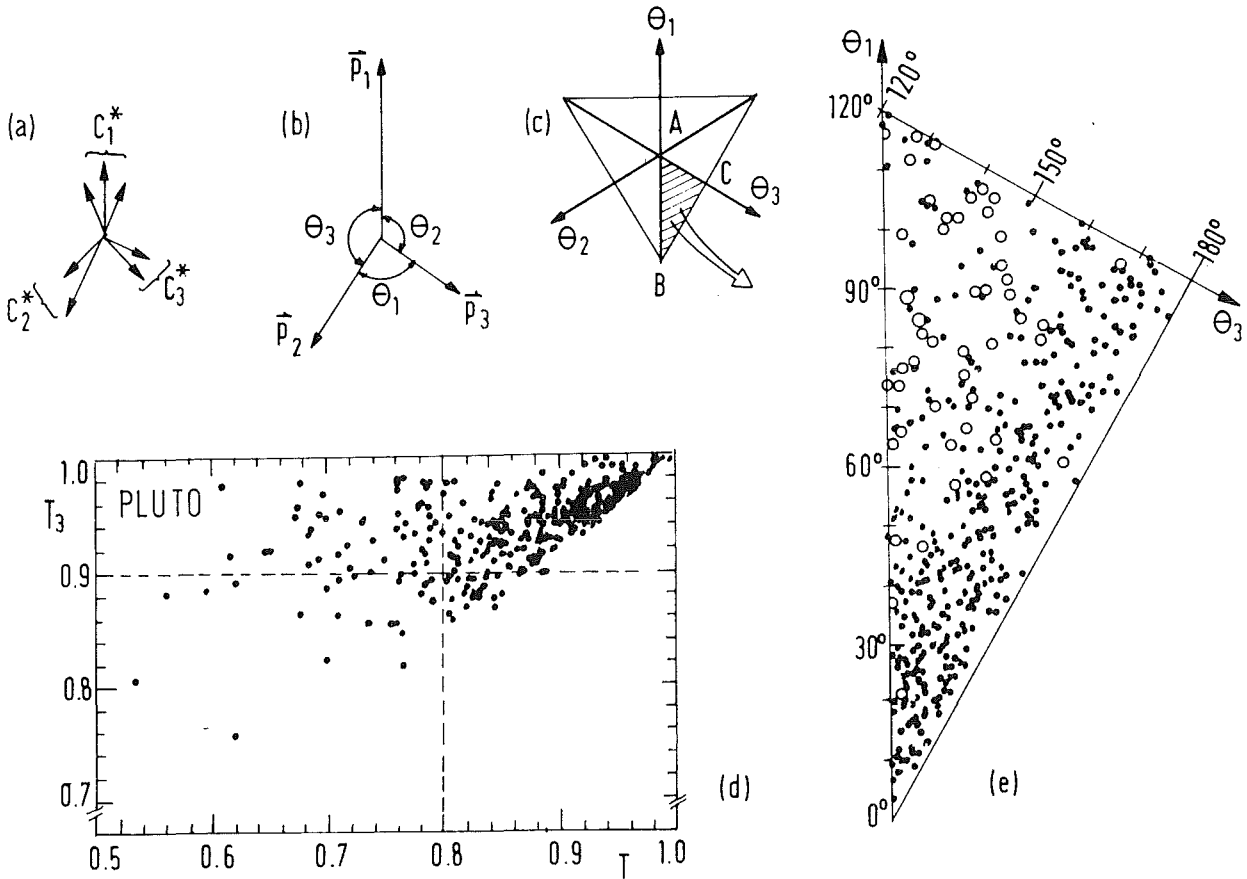analysis (fig. 58e) we realize that these events cluster around values of

Fig. 58   PLUTO: high energy data (27.4 to 31.6 GeV) are shown in a scatter
plot of triplicity T_3 vs. thrust T (d) and in a Dalitz plot of
the jet angles θ_i (e). Open circles in (e) correspond to the re-
gion (T < 0.8, T_3 ≮ 0.9). Fig. (a), (b) and (c) illustrate the
definition of θ_i.

$\theta_1 = \theta_3 \simeq 120^\circ$ (open circles in fig. 58e). Table 18 gives a quantitative
comparison of events observed and expected under various selection criteria
for three-jet candidates (T_3 > 0.9, T < 0.8, θ_3 < 150°). In addition, re-
sults for a selection similar to TASSO are given (S > 0.25, Q_1 < 0.03).
Whereas all numbers at low energies are well accounted for by simple $q\bar{q}$
models (with σ_q = 25o MeV) this model cannot reproduce the high energy da-
ta, even if σ_q is increased to 350 MeV.

Conclusion

In conclusion, all data indicate an increasing number of events with
planar structure which cannot be accounted for by a simple rise in $<p_T^2>$.

Table 18   Observed and expected numbers of events obeying different selection criteria

E_{CM} (GeV)	selected region	events observed	events expected (σ_q = 250 MeV/c)		events expected (σ_q = 300 MeV/c)		events expected (σ_q = 350 MeV/c)
			$q\bar{q}$	$q\bar{q}g$	$q\bar{q}$	$q\bar{q}g$	$q\bar{q}$
13 - 17	$T_3 > 0.9$, T < 0.8 (three-jet events)	24	11	15	15.5	17.5	20
	$\theta_3 < 150^o$	32	25	32	27	33	29
	S > 0.25, $Q_1 < 0.03$ (planar events)	7	8	8	9	9	11
27 - 32	$T_3 > 0.9$, T < 0.8 (three-jet events)	48	11	43	23.5	48.5	36
	$\theta_3 < 150^o$	52	19	51	25	50	31
	S > 0.25, $Q_1 < 0.03$ (planar events)	35	12	30	17	30	22

The effect is well reproduced by QCD predictions. Note, however, that
with the present event numbers, the statistical significance of this pla-
nar structure is not overwhelming.

c) Three Jet Events?

    We have seen that the number of planar events is well compatible with
the expectation of QCD. If q$\bar{\text{q}}$g is the source of these events, there should
be some hard gluon bremsstrahlung events with a visible three-jet struc-
ture. (At the T there was no chance to observe 3 jets, due to the low ener-
gy. At high PETRA energies about 1o GeV per jet should be sufficient to
see this structure.) Fig. 59g-i shows an example for such an event in the
TASSO data. For comparison, an event from the two-jet sample is given in
fig. 59a-c. The projections into the plane perpendicular to the smallest
extent in momentum space $\vec{n}_1$ are shown in fig. 59a and g (top view). Projec-
tions b, h view along the main event axis $\vec{n}_3$ and c, i give the side view.
a-c confirm the main characteristics of a two-jet event: elongation along
the main axis with limited p_T. Fig. 59, however, shows a broad distribution
of momenta with a clustering in three-jet directions (dashed lines).

    One may argue that only charged particles are shown here and the neu-
trals may destroy the threefold structure. However, including neutral ener-
gy detection, figs. 6o and 61 show a corresponding example of planar events
from PLUTO and JADE. Neutral (dashed) and charged (full lines) particles
are well collimated in three jets.(The jet axes are indicated by thick
bars in fig. 6o.)

d) Strong Coupling Constant

    In the preceeding comparison of data and QCD prediction a standard va-
lue of Λ = 0.5 GeV was used. Of course we can turn the argument the other
way and extract α_s (or Λ) from this comparison.

    A summary of values obtained for α_s by the different groups is given
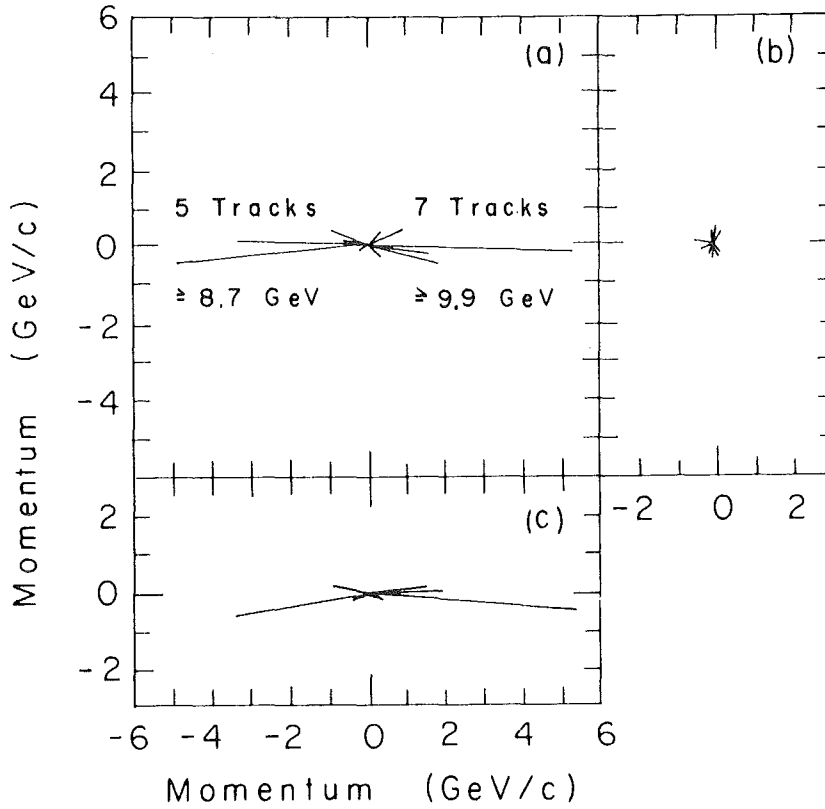in fig. 62. They agree within the error bars yielding an average of

TASSO: a typical two-jet event, (a), (b) and (c) are different views as defined in the text. Charged particle momenta are represented by full lines, the length is proportional to the particle momentum.
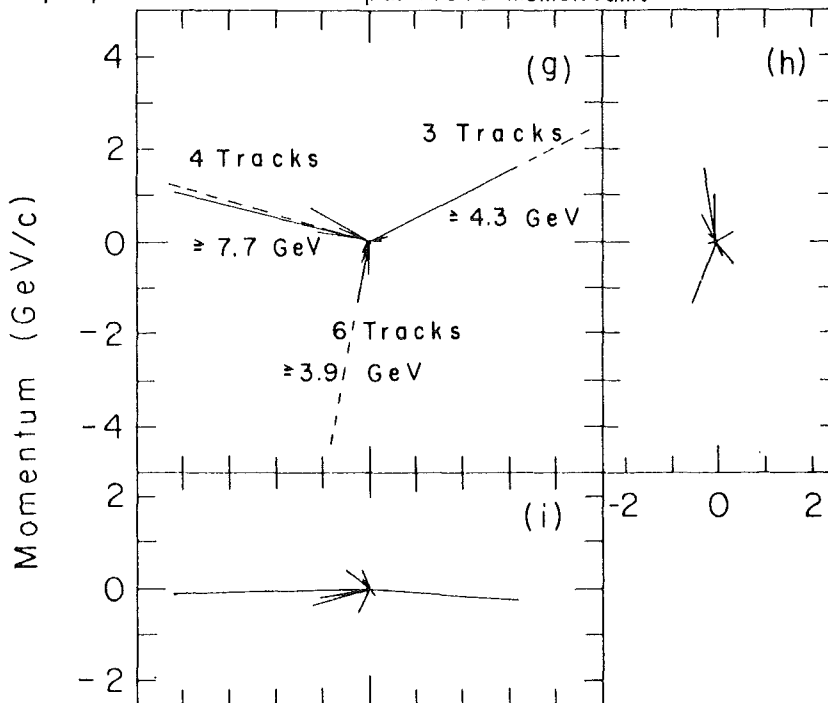
TASSO: a three-jet candidate, (g), (h) and (i) are different projections as defined in the text. The dashed lines indicate the three jet momenta.
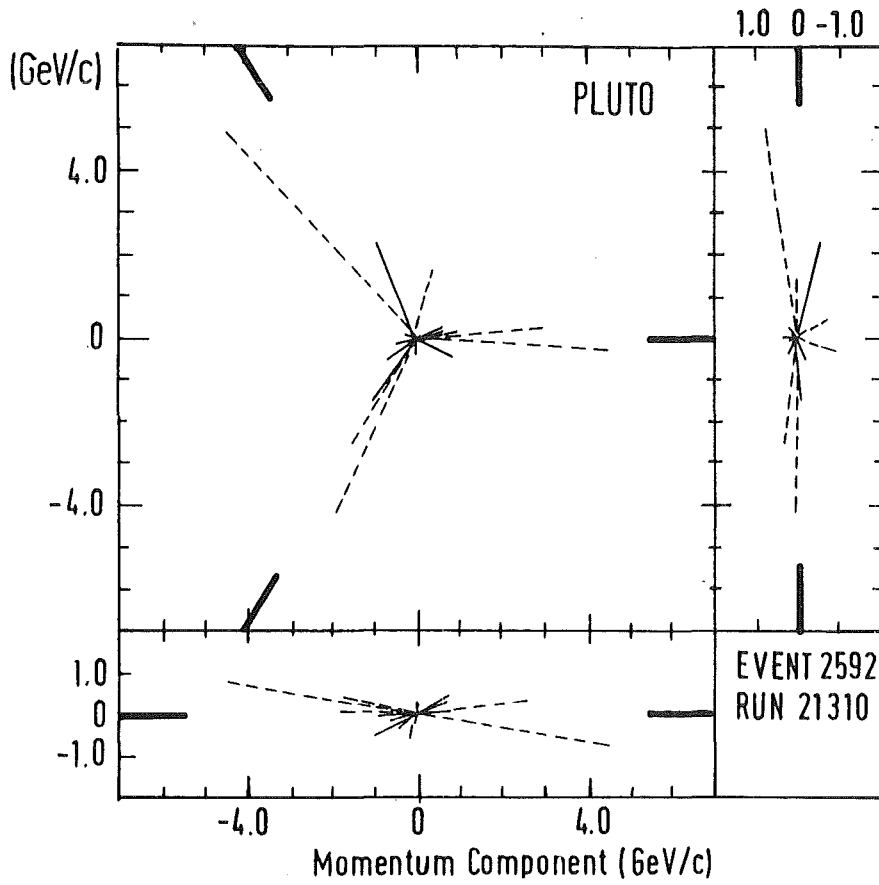
Fig. 6o   PLUTO: a three-jet candidate. Different projections are shown
(comp. fig. 59). The full lines correspond to charged particles,
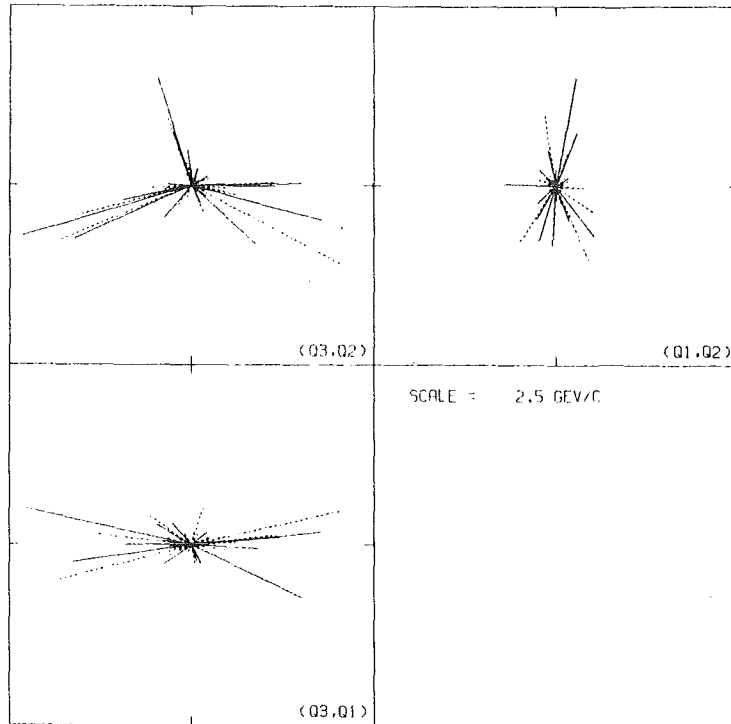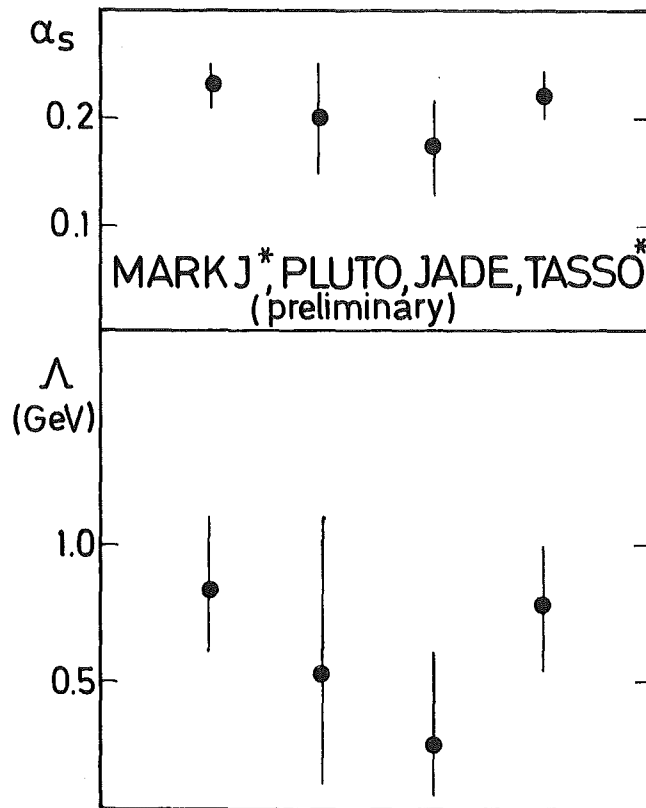the dashed lines to neutral energy. The thick bars indicate the
jet direction.

Fig. 61   JADE: The three projections of a three-jet event. The solid lines
           indicate charged particle tracks, the dashed photons.

Fig. 62   MARKJ[1o6,1o7], PLUTO[74], JADE[1o3], TASSO[1o7]: the strong coupling
           constant α_s at $E_{CM} \simeq 30$ GeV.

$$\alpha_S \ (30 \ \text{GeV}) \ \simeq \ 0.2$$

which corresponds to

$$\Lambda \ \simeq \ 0.5 \ \text{GeV} \ .$$

4. Conclusion

The jet analysis at highest PETRA energies has shown a clear deviation from a simple extrapolation of the two-jet behvaiour at low energies ($\leq$ 10 GeV).

In particular the p_T^2 distributions and the seagull effect can only be explained by an increase of $<p_T^2>$ with energy. The amount by which the $<p_T^2>$ is changed is an agreement with QCD.

In addition, a (low) fraction of the high energy events exhibits a planar structure. Again, this effect can be well explained by gluon bremsstrahlung.

All observations are in quantitative agreement with QCD predictions. The value of α_S extracted from these data is α_S (3o GeV) $\simeq$ 0.2.

REFERENCES

1) G. Wolf, DESY Report 8o/13 (198o)
   G. Flügge, VIII Topical Conference in Particle Physics, Hawaii, 1979
   E. Lohrmann, Erice School, 1979

2) C. Bernardini, G.F. Corazza, G. Ghigo and B. Touschek, Nuovo Cim. 18 (196o) 1293

3) J. Le Francois, raporteur talk, Cornell Conf. 1971
   V. Sidorov, raporteur talk, Cornell Conf. 1971
   Pioneering work: G.K. O'Neill, Bulletin A. Phys. Soc. Ser. 23 (1958) 158

4) B.H. Wiik and G. Wolf, DESY Report 78/23 (1978)
   P. Waloschek, Kerntechnik, Isotopentechnik und -chemie 12 (197o) 525

5) PETRA proposal, unpublished

6) J.J. Aubert et al., Phys.Rev.Lett. 33 (1974) 14o4
   J.-E. Augustin et al., Phys.Rev.Lett. 33 (1974) 14o6

7) PETRA proposal, unpublished

8) PETRA proposal, unpublished

9) PETRA proposal, unpublished

1o) PETRA proposal, unpublished

11) PETRA proposal, unpublished

12) G.A. Voss, 1979 Particle Accelerator Conf., San Francisco, 1979
    and DESY M79/16

13) A. Febel, G. Hemmie, 1979 Particle Accelerator Conf., San Francisco, 1979 and DESY M79/13

14) M. Kobayashi, K. Maskawa, Prog. Theor. Phys. 49 (1973) 652

15) L. Criegee et al., Proc. 1973 Int. Conf. on Instrum. for HEP, Frascati 1973
    PLUTO Coll., J. Burmester et al., Phys.Lett. 64B(1976) 369

16) T. Kinoshita et al., Phys.Rev. D2 (197o) 91o

17) Recent experimental limit: T. Himel et al., Phys.Rev.Lett. 41 (1978) 449
    Recent review: J.J. Sakurai, III. Int. Symp. on HEP with Pol. Beams
    and Targets, Argonne, 1978

18) T. Appelquist and H.D. Politzer, Phys.Rev. D12 (1975) 14o4
    and Phys.Rev.Lett. 34 (1975) 43

19) PLUTO Coll., J. Burmester et al., Phys.Lett. 66B (1977) 395
    A. Bäcker, Thesis, Siegen (1977)

2o) G. Feldman, Proc. of the XIX Int. Conf. on HEP, Tokyo 1978
    and SLAC-PUB-2224 (1978)

21) J. Siegrist et al., Phys.Rev.Lett. 36 (1976) 7oo

22) DASP Coll., R. Brandelik et al., Phys.Lett. 7oB (1977) 125
    and Phys.Lett. 73B (1978) 1o9

23) J. Kirz, Contrib. to the XIX Int. Conf. on HEP, Tokyo 1978

24) Recent reviews:
    G. Goldhaber, EPS conf. Budapest, 1977
    G. Feldman, Banff Summer Inst., Alberta (CA), 1977
    H. Schopper, DESY-report 77/79 (1977)
    B.H. Wiik and G. Wolf, DESY-report 78/23 (1978)
    A. Barbaro-Galtieri, XVI Int. School, Erice, 1978
    M. Davier, EPS Conf. Geneva, 1979

25) V. Lüth, 1979 Int. Sy mp. on Lepton and Photon Interactions at
    High Energies, FNAL, 1979

26) M. Krammer and H. Krasemann, Int. Universitätswochen, Schladming,
    1979 and DESY 79/2o (1979)

27) DASP Coll., W. Braunschweig et al., Phys.Lett. 67B (1977) 243 and 249
    W.D. Apel et al., Phys.Lett. 72B (1978) 5oo

28) W. Bartel et al., Phys.Lett. 79B (1978) 492
    C.J. Biddik et al., Phys.Rev.Lett. 38 (1977) 1324
    W. Tannenbaum et al., Phys.Rev.Lett. 35 (1975) 1323
    PLUTO Coll., V. Blobel, XII Rencontre de Moriond, Flaine, 1977
    S. Yamada, Hamburg Conf., 1977
    Recent results from the MARK II group do not confirm the χ (3.45)
    (J.M. Weiss, EPS Conf. on HEP, Geneva, 1979)

29) E. Bloom, 1979 Int. Symp. on Lepton and Photon Interactions at High Energies, FNAL, 1979

3o) G. Goldhaber et al., Phys.Rev.Lett. 37 (1976) 255
I. Peruzzi et al., Phys.Rev.Lett. 37 (1976) 569

31) DASP Coll., R. Brandelik et al., Phys.Lett. 70B (1977) 132
and 80B (1979) 412

32) G. Flügge, Z. Physik C1 (1979) 121 and
Proc. of the Int. Conf. on HEP, Geneva, 1979
J. Kirkby, 1979 Int. Symp. on Lepton and Photon Interactions at
High Energies, FNAL, 1979

33) M.L. Perl et al., Phys.Rev.Lett. 35 (1975) 1489 and 38 (1976) 117
PLUTO Coll., J. Burmester et al., Phys.Lett. 68B (1977) 297 and 3o1

34) W. Bacino et al., Phys.Rev.Lett. 41 (1978) 13

35) W. Bacino et al., Phys.Rev.Lett. 42 (1979) 749

36) G.J. Feldman, Proc. of the 19th Intern. Conf. on High Energy Physics,
Tokyo, August 1978

37) TASSO Coll., R. Brandelik et al., DESY Report 80/12 (1980)

38) Y.S. Tsai, Phys.Rev. D4 (1971) 2821; SLAC-PUB-21o5 (1978)
H.B. Thacker, J.J. Sakurai, Phys.Lett. 36B (1971) 1o3
J.D. Bjorken, C.H. Llewellyn-Smith, Phys.Rev. D7 (1973) 887

39) A.M. Cnops et al., Phys.Rev.Lett. 40 (1978) 144

40) S.W. Herb et al., Phys.Rev.Lett. 39 (1977) 252
W.R. Innes et al., Phys.Rev.Lett. 39 (1977) 124o

41) PLUTO Coll., Ch. Berger et al., Phys.Lett. 76B (1978) 243

42) C.W. Darden et al., Phys.Lett. 76B (1978) 246

43) PLUTO Coll., Ch. Berger et al., Z. Physik C1 (1979) 343

44) C.W. Darden et al., Contr. to the XIX Int. Conf. on HEP, Tokyo 1978

45) J.K. Bienlein et al., Phys.Lett. 78B (1978) 36o

46) $B_{\mu\mu}$ is taken from Heinzelmann, Tokyo Conference 1978

47) G. Flügge, XIX Int. Conf. on HEP, Tokyo 1978

48) K. Ueno et al., Phys.Rev.Lett. 42 (1979) 486

49) PLUTO Coll., Ch. Berger et al., DESY Report 80/15 (1980)

50) H. Albrecht et al., DESY Report 80/30 (1980)

51) D. Andrews et al., Phys.Rev.Lett. 44 (1980) 1108

52) T. Böhringer et al., Phys.Rev.Lett. 44 (1980) 1111

53) C. Quigg and J.L. Rosner, Phys.Lett. 72B (1978) 462
    J.L. Rosner, C. Quigg, H.B. Thacker, Phys.Lett. 74B (1978) 35o

54) G. Bhanot, S. Rudaz, Phys.Lett. 78B (1978) 119

55) S. Herb and P. Skubic, XV Rencontre de Moriond, March 1980

56) S.D. Drell, Ann. Phys. 4 (1958) 75
    H. Salecker, Z. Physik 16o (1960) 385

57) D. Barber et al., Phys.Rev.Lett. 42 (1979) 111o
    D. Barber et al., MIT report 1o7 (1979), subm. to Nucl.Phys. B

58) PLUTO Coll., Ch. Berger, talk at the 1979 Int. Symp. on Lepton and
    Photon Interactions at High Energies, FNAL, August 1979

59) TASSO Coll., 1979 EPS Int. Conf. on HEP, Geneva, 1979

60) JADE Coll., W. Bartel et al., DESY Report 80/14 (1980)

61) J.E. Augustin et al., Phys.Rev.Lett. 34 (1975) 233
    L. H. O'Neill et al., Phys.Rev.Lett. 37 (1976) 395
    B.L. Beron et al., Phys.Rev.Lett. 33 (1974) 663 and
  , Phys.Rev. D17 (1978) 2187 and 2839

62) F.A. Berends et al., Nucl.Phys. B57 (1973) 381, B63 (1973) 381,
    B68 (1974) 541, B1o1 (1975) 234 and Phys.Lett. 63B (1976) 433

63) O. Meyer, DPG Frühjahrstagung, Dortmund, 1980

64) PLUTO Coll., Ch. Berger et al., Phys.Lett. 81B (1978) 410,
    86B (1979) 413, and 86B (1979) 418

65) D. Barber et al., Phys.Rev.Lett. 42 (1979) 111o, 1113, and
    D. Barber et al., MIT-LNS Report 1o7 (August 1979)

66) TASSO Coll., R. Brandelik et al., Phys.Lett. 83B (1979) 261,
    86B (1979) 243, and 89B (1980) 418

67) W. Bartel et al., Phys.Lett. 88B (1979) 171

68) G. Sterman and S. Weinberg, Phys.Rev.Lett. 39 (1977) 1436

69) A. De Rujula, J. Ellis, E.G. Floratos and M.K. Gaillard,
    Nucl.Phys. B138 (1978) 387

70) G. Hanson et al., Phys.Rev.Lett. 35 (1975) 16o9
    G. Hanson, XIII Rencontre de Moriond, Les Arcs (1978) and
    SLAC-PUB-2118 (1978)

71) PLUTO Coll., Ch. Berger et al., Phys.Lett. 78B (1978) 176

72) J.D. Bjorken and S.J. Brodsky, Phys.Rev. D1 (197o) 1416

73) E. Fahri, Phys.Rev.Lett. 39 (1977) 1587. See also S. Brandt,
    Ch. Peyrou, R. Sosnowski and A. Wroblewski, Phys.Lett. 12 (1964)
    57; S. Brandt and H. Dahmen, Z. Physik C1 (1979) 61

74) O. Achterberg, Frühjahrstagung DPG, Dortmund, 198o

75) A. Ali, J.G. Körner, G. Kramer, J. Willrodt, Z. Physik C1 (1979)
    2o3 and DESY report 79/63 (1979), to be published

76) M. Kobayashi, T. Maskawa, Prog. Theor. Phys. 49 (1973) 652

77) e.g.: J.J. Sakurai, VIII Hawaii Topical Conf., 1979

78) A. Barbaro-Galtieri, Erice School 1978,

79) R.D. Field and R.P. Feynman, Phys.Rev. D15 (1977) 259o and
    Nucl.Phys. B136 (1978) 1

80) TASSO Coll., R. Brandelik et al., Phys.Lett. 88B (1979) 199
    PLUTO Coll., Ch. Berger et al., Phys.Lett. 91B (1980) 148
    JADE Coll., W. Bartel et al., Phys.Lett. 91B (1980) 152
    D.P. Barber et al., MIT-LNS Report 11o (March 198o)

81) H. Fritzsch, M. Gell-Mann and H. Leutwyler, Phys.Lett. 47B (1973) 365
    D.J. Gross and F. Wilczek, Phys.Rev.Lett. 30 (1973) 1343
    H. Politzer, Phys.Rev.Lett. 3o (1973) 1346

82) K. Koller, H. Krasemann, T.F. Walsh, Z. Physik C1 (1979) 71
K. Koller, T.F. Walsh, Phys.Lett. 72B (1977) 227,
73B (1978) 5o4, and Nucl.Phys. B14o (1978) 449

83) T.A. De Grand et al., Phys.Rev. D16 (1977) 3251
S. Brodsky et al., Phys.Lett. 73B (1978) 2o3
H. Fritzsch, K.H. Streng, Phys.Lett. 74B (1978) 9o

84) e.g.: K. Shizuya, S.H.H. Tye, to be published
with further references

85) F.H. Heimlich et al., Phys.Lett. 86B (1979) 399

86) C.W. Darden et al., ref. 44

87) PLUTO Coll., Ch. Berger et al., Phys.Lett. 82B (1979) 449

88) A. Ore, J.L. Powell, Phys.Rev. 75 (1949) 1696

89) Compare also: K. Hagiwara, Nucl.Phys. B137 (1978) 164

90) S. Brandt and H. Dahmen, Z. Physik C1 (1979) 61

91) PLUTO Coll., S. Brandt, talk at the Int. Conf. on HEP, Geneva, 1979

92) H. Meyer, 1979 Int. Symp. on Lepton and Photon Interactions
at High Energies, FNAL, 1979

93) K. Koller, H. Krasemann, Phys.Lett. 88B (1979) 119

94) J. Ellis, M.K. Gaillard and G. Ross, Nucl.Phys. B111 (1976) 253
T.A. De Grand, Y.J. Ng., S.H.H. Tye, Phys.Rev. D16 (1977) 3251

95) I.I.Y. Bigi, R.F. Walsh, Phys.Lett. 82B (1979) 267
I.I.Y. Bigi, to be published

96) C.L. Basham et al., Phys.Rev. D17 (1978) 2298
F. Steiner, DESY 78/59 (1978)

97) G. Kramer, G. Schierholz, Phys.Lett. 82B (1979) 1o8

98) P. Hoyer, P. Osland, H.G. Sander, T.F. Walsh, P.M. Zerwas,
DESY 79/21, to be published

99) TASSO Coll., talks presented by R. Cashmore, P. Söding, G. Wolf
at the Int. Conf. on High Energy Physics, Geneva, June 1979

100) D.P. Barber et al., Phys.Rev.Lett. $\underline{43}$ (1979) 83o

101) TASSO Coll., R. Brandelik et al., Phys.Lett. $\underline{86B}$ (1979) 243

102) PLUTO Coll., Ch. Berger et al., Phys.Lett. $\underline{86B}$ (1979) 418

103) JADE Coll., W. Bartel et al., Phys.Lett. $\underline{91B}$ (198o) 142

104) G. Alexander, XIX Int. Conf. on HEP, Tokyo, 1978

105) S.L. Wu, G. Zobernig, Z. Physik $\underline{C2}$ (1979) 1o7

106) D.P. Barber et al., Phys.Lett. $\underline{89B}$ (1979) 139

107) A. Ali, E. Pietarinen, G. Kramer, J. Willrodt, DESY Report 79/86 (1979)